Study on the Loading Frequency Effect on the Fatigue Properties of Metallic Materials Mainly Focused on Low Carbon Steel

A Thesis Submitted to the Faculty
in Partial Fulfillment of the Requirement for the
Degree of Doctor in Mechanical Engineering

by

GUENNEC Benjamin Morgan Francois Paul

Doctoral Program in Integrated Science and Engineering
Graduate School of Science and Engineering
Ritsumeikan University
September, 2014

Acknowledgments

Before introducing some particular persons, which have contributed a lot in the researches related to this *PhD* thesis, my first words will be dedicated to *all* the different people who helped me by spending their time to allow me to go further at any stage of my doctoral program, as other student at Prof. Ueno's laboratory, or people met during my internship at IHI Corporation.

I want to thank particularly Profs. Akira UENO and Tatsuo SAKAI for their warm welcome at Ritsumeikan University. In a similar way, I want to thank also MM. Masahiro TAKANASHI and Yu ITABASHI for their kind help and support in the preparation of the manuscripts written based on the experiments presented in this report.

I want also to have a special word to Prof. Kei AMEYAMA and Ms. Mie OTA in order to express my thanks for improving significantly the progression of my *PhD* program.

I wish also deliver a sincere message to Mrs. SUGAHARA who also helped me more than she probably thought.

Finally, I want to thank also my family in France for their support during this period where their son, brother or uncle was far, far away.

Abstract

Use of ultrasonic testing method has not ceased to grow in the latest decades. This statement can be easily explained, as one of the topical subjects in metallic material fatigue is the gigacyclic property. Indeed, it is almost impossible to reach such kinds of number of cycles by using usual fatigue testing methods, as servo-hydraulic for instance.

Nevertheless, the main advantage of the ultrasonic fatigue method is based on its very high loading frequency, usually 20 kHz. Thus, ultrasonic method is driven at loading frequency 100 to 1,000 times larger than usual fatigue method ones. Consequently, an effect of the loading frequency on the fatigue properties of metallic materials is at stake. This is the problem so-called "frequency effect".

Naturally, previous outstanding works have already been conducted on this issue. However, up to now, the frequency effect still remains unexplained. Indeed, some metallic materials do not reveal a particular gap between *S-N* curves obtained by ultrasonic and usual methods, as high strength steels for instance. On the other hand, typical materials as Nickel alloys or low carbon steels let appear a significant effect of the loading frequency on the *S-N* property.

The aim of this *PhD* program is to better grasp the frequency effect by mainly undertaking two studies totally different. First one consists on a statistical point of view of the frequency effect by gathering a large amount of data from literatures in this field. Particular discussions will be held for materials where the frequency effect is not clear, as high strength steels and aluminum alloys. This first study will be detailed in Chapter 2.

The second study is related to the frequency effect in the case of low carbon steel (JIS S15C, 0.15 %C). We will first reconfirm the presence of such a frequency effect in the case of low carbon steels, and then discuss on the causes of this phenomenon. This study will be discussed in Chapters 3, 4 and 5.

According to these studies, as a general trend, it is true that high strength steels or aluminum alloys do not reveal so significant loading frequency effect, even though such a result needs to be further detailed. In addition, the effect of the loading frequency on the fatigue properties of low carbon steels has been found to be a consequence of a particular behavior of B.C.C. material, as ferrite. Under specific temperature and strain rate conditions, changes of dislocation structure and crack initiation mode have been detected. The longer fatigue lives of S15C steel observed at ultrasonic frequency are a direct consequence of the change of crack initiation mechanism.

NB: *Important figures and tables of this report are set in the continuity of the text. However, in order to save this continuity, some results taken from other literatures are gathered in the appendix of this report. Such figures are labeled as* Fig_Apx*, to highlight their presence in the Appendix of this report.*

Table of contents

Chapter 1. Research background and problems left unsolved

1.1. Ultrasonic fatigue testing method

1.1.1. Purpose

Fatigue testing in mechanical engineering has always had the same purpose: to assess the resistance of a specific material against a cyclic stress pattern. This pattern, in order to clarify the situation of the test, follows usually a sinusoidal curve against time. Evolution of the stress is the main parameter that influences the results of a fatigue test.

As all sinusoidal curves, loading pattern is defined by two main parameters: on the one hand the mean stress level and amplitude; on the other hand, the frequency. To increase the stress amplitude will, of course, decrease the life span of the specimen; to increase the frequency will decrease the time needed for a specimen to hit a certain number of cycles. Wohler has defined the fatigue behavior of ferrous materials by a bilinear model. This model is represented in Fig. 1.

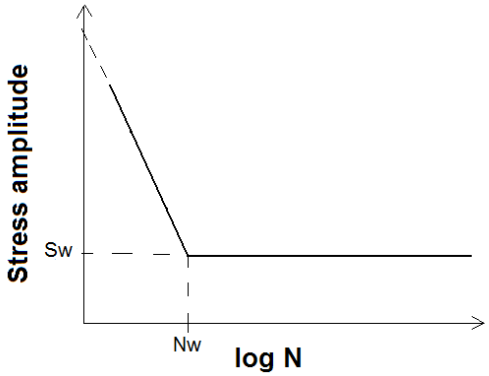

Figure 1 Representation of the bilinear model

This model is composed of two linear regressions. For low cycle regime, fatigue life decreases up to a certain number of cycles, named "knee point" (N_w). This point is usually situated from 10^5 to 10^6 cycles. After this point, the second regression is parallel to the cycle axis such as there is no evolution of the fatigue life, even though the number of cycles is increasing. This stage is usually so-called the "infinite life" and the associated stress level is the "fatigue limit" S_w. It is usually said that, at this stage, specimen would be prone to a failure from another phenomenon than fatigue. That is the reason why for a very long period, fatigue tests of metallic materials were carried out up to 10^7 cycles.

However, reliability design of mechanical parts has changed. Indeed, some now-a-days devices, as automobile crankshafts or shafts of very high speed train, are asked to hit number of cycles up to 10^9 or 10^{10} cycles. This domain of the fatigue property of metallic material is usually so-called the very high cycle fatigue (VHCF) or gigacyclic fatigue.

To reach these kinds of number of cycles by using usual devices, which have usually a loading frequency around 50 Hz, requires a little more than 3 years. In order to make more reasonable tests up to gigacyclic fatigue regime, ultrasonic testing method is much more convenient. Indeed, the specimen is placed into resonance, which allows us to hit very high loading frequencies. In general, frequency used is equal to 20 kHz. As a consequence it requires less than 6 days in order to reach 10^{10} cycles, if the test is performed continuously.

1.1.2. History of ultrasonic fatigue testing use

The ultrasonic fatigue test method is totally different from the conventional ones. Indeed, specimen is not just prone to a cyclic stressing cycles obtained by displacement of the machine's chucks. For ultrasonic device, the specimen itself is placed into resonance.

The application of resonance fatigue testing started in 1911 by its first using by Hopkinson[1]. By this way, he was able to reach a frequency of 116 Hz, instead of a maximum of 33 Hz by conventional machines at this time. In 1925, Jenkins[2] used a similar device and reached a frequency of 2.5 kHz. Four years after, Jenkins and Lehmann were able to hit a frequency of 10 kHz with a pulsating air resonance system.

We must wait up to the 1950's to highlight a critical improvement in the ultrasonic testing technics. Indeed, Mason[3] in 1950 introduced a piezoelectric or magnetostrictive material in the typical design of ultrasonic machine. In such a way, we can transform an electric signal into mechanical vibrations with the same frequency. For instance, Mason used a frequency of 20 kHz.

After this introduction, some researchers had reached even higher frequencies: Girard[4] conducted fatigue tests up to 92 kHz and Kikukawa[5] up to 199 kHz. However, such very high frequencies have a main drawback discussed in Section 1.1.4.

The 1960's correspond to the first age of ultrasonic fatigue tests. Some very important studies have been performed during this period. It was at that time where the first studies on loading frequency effect were carried out. However, in the following two decades, studies on ultrasonic fatigue testing have been almost given up. It was due to some intrinsic problems of ultrasonic testing method, in addition with the absence of the main purpose of ultrasonic testing use.

Indeed, in the middle of 1980's some Japanese researchers had found the main reason of ultrasonic fatigue test use. Kikukawa, Ebara and Murakami[6] pointed out some fatigue failures after 10^7 or 10^8 cycles. In other words, the "infinite life" introduced by Wohler does not really exist. We have now replaced the term of "infinite life" by "conventional infinite life".

Thus, since a fatigue failure can occur even for number of cycles of 10^9 and sometimes more, gigacyclic regime has become a topical issue in the metallic materials fatigue researches. As already mentioned, ultrasonic testing method represents a huge time saving process compared to usual testing methods. So a lot of researches have been started in order to improve the ultrasonic fatigue techniques.

One major problem of the ultrasonic device is to control the stress pattern that specimen has to cope with, which is much complicated than usual fatigue methods. This control was improved by progresses of computer science. Bathias, Wu and Ni[7,8] developed some computer control systems using PC 486 (at least) computers. With these kinds of system, we can obtain an accuracy of 99% on the stress level observed by the specimen. In addition cyclic stressing could have variable amplitude of loading, which is impossible for conventional tests.

About 30 years after this second main improvement, ultrasonic fatigue method is now present all around the world in all the industrial fields were mechanical reliability is important as aircraft, automobile, railway, offshore...

1.1.3. Presentation of ultrasonic machine

Let us now pay more attention on the principles and the main components of an ultrasonic fatigue testing machine. This kind of machine exists up to now only for axial and torsion loadings. In this part, we will make a focus on the far more used testing condition, which is the axial loading one. As already mentioned, the main idea of this technique is to place the metallic material's specimen into resonance. Fig. 2 and Photo 1 show the general situation of an ultrasonic fatigue testing device.

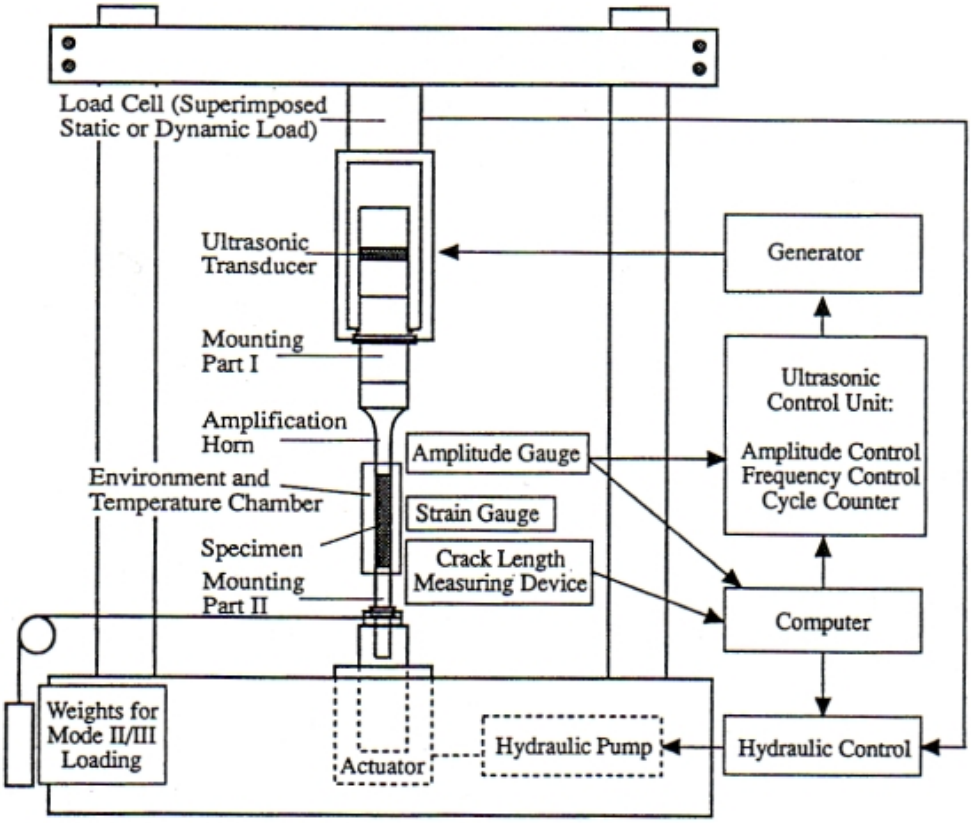

Figure 2 General hardware of ultrasonic fatigue machine

The electric generator is a relatively low power output (several hundreds of Watts). It supplies a sinusoidal signal; its frequency is equal to the loading frequency. This signal is transmitted to the piezoelectric (or magnetostrictive) transducer called "converter". It will transform the electric signal into mechanical vibrations. The direct environment of the specimen, called "mounting part I" in Fig. 2, will be discussed in a second time.

The control unit is one displacement gauge (or a gap sensor), an amplitude control unit, a frequency control unit and a cycle counter. The gauge or gap sensor is essential as it will give the information of the displacement of extremity of specimen, and so to allow the calculation of the stress observed by the specimen. In addition, a computer is very important for random loading tests, since it will record the stress pattern of the fatigue test. It is also useful to record the crack length if

the crack propagation is studied. Depending on the test's objectives, some additional facilities can be admitted. It could be a cooling system, furnace, corrosion chamber or crack length acquisition.

If the stress ratio ($R = \sigma_{min} / \sigma_{max}$) is strictly -1, which is corresponding to a fully reversed tension/compression situation with a mean stress equal to 0, the second extremity of the specimen is free. Otherwise, or if the loading conditions are mixed, we had to set a second mounting part.

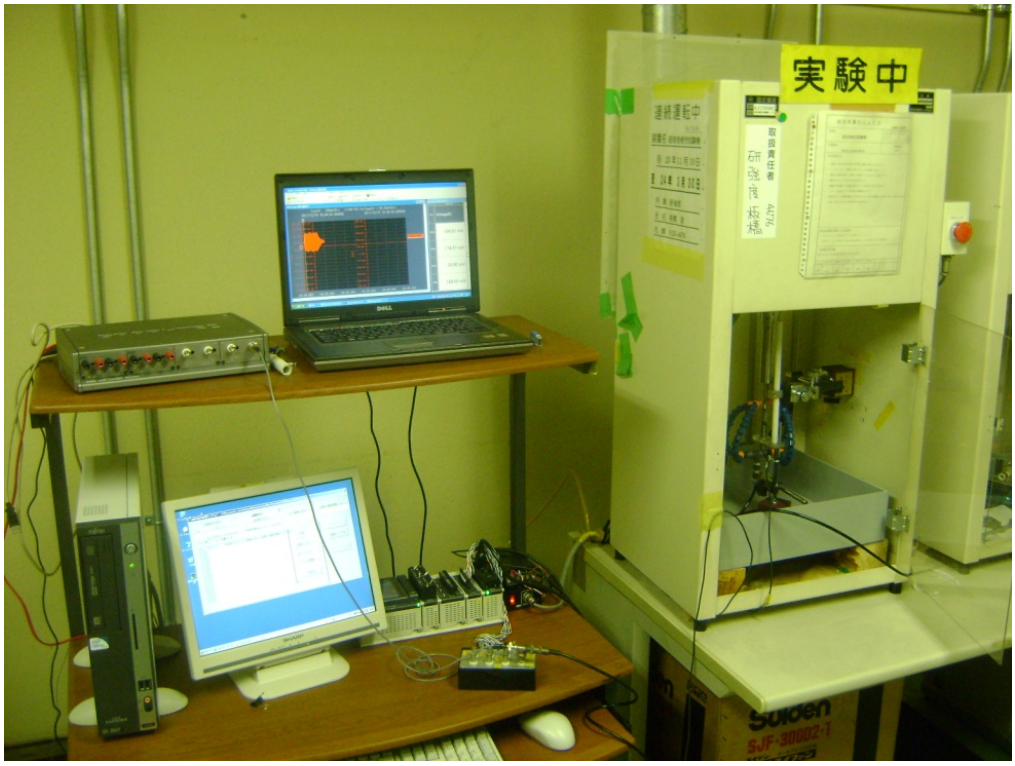

Photo 1 Ultrasonic fatigue testing machine (right) and some control devices (left)

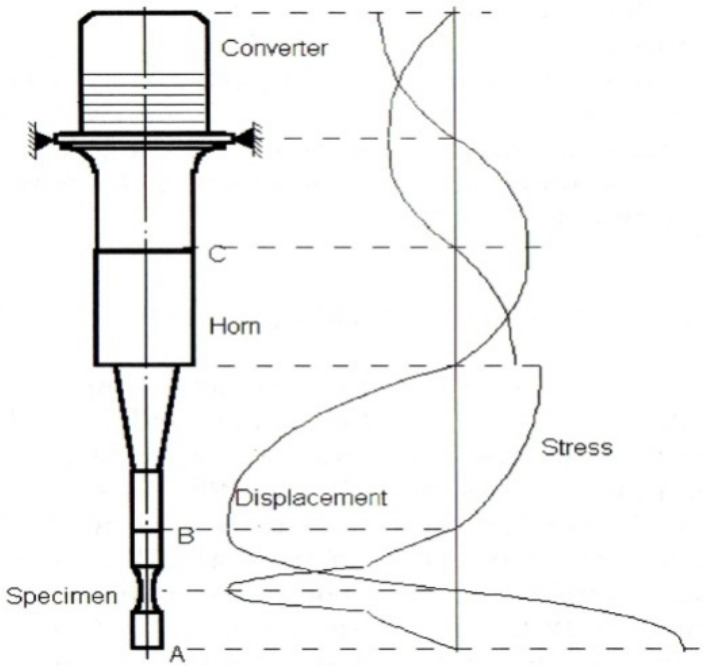

Figure 3 Direct environment of the specimen, ultrasonic test

Let us now talk about the direct specimen's environment, presented in Fig. 3. As seen previously the *converter* is directly linked to an electric current source and will excite the *horn* at the same frequency of the current. However, since the amplitude of this movement is very tiny, an ultrasonic horn is needed to amplify it. At the extremity of the horn, named *B* in Fig. 3, is attached the specimen.

As you can see on Fig. 3, displacement and stress repartition all along this system is plotted in the case where the second extremity *A* is free. In order to have a peak of stress at the center of the specimen, and thus a node of displacement pattern, specimen has to have a strict length that can be of course calculated, using resonance theory. Calculation of the stress distribution along the specimen under ultrasonic fatigue loading will be introduced in the Section 1.1.4.

1.1.4. Calculation of stress distribution

This section will introduce the calculation of the stress distribution along the metallic material specimen under ultrasonic loading. These calculations are taken from *Gigacycle Fatigue in Mechanical Practice*, by C. Bathias and P.C. Paris, edited by Dekker, New York. Let us first have a look on the different definitions before introducing equations.

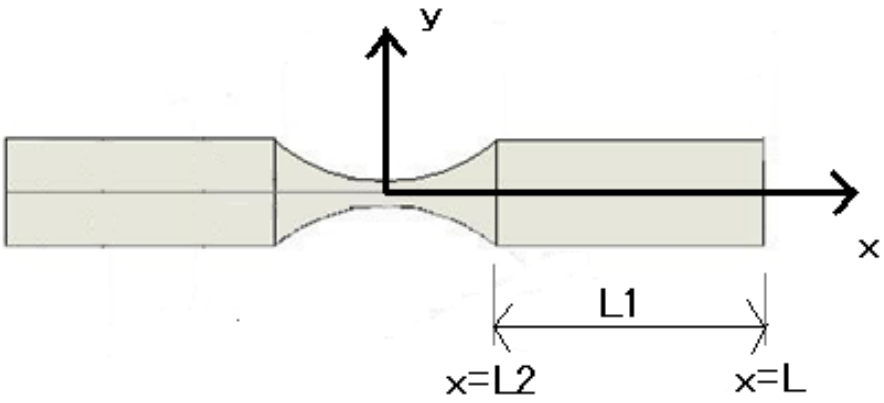

Figure 4 Schematic overview of an hourglass shaped specimen

Definitions:

U(x): displacement.
U'(x),ε(x): strain.
S(x): cross section area.
L: semi-length of specimen.
L2: semi-length of hourglass shape.
L1: length of both cylindrical sections of specimen.
R1: semi-diameter at the center of specimen.
R2: semi-diameter of both cylindrical sections.
y(x): profile in the hourglass profile.
f: loading frequency.
ρ: volume weight of metallic material.
E: Young's modulus of metallic material.
σ_a: stress amplitude of fatigue test.

Here, we will consider that profile of hourglass shape is equivalent to an exponential shape. At a result, we can consider that:

Where α depends on the specimen geometry.

Displacement along the specimen follows this differential equation:

$$U''(x) + p(x)U'(x) + k^2U(x) = 0$$

$$\text{with } p(x) = \frac{S'(x)}{S(x)} \text{ and } k = \frac{\omega}{c} = 2\pi f\sqrt{\rho/E}$$

We are solving this equation.

- In the cylindrical part (L2 < x < L), p is null. As a consequence:

$$U(x) = C1 * \cos(kx) + C2 * \cos(kx)$$

There is one limit condition: at the edge of specimen ($x = L$), we have a peak of displacement, so called A_0.

- In the central part (L2 < x < L), $p(x) = 2\alpha * \tan(\alpha x)$

The general solution for this differential equation is:

$$U_2(x) = \frac{C3 * \exp(\beta x) + C4 * \exp(-\beta x)}{\cosh(\alpha x)}$$

$$\text{with } \beta = \sqrt{\alpha^2 - k^2}$$

There is one limit condition: at the center of specimen ($x = 0$), we have a node of displacement. So $C3$ and $C4$ are opposite.

$$U_2(x) = \frac{2C3 * \sinh(\beta x)}{\cosh(\alpha x)}$$

In the case of the hourglass shape considered here, we have geometrically:

$$\alpha = \frac{1}{L2}\arg\cosh\left(\frac{R2}{R1}\right)$$

In addition, two continuity conditions can be involved for both displacement and strain at $x = L2$ to determine the expressions of U_1 and U_2. Thus:

$$A_0 * \cos[k(L - L2)] = \frac{2C3 * \sinh(\beta L2)}{\cosh(\alpha L2)}$$

$$U_1'(L2) = U_2'(L2)$$

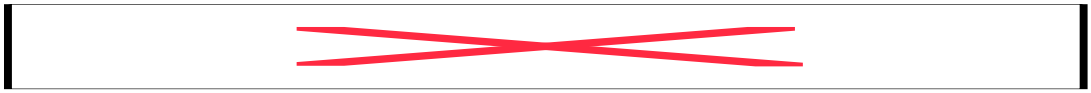

If we divide the second equation by the first one, in such a way to keep in mind that L - $L2$ is equal to $L1$, we obtain the Eq. (1):

$$k\tan(kL1) = \beta\coth(\beta L2) - \alpha\tanh(\alpha L2) \qquad (1)$$

In the same way, one can find the expression of strain inside the material, Eq. (2):

$$\varepsilon(x) = A_0 * \varphi(L1, L2)\frac{\beta\cosh(\beta x)\cosh(\alpha x) - \alpha\sinh(\beta x)\sinh(\alpha x)}{\cosh^2(\alpha x)} \quad (2)$$

Where,

$$\varphi(L1, L2) = \cos(kL1)\frac{\cosh(\alpha L2)}{\sinh(\beta L2)} \text{ and } \boxed{\times}$$

In this Eq. (2), all terms otherwise *L1* (length of cylindrical parts of specimen) are known. Thus, we can obtain the suitable length in order to place specimen in the resonance condition.

One can note that for a same metallic material, an increase of the loading frequency will increase only parameter *k* in this equation. As a consequence, lengths of cylindrical parts *L1* will decrease. This is the reason why ultrasonic tests are usually conducted at a loading frequency of 20 kHz. Indeed, as dimensions of the specimen become small, self-heating phenomenon (introduced in the Section 1.1.5) is more severe. In addition, 20 kHz is a sufficient frequency to reach gigacycle regime in a convenient period.

1.1.5. Temperature rising

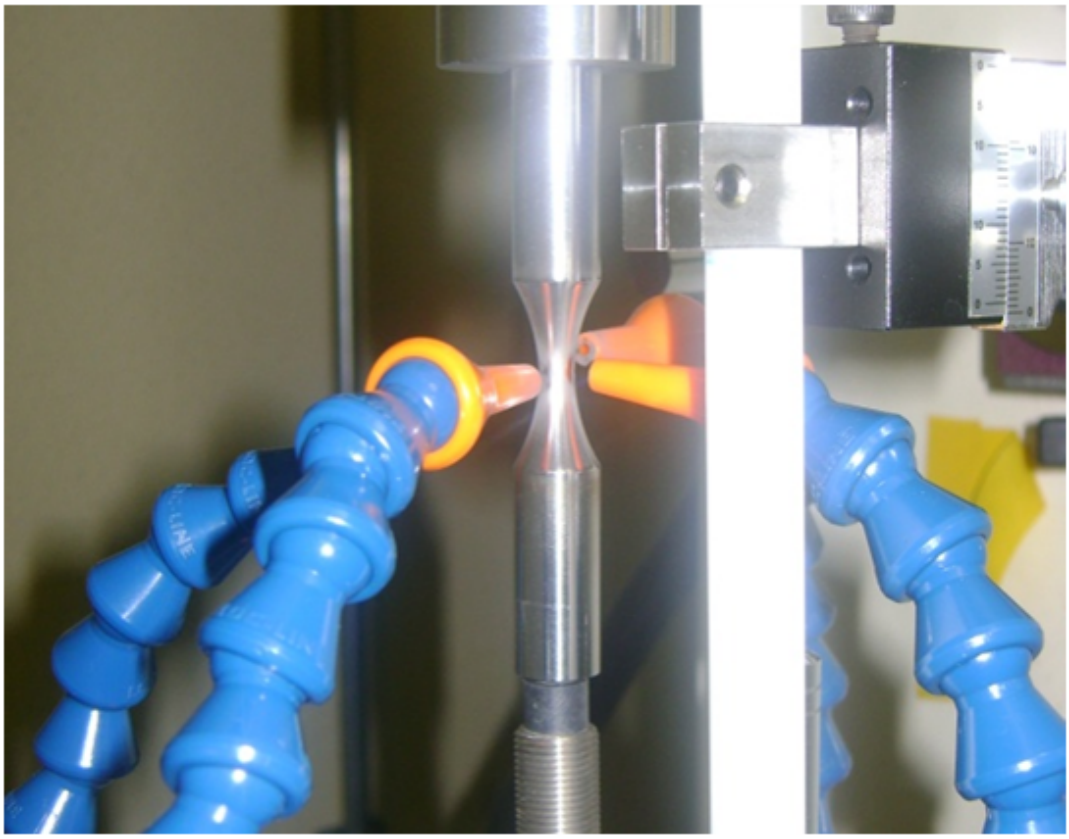

Photo 2 Air-cooling condition for ultrasonic tests

To apply a stress cycling pattern with a loading frequency as high as 20 kHz will cause the phenomenon so called “self-heating”. In other words, the temperature of metallic materials rises due to the stressing cycles. In a general way, the higher is the stress level, the higher will be this temperature rising. This increase is so high that it can change the properties of the material tested, as the Young’s modulus, ductility and so on… In order to avoid this temperature increase, a cooling system is usually added. In most of cases, this cooling system consists of flowing air on specimen surface, as depicted in Photo 2. For more specific uses, a water-cooling can also be admitted.

One other way frequently used to cool the specimen is to stop momentary the test (intermittent loading condition). Usually, test is effectively conducted for several milliseconds and then stopped for 1 second or more. This technique is practically not admitted alone, but in complement of a cooling system introduced before.

1.2. The “frequency effect”

Ultrasonic testing method is now widely used in most of the fields where product reliability in gigacyclic regime is particularly important. In addition, regardless its very high loading frequency, ultrasonic fatigue device has other advantages. Even though price of this kind of devices is still pretty high, possibility to implement a random amplitude pattern in addition to the low maintenance cost compared to servo-hydraulic machine incites to choose this method if possible.

Nevertheless, such a huge gap of loading frequency between the usual range of 1 to 100 Hz and ultrasonic frequency of 20 kHz urges us to engage a discussion about a potential influence of loading frequency on the fatigue testing results. This is the so-called “frequency effect”.

As it will be introduced in more details in the Chapter 2, various literatures for several decades have been published about this frequency effect. However, as various kinds of other parameters can influence also fatigue properties of metallic materials, it is really difficult to isolate and indentify it.

As a general trend, if a frequency effect has been found, the *S*-*N* property at ultrasonic frequency is higher than corresponding one in the usual loading frequency range. This phenomenon is usually observed for low carbon steels. However, such a frequency effect lefts, most of the time, unseen in the case of high strength steels, for instance.

The present situation is not satisfactory. Indeed, the frequency effect needs to be more studied, in a general way, and also for typical materials where frequency effect is obvious. That is why the present doctoral thesis consists of two main studies:

(1) A general meta-synthesis based on various valuable literatures published in the latest 50 years in the field of metallic material’s fatigue, initially related or not to the subject of frequency effect. This study is introduced in Chapter 2.

(2) The effect of the loading frequency on fatigue properties of JIS S15C low carbon steel was studied by conducting fatigue tests in a wide range of frequency of 0.2 Hz to 20 kHz. Some discussions deals with phenomena related to the frequency effect. This work, due to its length, is divided into Chapters 3, 4 and 5. Chapter 3 will discuss the effect of the loading frequency in the usual frequency range, up to 140 Hz in this work. Chapter 4 will introduce the fatigue experiment results obtained at ultrasonic frequency. Some irregularities on the fatigue properties of S15C steel

at ultrasonic frequency will be pointed out. Finally, Chapter 5 will be dedicated to the observation of dislocations, which will allow us to determine the particular behavior of B.C.C. ferrite that causes the significant frequency effect of S15C steel at ultrasonic frequency.

Chapter 2. Reconfirmation and new discussions on the frequency effect of fatigue properties of metallic materials based on numerous data in literatures[ii]

2.1. General approach of this study

As already mentioned in the previous section, the aim of such a study is to give the more overall point of view possible of the loading frequency effect in fatigue properties of metallic materials. In order to catch the principle of frequency effect in the large amount of fatigue tests result available around the world, one important part consists to select the most reliable results by introducing selection criteria, which will be discussed in more details in Section 2.3.

Even though those kinds of criteria are needed in order to have a better reliability of such a study, another key point consists to take into consideration only the *S-N* curve obtained from the numerous fatigue test data. It is usually said that around 15 fatigue tests at various stress amplitudes are needed to undertake a reliable *S-N* curve. The *S-N* curve represents the line where 50% of specimens would fail before this curve and 50% after it. For the sake of simplicity, we will consider only linear and bilinear *S-N* models. By considering only *S-N* curve rather than all the data, we minimize the data recorded in 3 or 4 figures, corresponding to *S-N* curve parameters. These parameters are presented in Fig. 5.

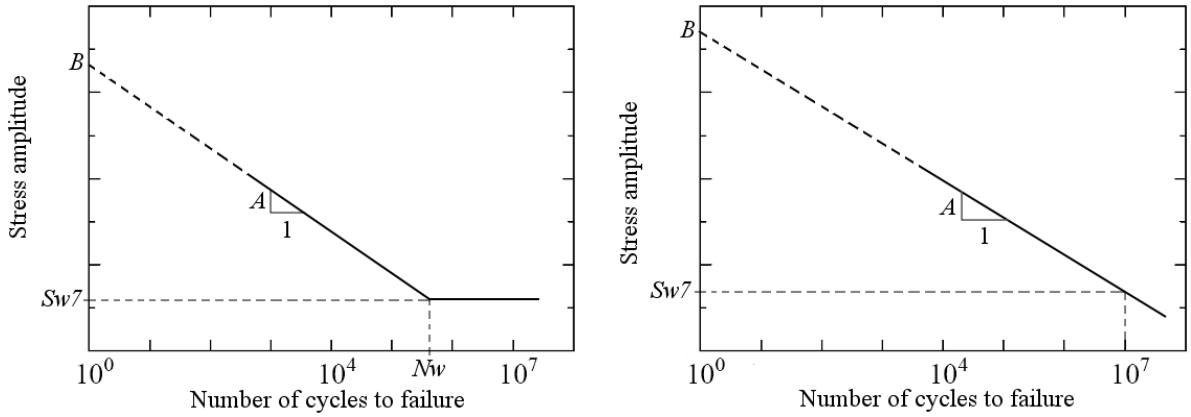

(a) Case of bilinear model **(b) Case of linear model**

Figure 5 Parameters obtained from *S-N* curves

For all selected *S-N* diagrams, the following parameters have been collected: (1) the slope of the decreasing line in absolute value, so-called "*A*"; (2) the intercept of the decreasing line with the ordinary axis in a logarithm scale, so-called "*B*"; (3) the fatigue strength at $N = 10^7$ cycles, so-called "S_w7"; and (4) the knee point cycle, so-called "N_w", in the *S-N* bilinear is more appropriate than the linear one.

For the sake of homogeneity, all the fatigue tests have been plotted again and *S-N* curves parameters have been obtained using JSMS (Society of Materials, Japan) way of calculation.

[ii] [International Journal of Materials and Structural Integrity] [To be published]© Inderscience Enterprises Ltd.

2.2 Review of several previous studies from literatures

Ultrasonic fatigue testing method has been used from the 1960's up to now. As the problem of frequency has not been solved up to now, influence of loading frequency on fatigue test results remains an issue in the field of fatigue experiments.

As a consequence, first really valuable literatures, which have been published on the frequency effect, appeared in the 1960's. Nevertheless, most of the ultrasonic data are relatively recent (from the 1990's). Now a day some new studies are still conducted in order to better grasp this particular phenomenon.

2.2.1. Literatures from 1960's

The most interesting publication from this period comes from Prof. M. Kikukawa[5] in 1965. In this literature, a comparison of fatigue results undertaken for two low carbon steels in axial loading condition (R = -1) has been made for a large range of loading frequency from 40 Hz to 100 kHz.

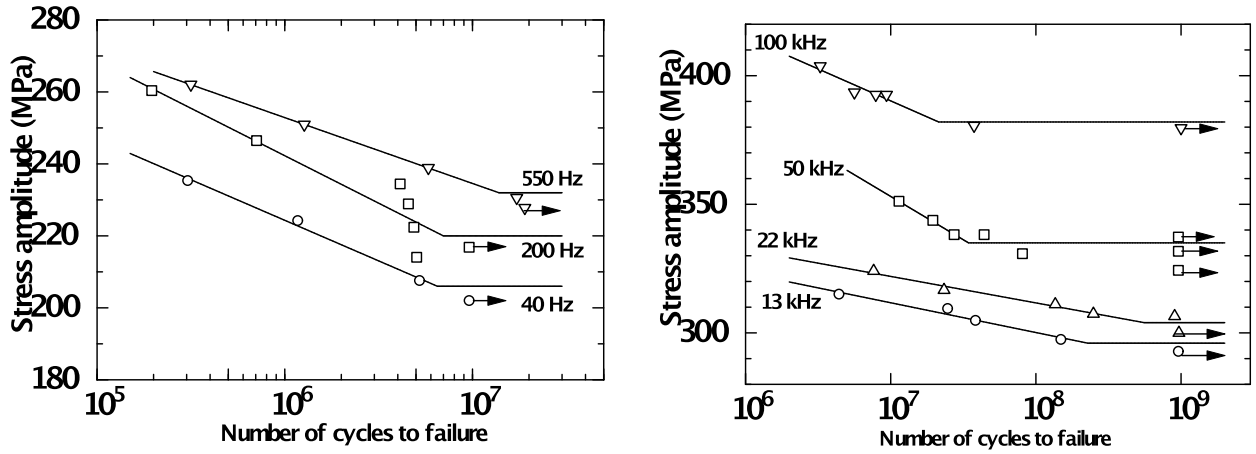

Figure 6 *S-N* diagrams from Kikukawa's study on S10C steel[5]

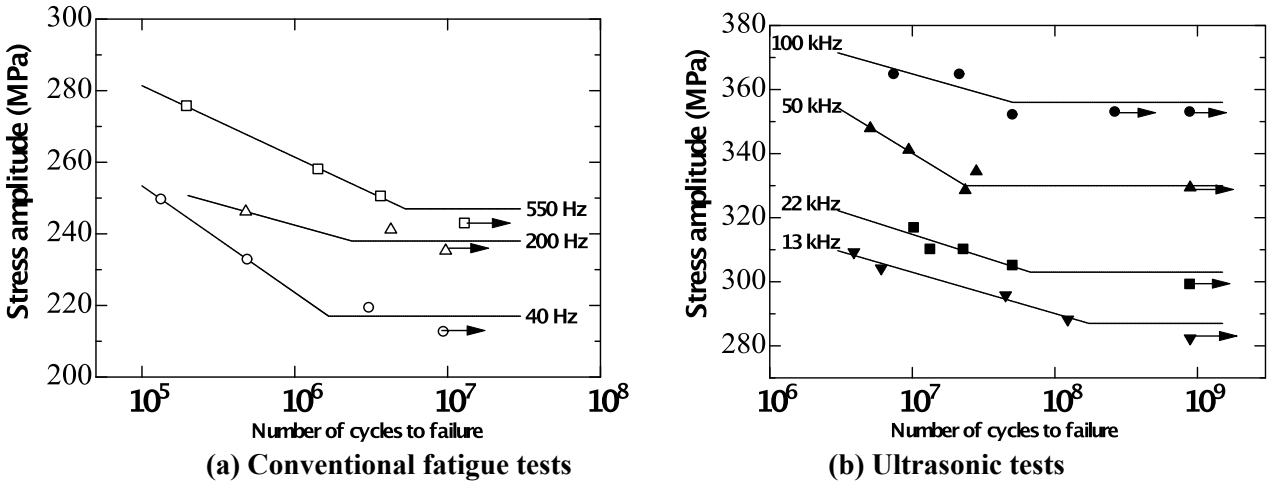

Figure 7 *S-N* diagrams from Kikukawa's study on S20C steel[5]

In addition, this literature deals with the problem of self-heating during test. Indeed, it was established that thermal stresses, from a cooling system, have a negligible influence on fatigue data. As a consequence, Kikukawa introduced a water-cooling system. A study to indentify the best coolant, paying a particular attention of the corrosion phenomenon, was also carried out. At last, a specific new system to control stress level applied on specimen has been designed.

Kikukawa have studied the S-N properties of both S10C (0.10% C) and S20C (0.20% C) carbon steels. *S-N* diagrams obtained for these two types of low carbon steel are presented in Figs. 6 and 7, respectively. Each of these figures consists of two *S-N* diagrams, which presents fatigue data for conventional tests (from 40 Hz to 550 Hz) and ultrasonic tests (from 13 kHz to 100 kHz), in (a) and (b) respectively. For both diagrams, it is clear that fatigue strength tends to increase when loading frequency is increasing.

At last, Kikukawa has confronted his own results with other results in the subject of frequency effect at that time. Figure 8 sums up this comparison. This diagram represents the evolution of the fatigue limit against the loading frequency in logarithm scale. In addition, two other curves are added to this diagram. Correspondent data come from two other literatures, written by Yamane[9] and Taira *et al.*[10]. For both literatures, loading type was not axial. Nevertheless, one can see that the general trend illustrated by Kikukawa's data is reconfirmed.

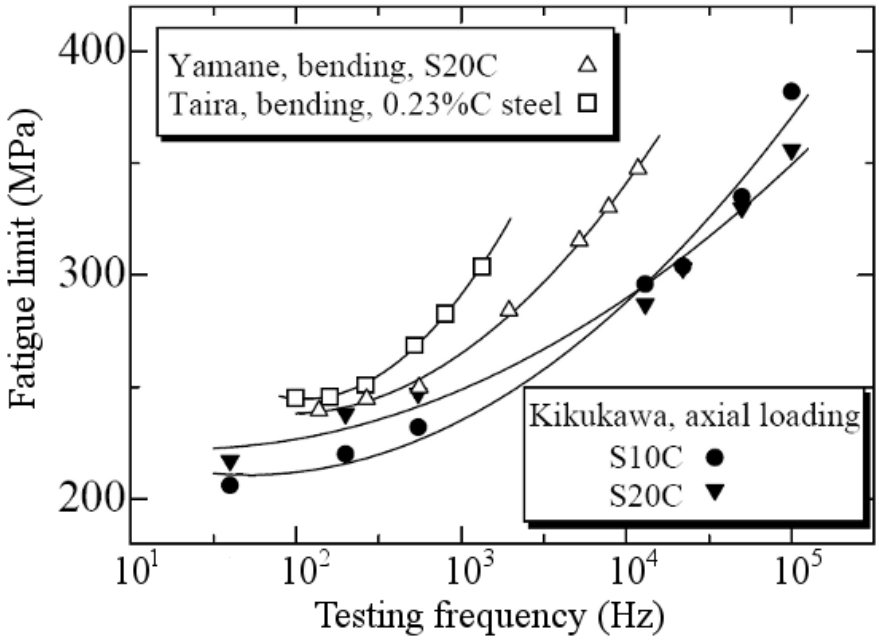

Figure 8 Fatigue limit to the loading frequency for various literatures[5]

2.2.2. Recent literatures

For the latest two decades, a lot of ultrasonic fatigue data have been published. Indeed, improvement of computer science has allowed a better accuracy on stress control. In addition, research on VHCF domain (10^8 cycles and more) has become one of the most topical issues in material fatigue testing field.

As a general trend, literatures carried out in this period point out a good agreement for both conventional and ultrasonic tests results in the domain of the high cycle fatigue (HCF). Figure 9

represents an *S-N* diagram published in by Furuya[11] in 2008. One can note see that there is a good match between ultrasonic and conventional data. In addition, the same author has published several years before (2003) another literature where conventional rotating bending fatigue tests carried out up to 10^{10} cycles has revealed similar *S-N* property to ultrasonic tests. As a consequence, for numerous researchers in the field of metallic material fatigue, the frequency effect is not significant. Indeed, it is usually said that even though some frequency effect could occur, influence of the loading frequency is negligible compared with the phenomenon of statistical dispersion of *S-N* property of metallic materials.

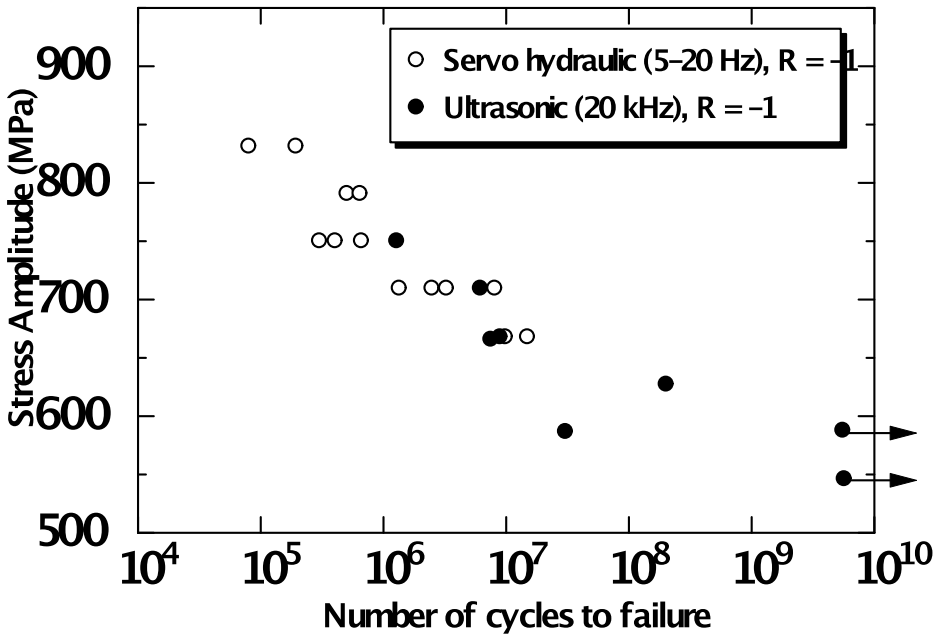

Figure 9 *S-N* diagram on a molybdenum chrome steel[11]

Nevertheless, some divergent data exist too. Figure 10 presents two *S-N* diagrams from the same literature[12], where the procedure to carry out the tests was exactly the same for both diagrams. The raw material of Ti-6Al-4V comes from 2 different companies (named here *B* and *C*) and these materials have been tempered in the same way. Figure 10 presents fatigue data results for both materials *B* and *C*, (a) and (b) diagrams, respectively.

In the one hand, Fig. 10(a) shows that ultrasonic and conventional data are in a good agreement. One the other hand, Fig. 10(b) depicts a clear frequency dependence of fatigue properties, equivalent to the observation by Kikukawa. According to the author, this fact can be explained that type of failure was not the same: we have only surface fracture for *C*; both surface and interior fracture for *B*, which is the more typical case.

Another example will be highlighted here in the case of low carbon steel. Prof. Nonaka[13] has conducted these experiments for S38C steel, designed for rail base component. Fatigue strength of this kind of steels has been measured under several loading frequencies conditions (10 Hz, 400 Hz and ultrasonic tests at 20 kHz frequency). Fatigue results are shown in Fig. 11, where ultrasonic fatigue results reveal obviously higher fatigue strength.

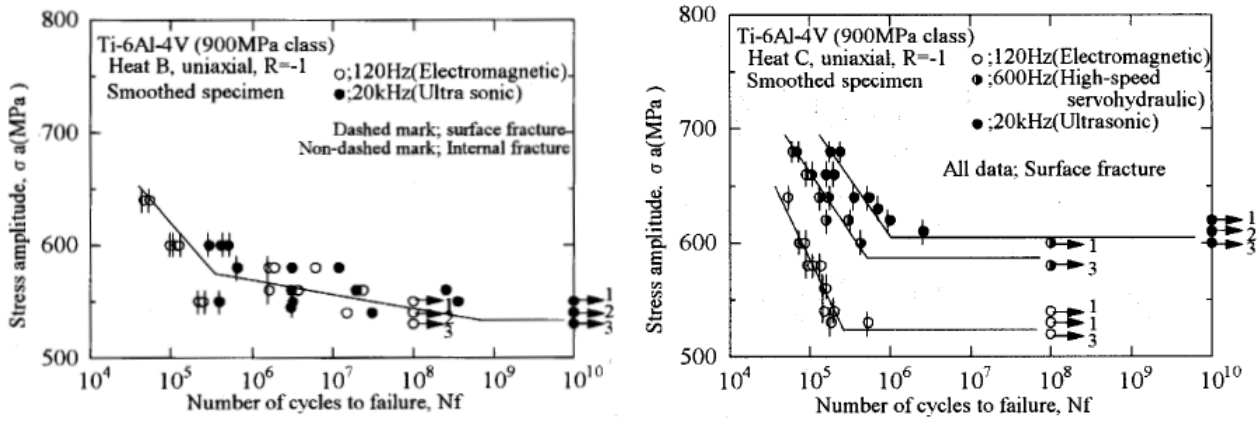

(a) Heat B **(b) Heat C**

Figure 10 *S-N* diagram from titanium alloy[12]

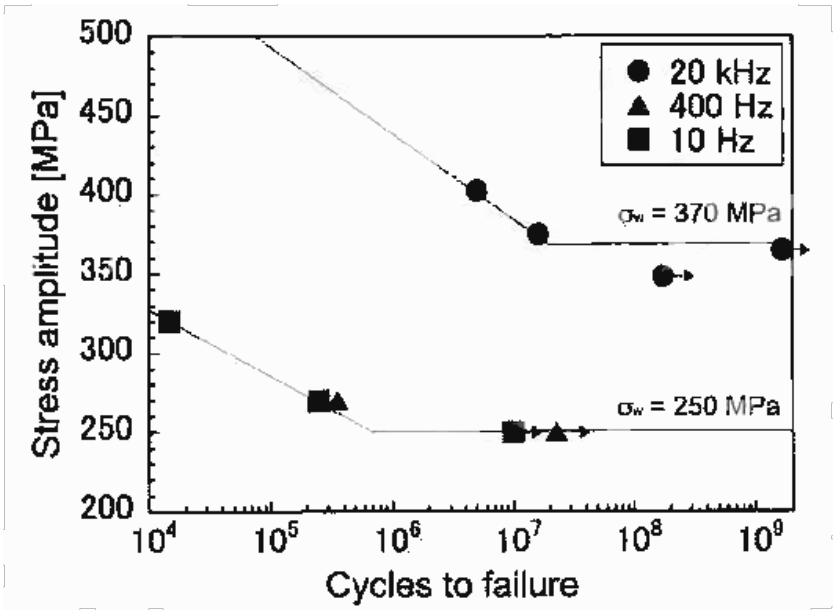

Figure 11 S38C rail steel fatigue behavior under several loading frequency[13]

Therefore, for many researchers in the field of fatigue of metallic materials, if some usual conditions are admitted, as cooling-system for instance, ultrasonic device could be used to obtain fatigue properties of a material in both HCF (from 10^4 to 10^7 cycles) and VHCF (more than 10^7 cycles) domains for most of materials. In particular, it is almost known that low carbon steels usually reveal a significant frequency effect.

However, due to some other divergences, it seems useful to undertake further discussions in the study on the frequency effect in fatigue. Thus, we have chosen to conduct a meta-synthesis to get the most overall point of view possible on this issue, as a sufficient amount of data is available now from literatures.

2.3. Explanation of the studies conducted

Based on the previous observations and discussions, as a sufficient amount of reliable fatigue tests results are available, this kind of meta-synthesis would be fruitful. Indeed, up to now, studies on the frequency effect have always been carried out with almost the same approach, which

consists of making a discussion based on *S-N* property of a similar material fatigued with conventional and ultrasonic devices.

In this Chapter 2, our approach is different. Indeed, our idea is to highlight as much as possible the presence or inexistence of the frequency effect for various kinds of metallic materials. To carry out this study, we have collected all the most reliable *S-N* data from various literatures first, and then to present these data in a way to estimate more clearly the frequency effect.

2.3.1. Direct comparison

This work represents the first step of this study. The purpose is very simple, since it consists of directly monitoring the differences of fatigue properties from conventional and ultrasonic tests. To do so, we have selected the publications where the same material has been tested at both conventional and ultrasonic frequencies with the same external conditions. For all the tests here, the stress ratio *R* is strictly -1, and tests are made in room temperature condition with a coolant system.

By this way, we have picked up about a dozen distinct literatures[5,12-22], which deal with both ferrous and non-ferrous metals. From these literatures, we have selected 21 comparisons between ultrasonic and conventional data.

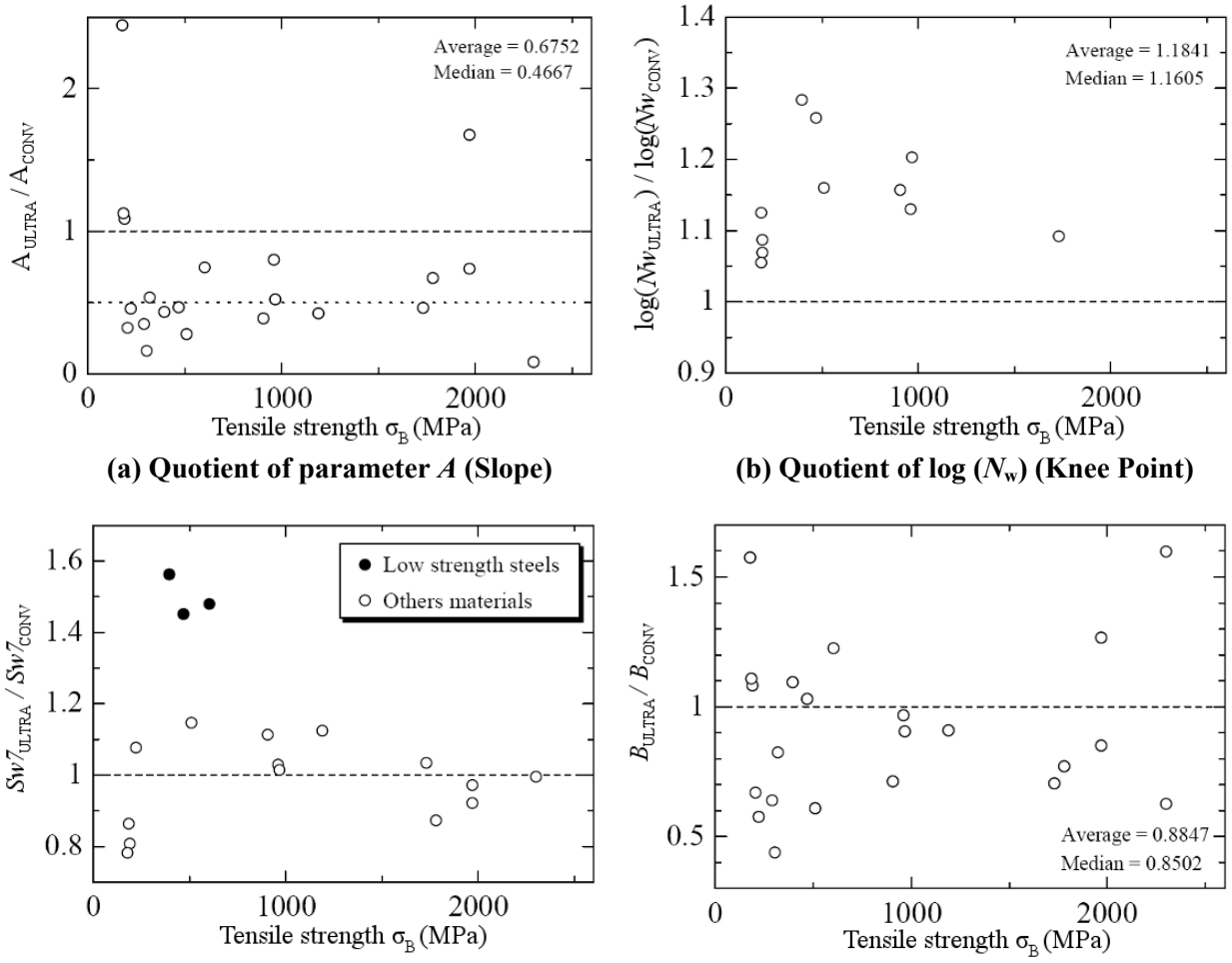

(a) Quotient of parameter *A* (Slope) **(b) Quotient of log (N_w) (Knee Point)**

(c) Quotient of S_w7 **(d) Quotient of *B* (Intercept)**

Figure 12 Direct comparison results

In the case where the corresponding literature compares more than one frequency in conventional and ultrasonic domain each, we have kept only one frequency data for each. The selection is made by taking the data with the less scatter in the case of conventional tests; the loading frequency next to 20 kHz for ultrasonic one. The *S-N* diagrams corresponding to the initial data of this work are presented in Figs_Apx 1 to 21, available in the Appendix.

To compare the data, we used bilinear or linear model if no knee point was detected as presented in Section 2.1. According to such an approach, parameters of *S-N* curves are recorded and then plotted in a way to highlight a potential frequency effect. As a reminder, the parameters selected here are: the Slope (A), the Intercept (B), the fatigue strength at 10^7 cycles (S_w7) and knee point cycle (N_w) if exists.

In the case of the direct comparison study, as the material is exactly the same between conventional and ultrasonic data, we have decided to calculate directly the quotient of these parameters to compare the data. More precisely, we have divided the parameter from ultrasonic test by the corresponding parameter from conventional test, except for knee point value, if exists, where the logarithm value was used instead in the quotient calculation.

Figure 12 presents these quotients against tensile strength of the corresponding tested material. This type of figures allows us to have a first sight of the fatigue properties for both conventional and ultrasonic tests for a various kind of metallic materials.

Comparison of parameter A, in other words the absolute value of decreasing slope of *S-N* curve, is presented in Fig. 12(a). One can see clearly that points tend to appear in the area below the value of 1. It indicates that the slope tends to be lower for ultrasonic tests compared to conventional tests. Particularly, median of this distribution is about 0.5. As a consequence, for one half of these comparisons, conventional slope is at least 2 times steeper than the corresponding ultrasonic datum.

One other particularly clear result is presented in Fig. 12(b), which deals with the comparison of knee point cycle (N_w). For *all* comparison where this calculation was available, the quotient is larger than 1. It implies that the knee point tends to appear for a larger value of cycles.

One interesting result is available in Fig. 12(c). This diagram shows the corresponding results for the parameter S_w7, the fatigue strength found at 10^7 cycles. There are here two distinct trends depending on material tested. Indeed, in a general way, it is difficult to point out an effect of the frequency as points appear around value of 1. Nevertheless, 3 points do not follow the same trend, as they appear around value of 1.5. So, the fatigue strength in these cases is 50% higher from ultrasonic testing method than conventional one. If we pay attention to these 3 points, these results are related to low carbon steels. As previously discussed in the Section 2.2, this sort of materials lets usually appear a significant frequency effect. As a conclusion, this distinct behavior is not surprising at all.

Finally, let us have a look on the last figure involved in this direct comparison study in Fig. 12(d). This figure shows the corresponding results in the case of parameter B, the intercept of decreasing line from *S-N* curves. This diagram does not highlight an effect of the frequency, as distribution points' value is around 1, with a pretty high scatter.

Thus, such a direct comparison gave some first trends particularly useful in order to advance in the study of frequency effect in metallic materials. Of course, due to the strict selection, and thus the relative low number of data selected in this study, it is impossible to conclude on the frequency effect at this point. However, this work had two advantages. It does not require a long time to

conduct it, and it was an important step to have some clear ideas on the phenomena at stake when studying the frequency effect in metallic materials.

2.3.2. Overview analysis

2.3.2.1. Objectives of this overview analysis

Previous study so-called "direct comparison" has several advantages but reveals a decisive drawback, which is the strict limitation of data available. Indeed, in order to select a literature in the direct comparison, exactly the same material had to be fatigued at both conventional and ultrasonic frequencies. However, a lot of literatures, which deals with ultrasonic fatigue test results, do not undertake such an experiment. For instance, a lot of literatures in this field just compare ultrasonic results obtained with results from an almost similar material at conventional frequency from another literature, for the sake of reference. In such a case, of course, those data are not suitable to be included in the direct comparison study.

It implies that the amount of data selected is really tiny compared the large amount of reliable data available is numerous literatures. The objective of the following "overview analysis" is to better grasp the frequency effect in metallic material fatigue by gathering the largest as possible amount of data.

2.3.2.2. Approach of overview analysis

Nevertheless, to gather numerous data from different literatures in a meaningful way is not as simple as it may see. A lot of other parameters have to be considered in order to share all these data without distortion of the fatigue results. As a result, we have to select carefully the fatigue tests, which follow strict experimental conditions to obtain meaningful results. In this study, there are three populations: ultrasonic tests (always axial), rotating bending conventional tests and axial conventional tests. For each population, the criteria of selection are mentioned below:

- Ultrasonic tests: R = -1, specimen stress factor below 1.2, at room temperature, in air, with adding of a cooling system or at least under intermittent loading condition to cool the specimen. Most of these tests are performed at a loading frequency of 20 kHz.
- Rotating bending conventional tests: R = -1, specimen stress factor below 1.2, test in air, at room temperature.
- Axial conventional tests: exactly the same than rotating bending. Servo-hydraulic machines usually perform these conventional tests. In addition some tests are undertaken by electro-magnetic machine. Besides, the most of tests selected here are performed in a frequency range from 1 to 100 Hz, even though maximum frequency is 600 Hz.

In addition, tests on specimens where specific treatments were applied have not been selected in this study. Indeed, this sort of treatments has some special effects on the fatigue properties. Here is a list of such well-known phenomena, which can influence the fatigue strength results:

- Size effect: as specimen size increases, fatigue strength tends to decrease. This phenomenon has been also reviewed in the case of ultrasonic method by Furuya[11]. Consequently, *S-N* data related to specimens with a 10mm-diameter or higher tested portion do not have been taken into consideration here.

- Residual stress effect: a compressive or tensile residual stress profile can change drastically the fatigue properties of a metallic material. Thus, fatigue results obtained from specimens with a specific residual stress profile have not been taken into consideration.
- Some authors, as Bathias[23], has interpreted some isolated divergences between ultrasonic and conventional results by special materials' microstructure. The approach of overview analysis, which collects a lot of fatigue data minimize the influence of such isolated examples.

In addition, in order to verify the validity of *S-N* curves selected, we have checked that almost all *S-N* data selected from conventional data are in accordance with the stress level range verification in the JSMS Standard given by Eq. (3), where $(\sigma_a)_{MAX}$ and $(\sigma_a)_{MIN}$ are maximum and minimum stress amplitude in a series of *S-N* data, respectively. If such a criteria is not observed, the fatigue life range in the series of fatigue tests should be within 1.5 decade at least. Conventional *S-N* data are usually measured up to $N = 10^7$ cycles. In the case of ultrasonic *S-N* data, even though the fatigue life range tested is larger than 3 decades, the criterion introduced in Eq. (3) is sometimes not verified. Even in such a case, it was assumed that corresponding *S-N* data are reliable.

$$\frac{(\sigma_a)_{MAX}}{(\sigma_a)_{MIN}} \geq 1.2 \tag{3}$$

As the objective of such a study is to get an overall point of view of the frequency effect, it is obvious that structural steel material has to be studied. Besides, there are numerous data available on steels, so results are expected to be fruitful. In addition, such an approach was conducted also in the case of aluminum alloys, as amount of fatigue data in literatures are sufficient. Results and discussions will be presented in a distinct section for each material.

Most of references used in this overview analysis are listed in Table 1, for both structural steels and aluminum alloys. A lot of conventional fatigue records have been extracted from JSMS Database called "Fatigue Strength of Metallic Materials" published by Elsevier and JSMS in 1996[24]. At last, some fatigue data come from NIMS data sheet[25].

Results directly taken from this overview analysis are again based on the *S-N* curve's parameters (A, B, N_w and S_w7) changes. Results are presented in the way of each parameter evolution against tensile strength of the corresponding material.

Table 1 List of literatures used for overview analysis

	Authors	Publisher	Year	pp.
Steels	H. Koganei et *al.*	JSMS Vol.24(263)	1975	753-760
	M. Kikukawa et *al.*	J Basic Eng.-T. ASME D, Vol.87	1965	857-864
	Y. Murakami et *al.*	Int. J. Fatigue, Vol.16(9)	1998	661-667
	S. Setowaki et *al.*	Proceedings VHCF-5	2011	153-158
	N. Miyamoto et *al.*	Trans. Jpn. Soc. Mech., Ser.A, Vol.70(696)	2004	1080-1086
	Z.G. Yang et *al.*	Acta Mater., Vol.52(18)	2004	5235-5241
	T. Abe et *al.*	Fatigue Fract. Engng. Mater. Struct., Vol.27(2)	2004	159-167
	Y. Furuya et *al.*	Trans. Jpn. Soc. Mech., Ser.A, Vol.71	2005	1201-1206
	Y. Furuya	Trans. Jpn. Soc. Mech., Ser.A, Vol.73	2007	957-965
	Y. Furuya et *al.*	Fatigue Fract. Engng. Mater. Struct, Vol.26(7)	2003	641-645
	Y. D. Li et *al.*	Material Science and Engineering A, Vol.489(1-2)	2008	373-379
	Y.B. Liu et *al.*	Materials and Engineering A, Vol.497(1-2)	2008	408-415
	K. Yamaguchi et *al.*	Sci. Technl. Adv. Mat., Vol.8(7-8)	2007	545-551
	J.M. Zhang et *al.*	Int. J. Fatigue, Vol.29(4)	2007	765-771
	Y. Nie et *al.*	Acta Metallurgica sinica, Vol.43(10)	2007	1031-1036
	Q.Y. Wang et *al.*	Fatigue Fract. Engng. Mater. Struct., Vol.22(8)	1999	673-677
	I. Marines et *al.*	Int. J. Fatigue, Vol.25(9-11)	2003	1037-1046
	F. Novy et *al.*	Material and Engineering A, Vol.462(1-2)	2007	189-192
	T. Sakai et *al.*	Fatigue Fract. Engng. Mater. Struct., Vol.25	2002	765-773
	K. Tanaka et *al.*	Proceeding VHCF-3	2003	56-67
	K. Fukaura et *al.*	Metallurgical and Materials Transactions, Vol.35A(4)	2004	1289-1300
	C.R. Sohar et *al.*	Int. J. Fatigue, Vol.30(7)	2008	1137-1149
	C.R. Sohar et *al.*	Metal-powder.net, Elsevier	Feb. 2009	12-17
Aluminum alloys	N. Kawagoishi et *al.*	Trans. Jpn. Soc. Mech., SerA, Vol.70(696)	2004	1139-1145
	N. Kawagoishi et *al.*	Trans. Jpn. Soc. Mech., SerA, Vol.72(721)	2006	1356-1363
	K. Yamada et *al.*	Trans. Jpn. Soc. Mech., SerA, Vol.72(717)	2006	749-756
	H. Mayer	Int. J. Fatigue, Vol.28(11)	2006	1446-1455
	X. Zhu et *al.*	Int. J. Fatigue, Vol.28(11)	2006	1566-1571
	Q.Y. Wang	Int. J. Fatigue, Vol.28(11)	2006	1572-1576
	E. Bayraktar et *al.*	Int. J. Fatigue, Vol.28(11)	2006	1590-1602
	C.C. Engler-Pinto et *al.*	Proceedings VHCF-4	2007	421-435

2.3.2.3. Results found for steels

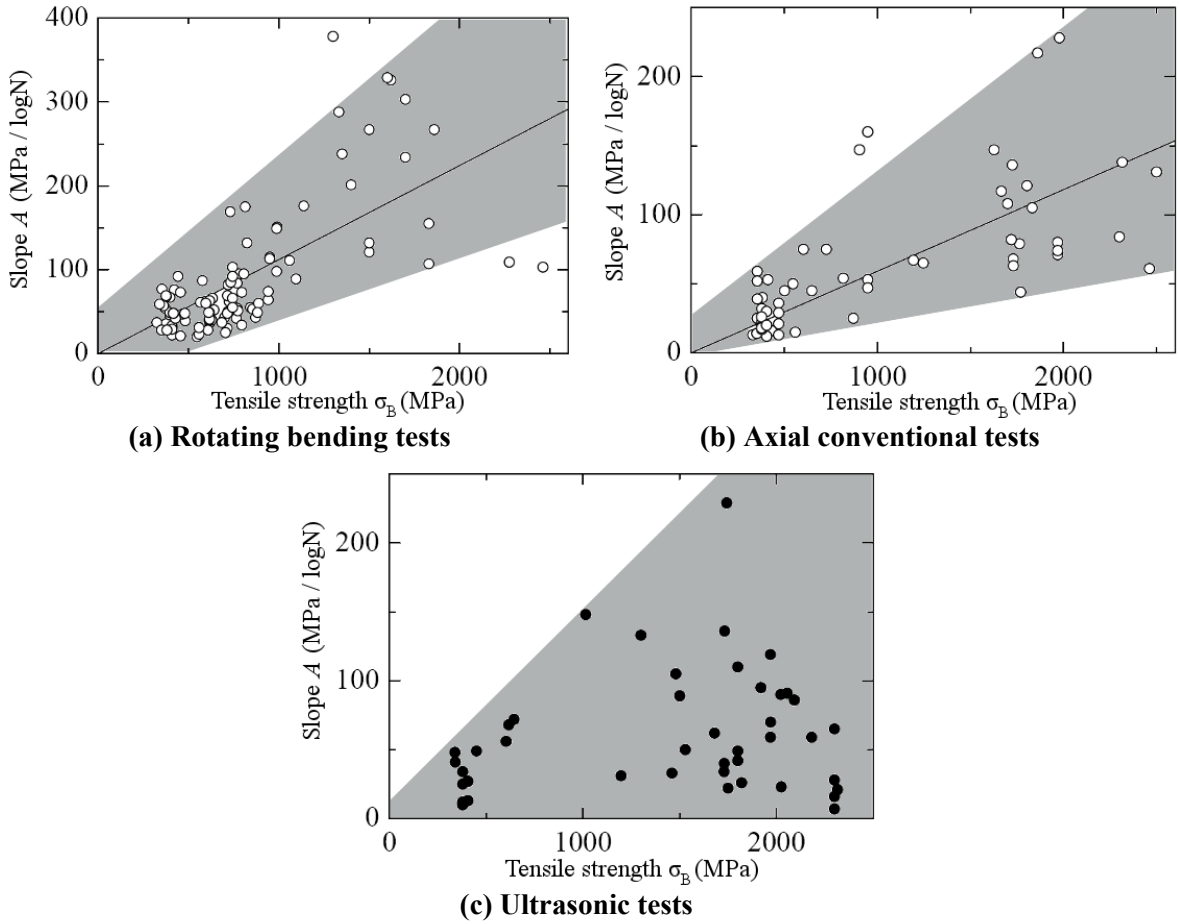

Figure 13 Strength dependence of slope (parameter *A*)

All discussions done in this section are based on the results given in Figs. 13 and 14. These figures show the behaviors of different parameters of the *S-N* curves selected. Indeed, Fig. 13 deals with the parameter *A*, in other words, the absolute value of decreasing slope. This figure consists of three different diagrams, which present the results in the case of conventional rotating bending tests, conventional axial tests and ultrasonic tests, in (a), (b) and (c), respectively.

In order to highlight the area of distribution of points in each diagram, a shadow has been included. It thus makes the result almost obvious. In the case of conventional fatigue tests Figs. 13(a) and (b), in both rotating bending and axial stressing conditions, one can see a rough linear relation between the slope and tensile strength of tested material. Indeed, linear regressions plotted in a solid line hit relatively high correlation coefficients *r*, compared to the number of points: $r = 0.684$ and $r = 0.678$ for rotating bending and axial loading respectively.

However, such a regression cannot be found in the case ultrasonic loading method, in Fig. 13(c). For the sake of comparison, a similar calculation gives a correlation coefficient of $r = 0.223$. Thus, clear regression does not exist in the case of ultrasonic tests.

Let us now have a look on the other parameters. Each diagram shown in Fig. 14 is dealing with one remaining parameter, the knee point cycle N_w, the intercept *B* and fatigue strength at 10^7 cycles S_w7, in (a), (b) and (c), respectively. From now, all selected *S-N* results are taken only from axial loading tests, *i.e.* no more rotating bending tests results are taken into consideration.

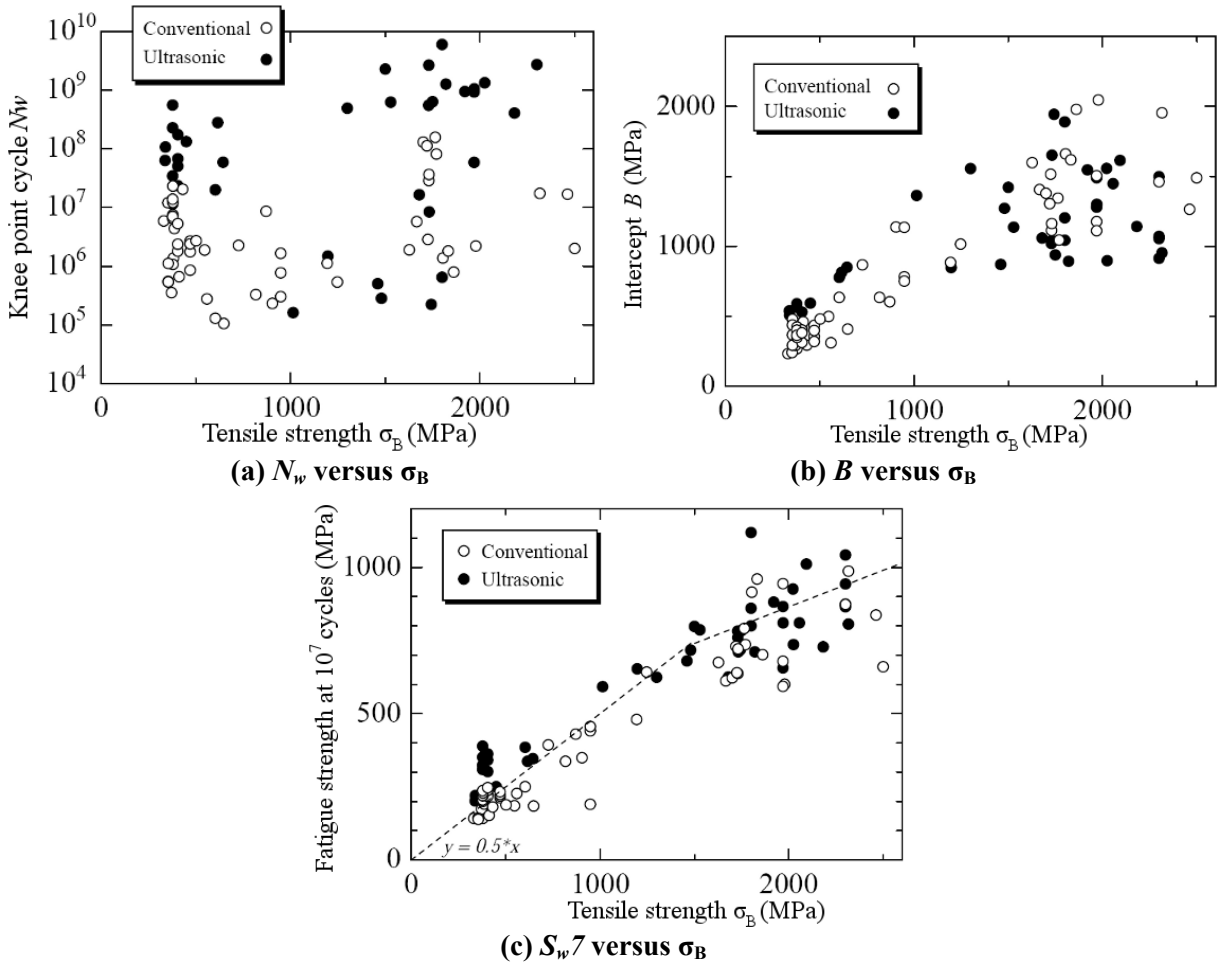

Figure 14 Strength dependence of other parameters for steels under axial loading tests

In Fig. 14(a), one can see an interesting point. Knee point cycles appear mainly in the long life region of N > 10^7 cycles. Nevertheless, some data points are found in the usual life region similar to the conventional tests. On the one hand in the case of low strength steels of σ_B < 700 MPa, ultrasonic knee points appear in the long life region only. On the other hand, for high strength steels of σ_B > 1000 MPa, knee point cycle tends to split into long life region and number close to value from conventional knee points. Diagram in Fig. 14(b) do not highlight an influence of the loading frequency on the parameter *B*, intercept of the decreasing slope. Indeed, distributions of points for both ultrasonic and conventional results are similar.

Now, let us have a look on Fig. 14(c), where the parameter S_w7 is studied. In this diagram, one can see pretty easily that general trend of fatigue strength at 10^7 cycles for both testing methods studied are in good correlation. However, such a general trend is not verified in the case of low strength steels. This is not surprising to detect such a particular case, as low strength steels are usually reported to be particularly sensitive to the loading frequency, as discussed before. In addition, one can note that S_w7 is almost one half of tensile strength σ_B, except for high strength steels, where this parameter is slightly lower. Such an observation is a typical common result of fatigue strength of steels, under general conditions selected here (tests in air, at room temperature, with a stress ratio *R* = -1).

Let us now make a discussion in order to gather all the results introduced previously. Before undertaken such a work, this discussion will not take into consideration the particular case of low strength steels. Indeed, this is less interesting for this overview analysis. Accordingly, the discussion here will be focused on middle and high strength steels.

Based on Figs. 13 and 14, overview behavior of different parameters related to *S-N* curve can be easily analyzed. Parameters A and N_w tend to be sensitive to the loading frequency. This is particularly obvious for slope parameter A, as shown in Fig. 13. Slope tends to be steeper for conventional tests, compared to ultrasonic one. In addition, knee point cycle from ultrasonic results tends to generally appear at a larger number of cycles, and most of the time after $N = 10^7$ cycles. However, Figs. 14(b) and (c) highlight a different behavior. Obviously, distributions from both testing methods are in a good agreement, as low strength steels are not taken into consideration here. As a result, parameters B and S_w7 are not sensitive to the frequency.

One additional criterion has been admitted in order to verify the validity of *S-N* data selected, particularly from ultrasonic testing method. Let us assume that N_0 is the minimum life datum among a series of *S-N* data. Then, this new criterion is: $N_0 < 3\times10^6$. Hopefully, all *S-N* data already selected for steels are following this new criterion. Thus, this criterion does not have any effect on the discussions already conducted in the case of steels.

According to the summary of parameters' behavior, a general model of *S-N* curves for both testing methods can be plotted, in Fig. 15. This diagram presents a pair of scheme *S-N* curves representing fatigue properties under conventional and ultrasonic loading frequency. As one can see, intercept B, and fatigue strength at 10^7 cycles S_w7 are exactly the same for both *S-N* curves. However, slope of conventional curve is steeper. As a result, conventional *S-N* curve is represented by a bilinear model, whereas ultrasonic model follows a linear model. As a consequence, ultrasonic fatigue strength is generally higher than conventional one in the fatigue life region before 10^7 cycles, usually called long life region. Besides, the highest fatigue strength difference takes place at the number of cycles corresponding to the knee point from conventional *S-N* model. This difference, indicated by an arrow in Fig. 15, is hereafter so-called "GAP".

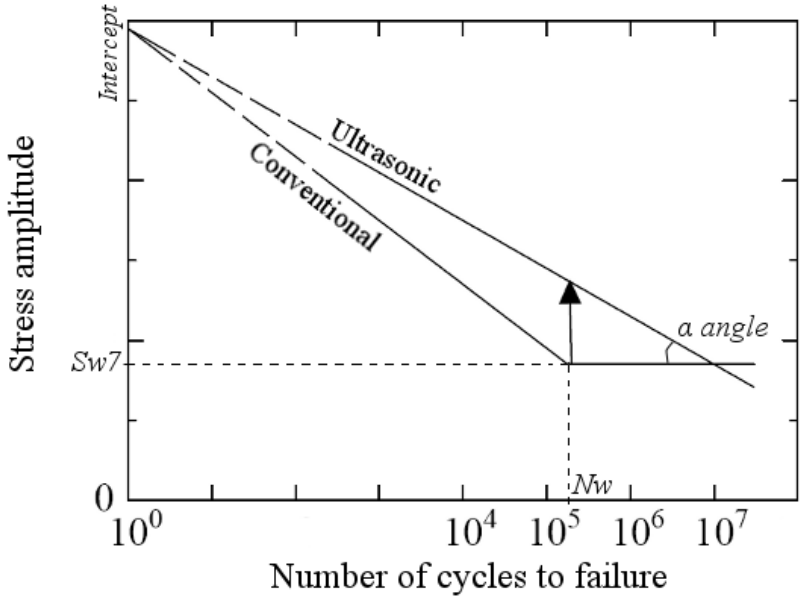

Figure 15 General model for steels

In order to carry out a quick calculation of this GAP, another condition is needed. Such a condition is given by the slope ratio q_s, defined in Eq. (4), and already introduced in the direct comparison study (Section 2.3.1). This value of q_s has a large scatter, according to the distributions presented in Figs. 13(b) and (c). Indeed, ultrasonic slope A_{ULTRA} data do not follow a linear regression with the tensile strength σ_B, whereas conventional slope A_{CONV} data are correlated with the tensile strength. Nevertheless, in order to get a value of q_s, linear regression was tentatively performed for ultrasonic data for the sake of reference. Thus, the value of 0.65 was obtained as q_s.

$$q_s = \frac{A_{ULTRA}}{A_{CONV}} \tag{4}$$

We can now make the calculation of *GAP*. By definition, we have:

$$\tan\alpha = A_{ULTRA} \quad \text{and} \quad \tan\alpha = \frac{GAP}{7 - \log Nw}$$

Thus, (5)

In addition:

$$B_{ULTRA} = S_w 7 + 7 \times A_{ULTRA}$$
$$B_{CONV} = S_w 7 + \log Nw \times A_{CONV}$$

Thus,

$$\log Nw = 7q_s \tag{6}$$

From Eqs. (5) and (6), we obtain Eq. (7)

(7)

A linear correlation between A_{CONV} and material's tensile strength σ_B is shown in Fig. 13(b). As a consequence, we are able to estimate *GAP* in correlation with material's tensile strength according to Eq. (7). Numerical application gives us a value of *GAP* equal to approximately 9% of tensile strength, *i.e.* potentially 18% of fatigue strength at 10^7 cycles, if we consider typical results of steels' fatigue behavior already verified here.

As a conclusion, based on this general model, a significant frequency effect exists for steels in the high cycle fatigue region, even for high strength steels. However, assumption of q_s equal to 0.65 is not verified widely by steels according to Fig. 13, and presents thus a large scatter. So, this value is only a rough average. Nevertheless, this general model is supposed to be useful to compare the fatigue properties in the high cycle fatigue regime.

2.3.2.4. Results found for aluminum alloys

Similar overview analysis has been undertaken in the case of aluminum alloys. Nevertheless, a typical fatigue property difference between structural steels and aluminum alloys

has to be pointed out first. Indeed, aluminum alloys do not usually reveal a knee point cycle on its *S-N* properties. As a consequence, all *S-N* models used in this section are following the linear model introduced in Fig. 5(b).

General behaviors of parameters A, B and S_w7 in the case of aluminum alloys are depicted in Fig. 16, in (a), (b) and (c), respectively. Again, all the corresponding data deal with only axial loading fatigue tests, under conventional and ultrasonic methods.

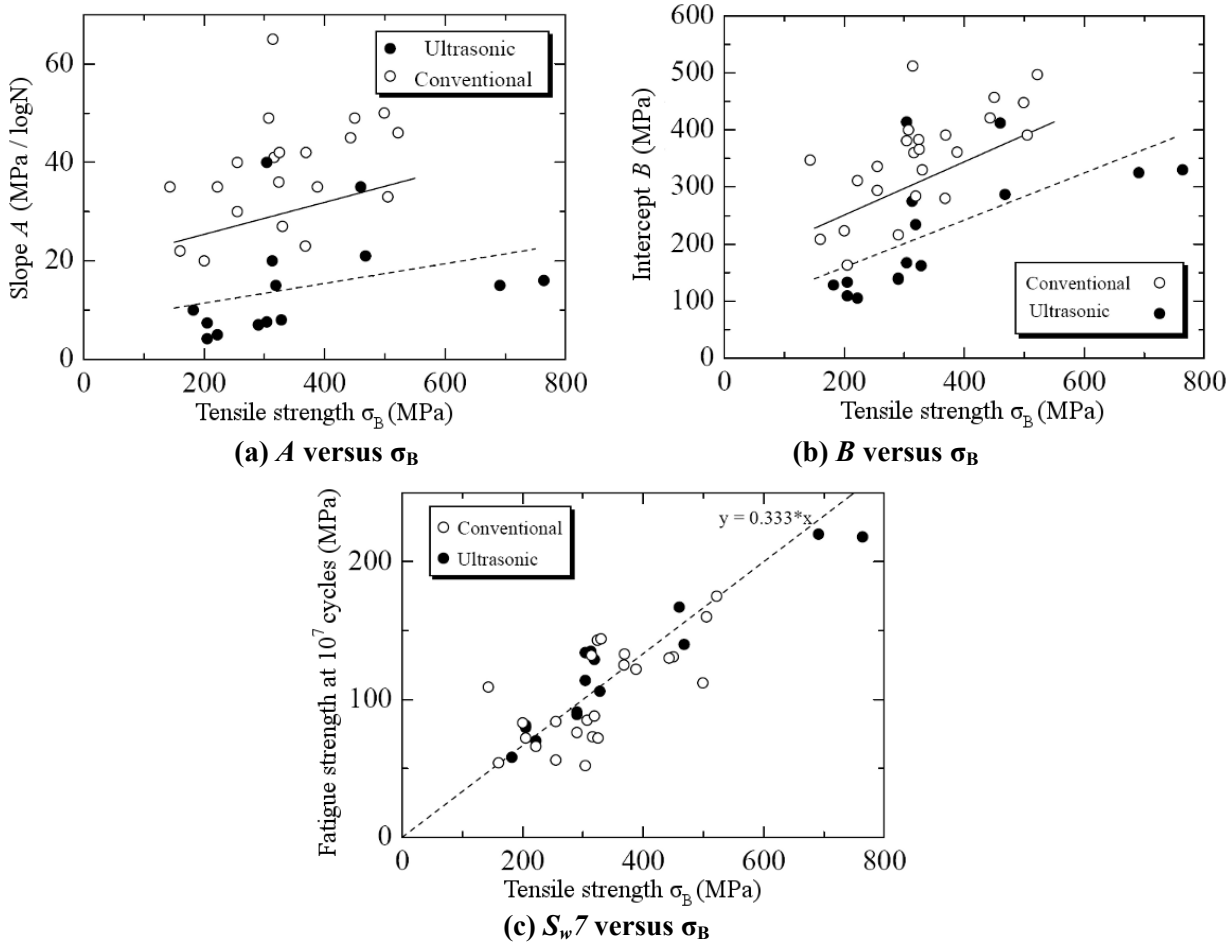

(a) A versus σ_B **(b) B versus σ_B**

(c) S_w7 versus σ_B

Figure 16 Strength dependence of parameters for aluminum alloys under axial loading

Let us make a discussion about diagram included in Fig. 16. Parameter A, the slope of decreasing linear *S-N* model, is again generally steeper for conventional test than ultrasonic one. Solid line corresponds to regression of conventional data distribution, whereas dashed line is the regression of ultrasonic data distribution. Correlation coefficient hit values of 0.360 and 0.320 for respective regressions.

A look at Fig. 16(b) let appear a similar general trend with Fig. 16(a). It indicates that conventional data have generally a higher intercept value B than ultrasonic one. However, regressions found for both distributions are much reliable, as coefficient correlation reach 0.676 and 0.652 for conventional and ultrasonic data, respectively.

At last, diagram which deals with fatigue strength at 10^7 cycles S_w7, in Fig. 16(c), do not highlight an obvious difference between ultrasonic and conventional data results. In addition, this diagram points out that S_w7 is almost one third of tensile strength σ_B. This fact has been often reported for aluminum alloys by some researchers[26].

As general behavior of parameters from *S-N* curve has been introduced, let us now make a discussion based on these results. As already mentioned in the previous section about structural steel study, the additional criterion has been accepted in order to verify validity of selected *S-N* data in the fatigue region $N_f < 10^7$ cycles. Three out of fifteen ultrasonic *S-N* data do not meet with this criterion, as the *S-N* data presented in the Fig_Apx 20. Such a removal does not have a significant effect on results presented before. Of course, aluminum alloys usually reveal *S-N* linear models. In addition, parameters *A* and *B* seem to be sensitive to the loading frequency, as conventional distribution values are higher than corresponding ultrasonic one.

Let us now pay a particular attention to the variation of fatigue strength of aluminum alloys. We will make a focus on the fatigue strength at three different stages included in the high cycle fatigue region, at $N = 10^5$, at $N = 10^6$ and $N = 10^7$ cycles. Some ultrasonic data selected do not have available data in the short life region. In such a case, the *S-N* curve has been extrapolated from around $N = 10^6$ cycles up to $N = 10^5$ cycles. Strength parameters S_w5, S_w6 and S_w7 thus obtained are depicted as a function of tensile strength in Fig. 17. All diagrams presented in this figure include linear regression and its correlation coefficients for both ultrasonic and conventional results. One can see relatively high coefficient values obtained. It implies a reliable strength dependence of each parameter.

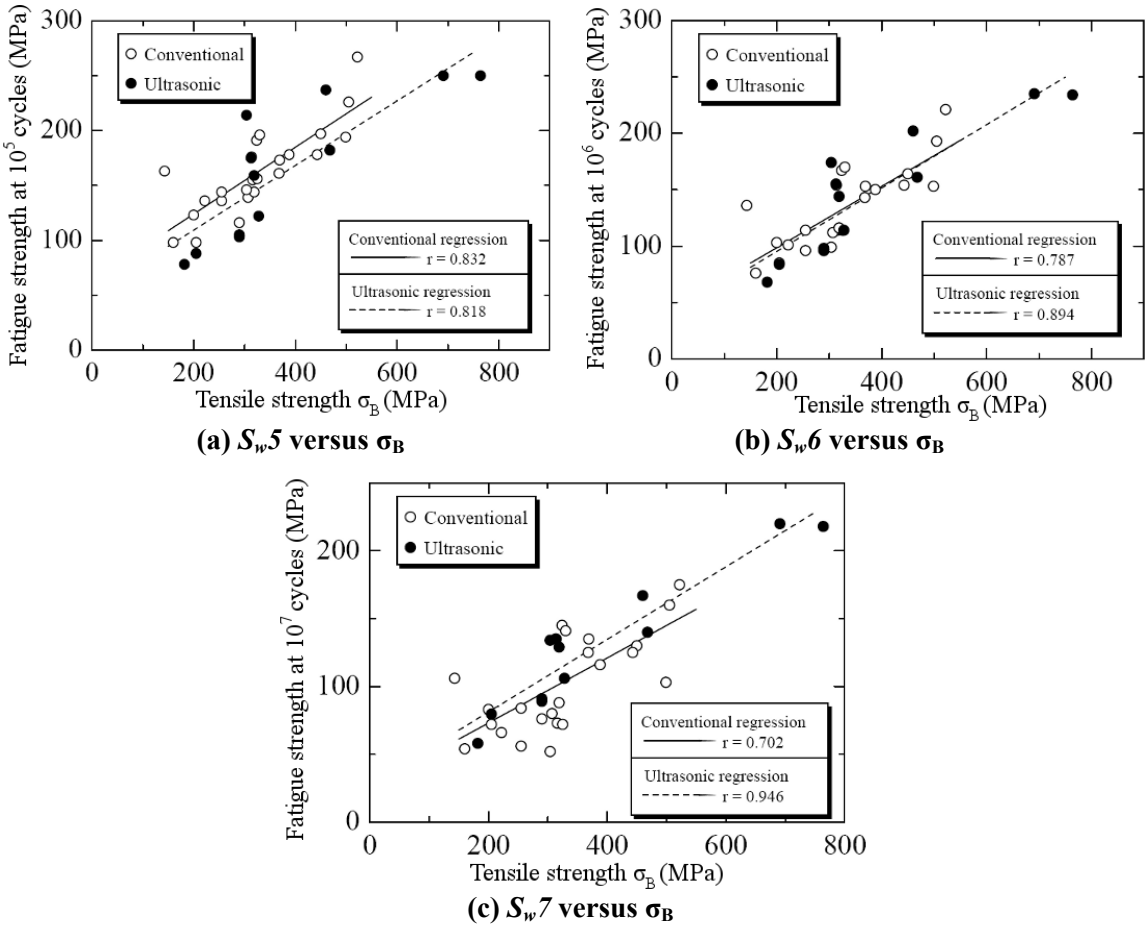

Figure 17 Fatigue strength in the high cycle regime for aluminum alloys under axial loading

Figure 17(a) presents two parallel linear regressions with a slight difference of fatigue strength. Based on both regression lines, S_w5 from ultrasonic tests is approximately 15 MPa lower

than conventional one. Figure 17(b), which depicts fatigue strength at 10^6 cycles, reveals almost the same regression line. So, we can assess that S_w6 is equivalent for both conventional and ultrasonic tests. In Fig. 17(c), regression line from ultrasonic tests is found now to be slightly higher than conventional one. As the regression lines are not really parallel in this case, difference of S_w7 tends to increase with an increase of the strength level. Such a difference is within a range of 8-16 MPa in the data range. It is noted that this difference is roughly comparable with the difference of S_w5 in Fig. 17(a).

Thus, a general model can also be undertaken in the case of aluminum alloys to highlight the frequency effect on these materials. This model is presented in Fig. 18. Accordingly to the results found from Fig. 17(b), fatigue strength at $N = 10^6$ cycles is the same for conventional and ultrasonic tests. However, S_w5 from conventional method is higher than ultrasonic one, whereas ultrasonic S_w7 is higher than conventional one, as seen in Figs. 17(a) and (c).

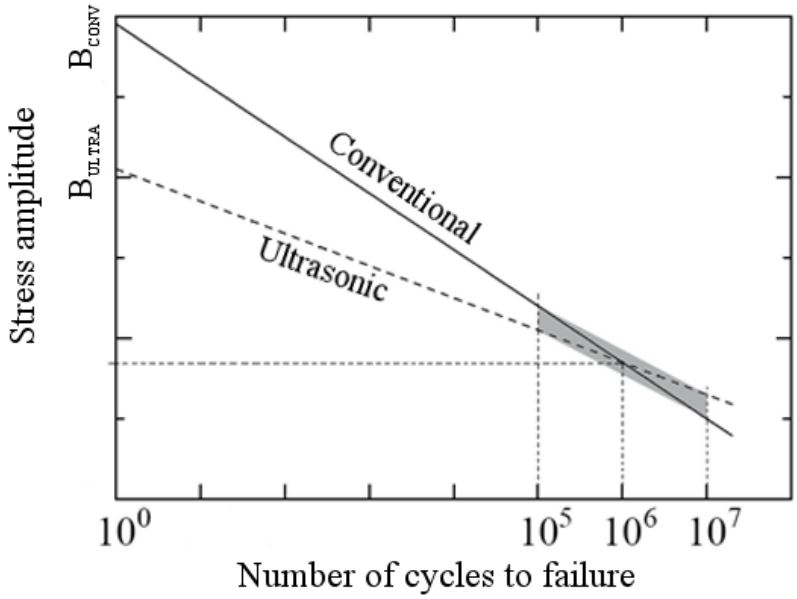

Figure 18 General model for aluminum alloys

Based on the values of fatigue strength differences at $N = 10^5$ and $N = 10^7$ cycles mentioned before, let us assume a numerical value of 15 MPa for both. As a result, one can estimate numerically the difference value of interception B between conventional and ultrasonic S-N models:

$$B_{CONV} - B_{ULTRA} = 90 \ MPa \tag{8}$$

Let us now moving back to the general behavior of intercept B in the case of aluminum alloys, presented in Fig. 16(b). This diagram depicts a difference of intercept B between 90 and 100 MPa for a wide range of tensile strength from σ_B = 150 MPa to σ_B = 550 MPa. This result is in correlation with the value found in Eq. (8). Such a result indicates that the general model presented in Fig. 18 is reasonable to compare fatigue behaviors in the high cycle fatigue regime from conventional and ultrasonic testing methods, as an attempt.

2.4. Conclusion

The work presented in this Chapter 2 of this report deals with a general overview of frequency effect on the fatigue behavior based on results from numerous literatures focused on structural steels and aluminum alloys. Bilinear *S-N* model or linear *S-N* model has been used in order to assess fatigue properties in the usual frequency and the ultrasonic frequency. The main results regarding frequency effect on fatigue properties are summarized as follows;

(1) For both steels and aluminum alloys, frequency has a clear effect on slope *A* such that the parameter in the ultrasonic frequency is significantly lower than in the usual frequency. In addition, if the *S-N* properties follow a bilinear model in structural steels, knee point cycles (N_w) for ultrasonic fatigue data tends to appear at the number of cycles larger than conventional tests results in the case of low strength steels, but the value of N_w tends to split into high value group and usual value group close to the conventional test results for high strength steel steels.

(2) Fatigue strength at 10^7 cycles is not affected by the testing frequency, for steels, except for low strength steels. For this type of steels, it is usually seen that the fatigue limit tends to increase under ultrasonic testing method.

(3) Intercept *B* parameter is not influenced by the testing frequency for steels, whereas *B* in the conventional frequency tends to be larger than the value in ultrasonic frequency in case of aluminum alloys.

(4) General model related to steels indicates a fatigue strength gap between conventional and ultrasonic methods in the high cycle fatigue region. Indeed, maximum difference value in this region, so-called *GAP*, represents potentially 18% of the fatigue limit. In the case of aluminum alloys, even though conventional and ultrasonic *S-N* models are not strictly the same, general model reveals only a slight difference on the fatigue behaviors, in the high cycle fatigue regime.

Damping characteristics and microscopic behaviour of dislocation motion are fundamentally important for the frequency effect of the fatigue property. However, such an aspect was not clear from a series of literatures in the present paper unfortunately.

Chapter 3. Effect of the loading frequency on fatigue properties of JIS S15C low carbon steel in the range of 0.2 to 140 Hz[iii]

Completion of the work presented in Chapter 2 deals with an overview analysis of the frequency effect of various kinds of metallic materials. It has revealed some interesting points. One of these points is the high frequency sensitivity of *S-N* properties of low carbon steels. As this kind of steels was not discussed in the previous work, it seems particularly fruitful to focus a study on it. In addition, accordingly to the literatures related to such a study, loading frequency effect is rather obvious. As a consequence, it seems sensible to detect the origin(s) of the frequency effect more easily.

3.1. Introduction of fatigue properties study of JIS S15C steel

The work presented in this Chapter 3 consists of an overall fatigue property study of JIS S15C low carbon steel (0.15 %C) in the loading frequency range from 0.2 to 140 Hz, thus excluding the ultrasonic tests. The final purpose of such a first step is to reconfirm a frequency effect, and in that case to indentify also its reasons.

As a consequence, in order to discuss on the reasons of the frequency effect, the present study involves not only fatigue tests results, but also a lot more other experiments. List of these experiments is presented in the next Section 3.2.

3.2. Experimental procedures

3.2.1. Raw material

Table 2 S15C chemical composition (mass %)

C	Si	Mn	Cu	Ni	Cr	Fe
0.15	0.21	0.40	0.02	0.02	0.15	*Re*

Table 3 Mechanical properties of S15C steel

Mechanical properties	Value
Lower yield stress (MPa)	273
Tensile strength (MPa)	441
Young modulus (GPa)	207
Elongation (%)	40.2
Reduction of area (%)	65.8
Vickers hardness (HV)	161

[iii] [International Journal of Fatigue][In press]© Elsevier Ltd.

Raw material in the present study is extracted from JIS S15C steel hot-rolled bar with a diameter of 30 mm. Chemical composition and general mechanical properties are indicated in Tables 2 and 3, respectively. In addition, Fig. 19 presents the microstructure of S15C steel. One can clearly see a usual ferritic and pearlitic structure. Besides, pearlite grains have a linear arrangement in the same direction of the rolling condition.

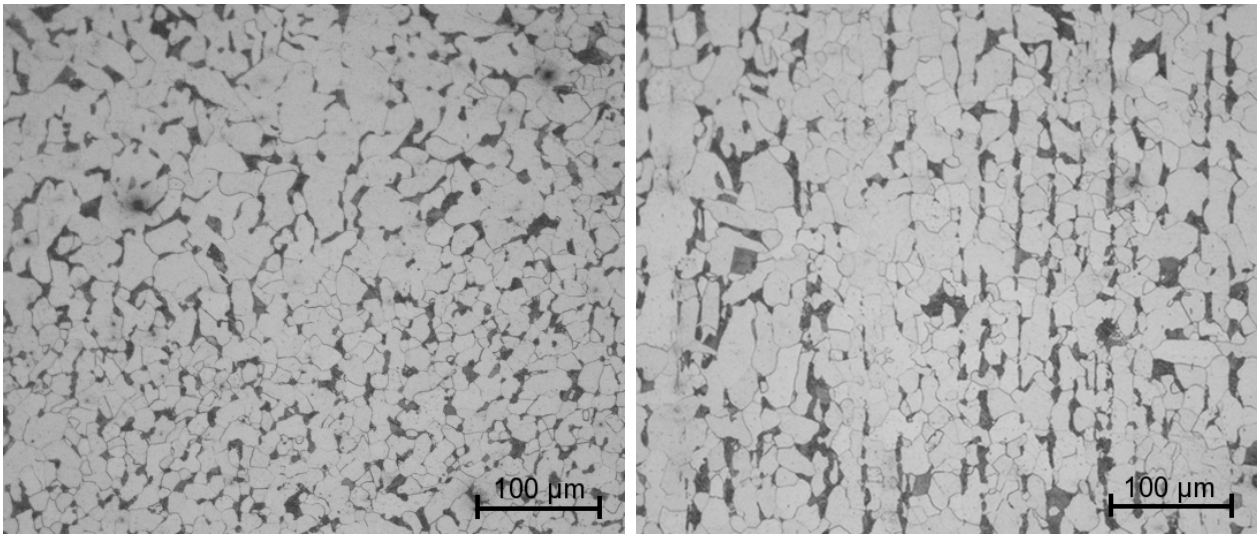

(a) Along transversal axis **(b) Along longitudinal axis**

Figure 19 Microstructure of S15C steel

3.2.2. Fatigue tests

As previously mentioned, fatigue tests were conducted here in the loading frequency range from 0.2 Hz to 140 Hz. For all these fatigue tests, common conditions are admitted: fatigue tests in air, at room temperature with a stress ratio R = -1. In addition, all fatigue tests were stress controlled. Nevertheless, two different fatigue machines were used to conduct all the fatigue tests in the present study. (1) usual servo-hydraulic machine. For this type of machine, a pump controls the oil pressure, which causes displacement of mobile chuck. This machine allowed us to perform tests at 0.2, 2 and 20 Hz loading frequencies. Shape of corresponding specimens used is presented in Fig. 20(a); and (2) electro-magnetic servo machine. Instead of a pump, here chuck displacement comes from magnet inside a coil. Even though principle technique is different, tests are equivalent from the point of view of the specimen, however it allows higher loading frequency. As a consequence, we used this type of machines to conduct 140 Hz fatigue tests. Specimen configuration is presented in Fig. 20(b). Due to the self-heating phenomenon, an air-cooling system has been admitted to minimize the temperature rising, in a condition similar to Photo 2 (in Section 1.1.5).

According to Fig. 20, one can note that tested portion diameter is 5 mm, whatever the test machine used. In addition, all specimens studied here have been subjected to an electrolytic polishing after machining. These previous two points implies that both size effect and residual stresses effect does not have a significant influence on the S15C steel fatigue properties here. Finally, concentration factor for specimens in Figs. 20(a) and (b) is K_t = 1.04.

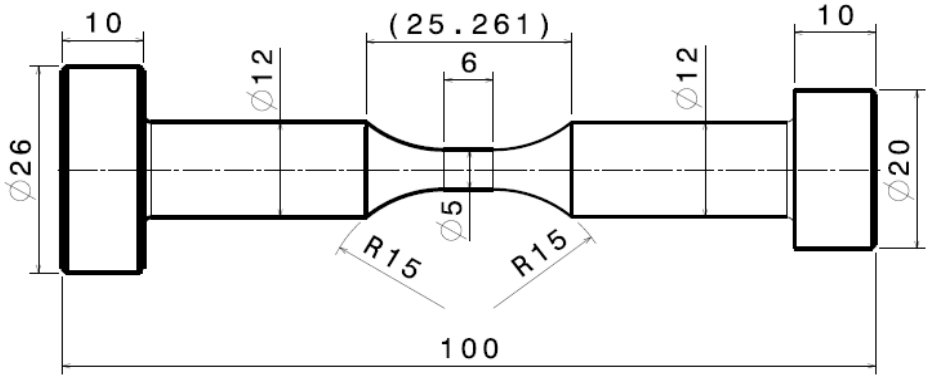

(a) Specimen for servo-hydraulic type machine

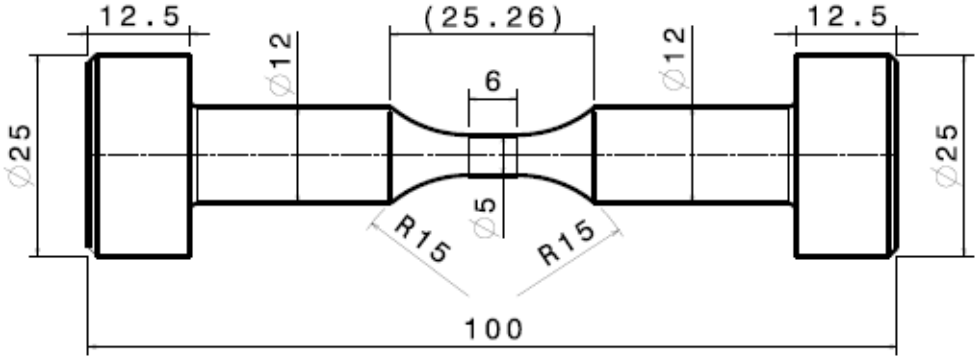

(b) Specimen for electro-magnetic type machine

Figure 20 Respective configurations of fatigue specimens

3.2.3. Tensile tests

Some tensile tests have been performed in order to evaluate some mechanical properties of S15C steels. These tests are following the JIS Z2201 standard. In such a way, specimen configuration is presented in Fig. 21. Tensile tests have been conducted at four different displacement speeds: 0.5 mm/s, 5 mm/s, 50 mm/s and 500 mm/s. More information about these tests will be provided in Section 3.4.1.

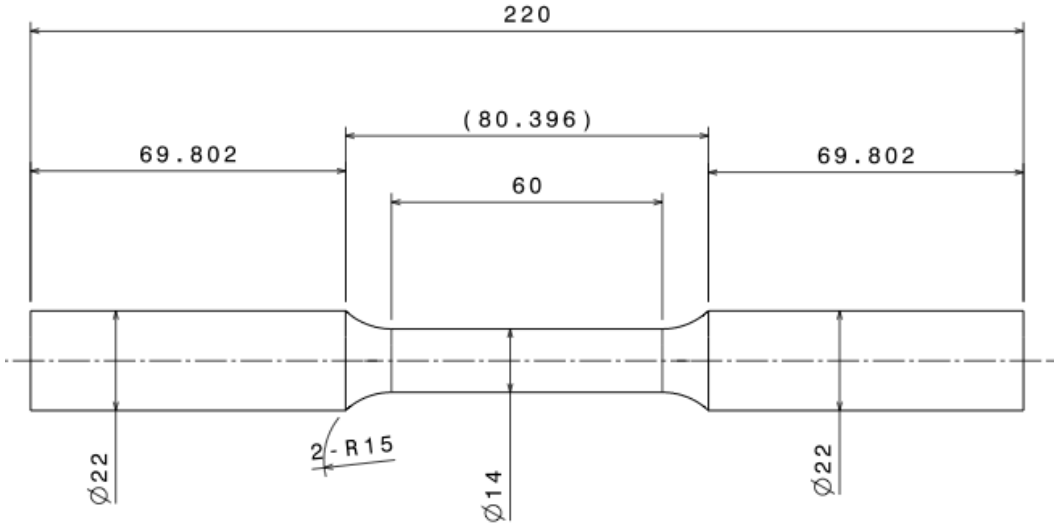

Figure 21 Configuration of specimen for tensile tests

3.2.4. Record of stress/strain properties

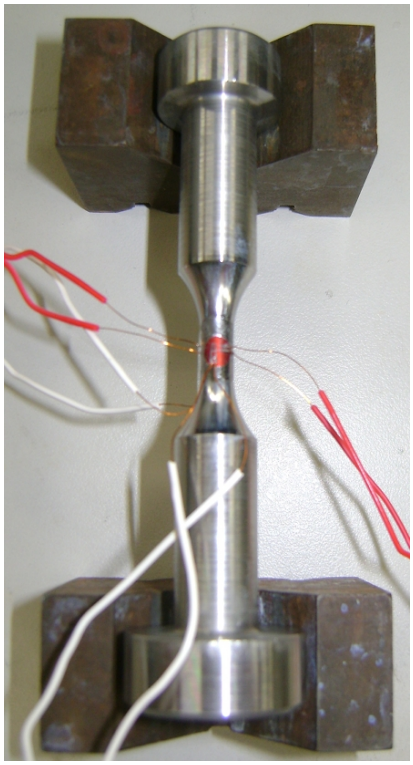

Photo 3 Strain gauge situation before fatigue test

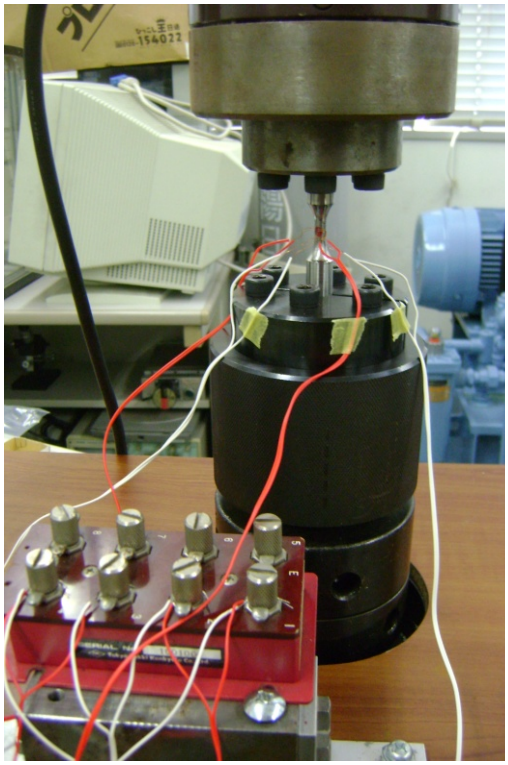

Photo 4 Strain gauge use during fatigue test

Stress and strain signals have been almost constantly recorded as fatigue tests at 0.2 Hz, 2 Hz, 20 Hz and 140 Hz were performed. Aim of these records is to analyze the micro-plasticity behavior of S15C steel subjected to fatigue loadings. A particular attention will be made on the well-known hysteresis loops phenomenon, which occurs even in the high cycle fatigue regime.

Regardless the fatigue machine used (servo-hydraulic or electro-magnetic device), the load cell voltage gives the stress signal, and thus can be easily recorded. In the case of strain signal, a full bridge gauge system, which consists of four strain gauges, has been carefully attached to the specimen center.

Besides, one can note that, in Fig. 20, the center portion of the corresponding specimens do not reveal the usual hourglass shape geometry. Instead, a cylindrical shape has been admitted for two main reasons; (1) paste of strain gauge is easier, (2) since fatigue failure is supposed to occur at stress concentration point at one of the extremities of this cylindrical shape, thus fatigue failure propagation will not influence the strain signal of gauges, at the center of specimen. Photo 3 illustrates the actual strain gauges condition before conducting fatigue test. Practically, two gauge bases including each 2 strain gauges are pasted in diametrically opposite locations. Photo 4 depicts the actual situation during the fatigue test, under servo-hydraulic machine in this case, however exactly the same system has been used in the case of tests conducted under electro-magnetic machine. One can see in this photo the bridge box necessary for this kind of strain measures.

The following data logger has performed record of stress and strain signals: *TML DC-204R*. Most of the time, sampling frequency was 100 times higher than fatigue test loading frequency. As a consequence, 100 points plot each hysteresis loop. This amount of points is enough to accurately

measure changes of hysteresis loops as fatigue goes. Figure 22 is a schematic overview of experimental instrumentation used to record the stress/strain behavior of S15C steel.

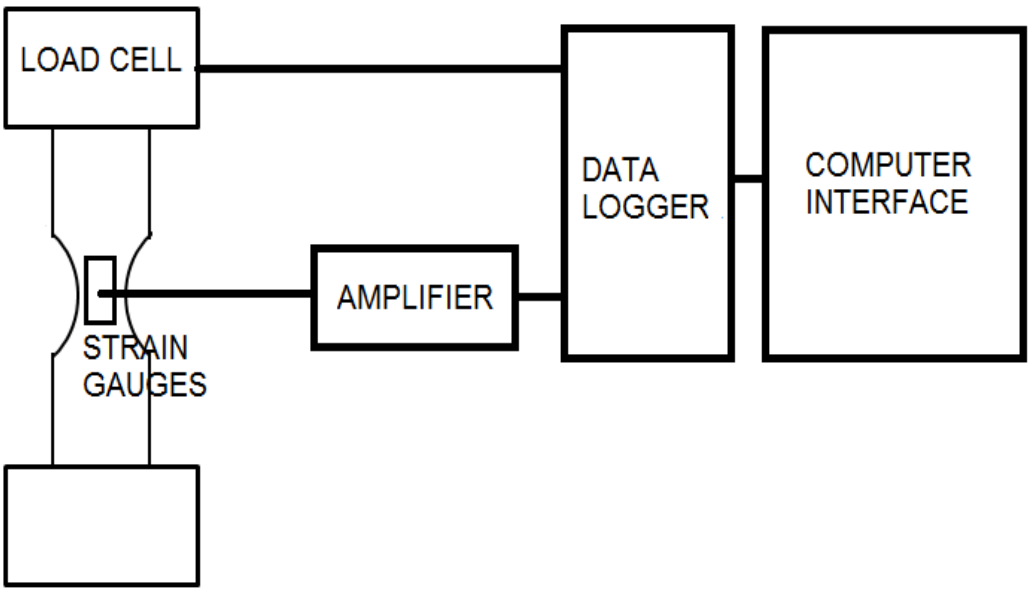

Figure 22 Instrumentation related to stress and strain record

3.2.5. EBSD observations

Aim of the EBSD observations made in this study is to analyze the lattice local misorientation in the ferritic phase of S15C steel. This kind of observations requires a particular surface condition, which is typically obtained by chemical attack electrolytic polishing. In the case of the present study, final preparation of samples has been done using OP-AA (Acidic Aluminum Oxide Polishing, *Struers*), which consists of both aluminum polishing and corrosion attack. EBSD observations have been conducted by using a *Hitachi SU6600* SEM equipped with a *NordlysF* camera for orientation acquisition.

Calculation of the local misorientation, θ, is presented in Fig. 23. In the general case, this calculation is based on the difference of the lattice orientation of one point with its directly neighbors, as presented in Fig. 23(a), where $\beta(p_0,p_i)$ denotes the misorientation between a fixed point p_0 and neighboring point p_i (i=1,2,…,8). However, in the case of the point studied is located at the edge of a grain or subgrain boundary, only neighbors points in the same grain/subgrain are taking into consideration, as indicated in Fig. 23(b). In the case of our study here, size of the unit square has been set as 0.3 μm × 0.3 μm. This choice has been done to get enough points even for small pearlite grains.

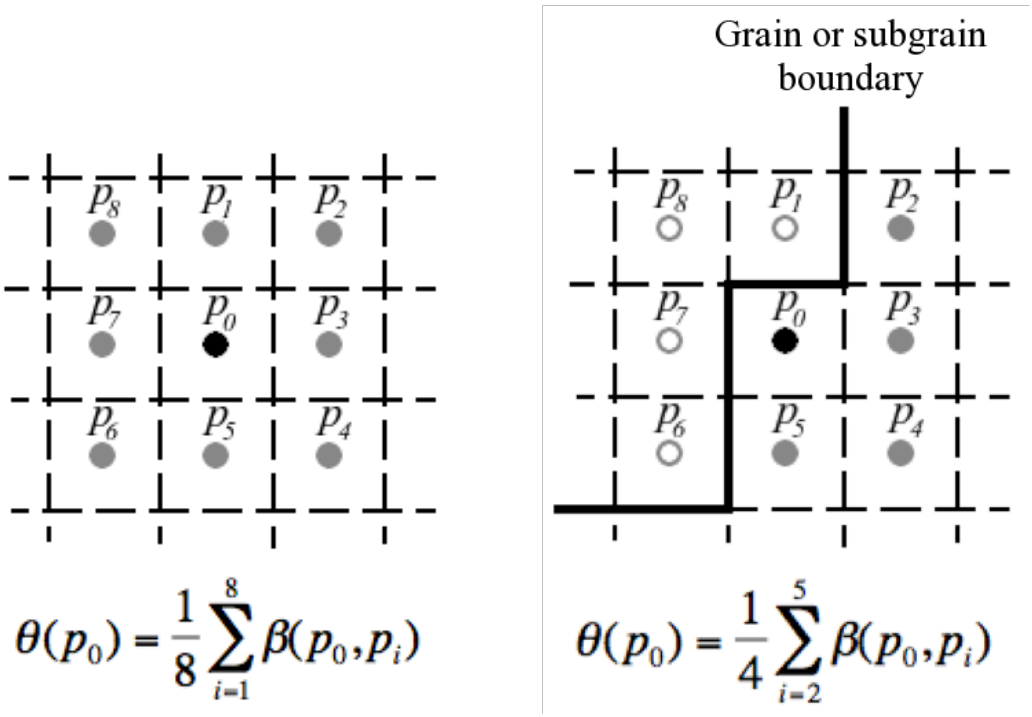

(a) Calculation in the general case **(b) Influence of subgrain or grain boundary**

Figure 23 Explanation of local misorientation calculation

3.3. Experimental results

3.3.1. *S-N* data

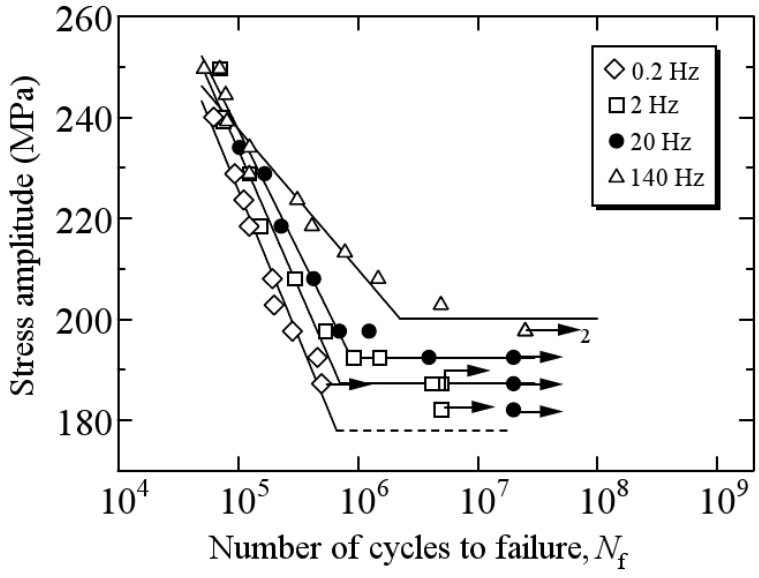

Figure 24 *S-N* diagram of S15C steel under usual loading frequencies

The most fundamental fatigue results in this study are presented in the *S-N* diagram in Fig. 24, for each frequency studied in this Chapter 2. *S-N* curves plotted in this diagram are determined by using the JSMS standard JSMS-SD-11-07 for curves[27]. Obviously, some extent of fatigue life

differences can be noted in the usual frequency loading range of 0.2 to 140 Hz. Even though fatigue lives are similar at high stress level conditions, differences become distinct as the stress level decreases. Thus, the fatigue limit also tends to increase gradually with an increase of the loading frequency: 187 MPa for 2 Hz tests, 192 MPa for 20 Hz tests, and 200 MPa for 140 Hz tests. Due to the time consuming aspect of fatigue tests operated at 0.2 Hz, the fatigue tests have been ceased at $N = 5\times10^5$ cycles, equivalent to approximately 1 month duration. Based on this difficulty, fatigue limit at 0.2 Hz was evaluated to be 178 MPa by a special procedure explained later (Section 3.4.1).

3.3.2. Stress-Strain properties

This section will be dedicated to the stress-strain properties and more particularly on hysteresis phenomenon during cyclic loading, of S15C steel for 0.2, 2, 20 and 140 Hz loading frequencies. General instrumentation of the following experiments has been already presented in Section 3.2.4. As a reminder, strain is recorded by a full bridge strain gauge system and stress is determined by load cell output. In order to record the hysteresis loop with a sufficient accuracy, the sampling frequency of stress and strain signals is 100 times the fatigue loading frequency. In other words, each hysteresis loop is composed of 100 points. As an example, hysteresis loop obtained at high stress level of σ_a = 230 MPa and at f = 20 Hz is presented in Fig. 25, for 3 different fatigue stages.

Variation of the hysteresis loop along the loading cycles in this study is depicted in Fig. 26. The hysteresis energy A_h calculated as the area of hysteresis loop is taken as the ordinate. One can find that, regardless both the loading frequency and the stress level, the hysteresis energy is increasing at the initial stage and then tends to decrease gradually after the peak point. However, in the case of low stress levels, such an increase can be retarded. The slope of the initial stage is roughly similar in this diagram with the logarithmic abscissa. Thus, the slope is actually decreasing with a decrease of the stress level. In other words, the slope in linear scale is more distinct at high stress levels. As hysteresis energy increases, one can find that S15C steel is subjected to a cyclic softening behavior.

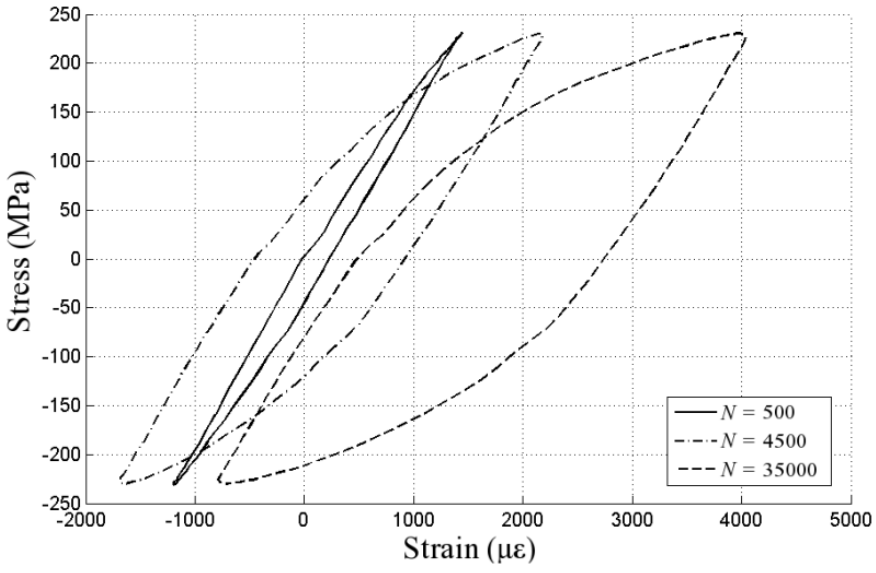

Figure 25 Stress-strain hysteresis loop evolution (f = 20 Hz, σ_a = 230 MPa, $N_f = 8.1\times10^4$)

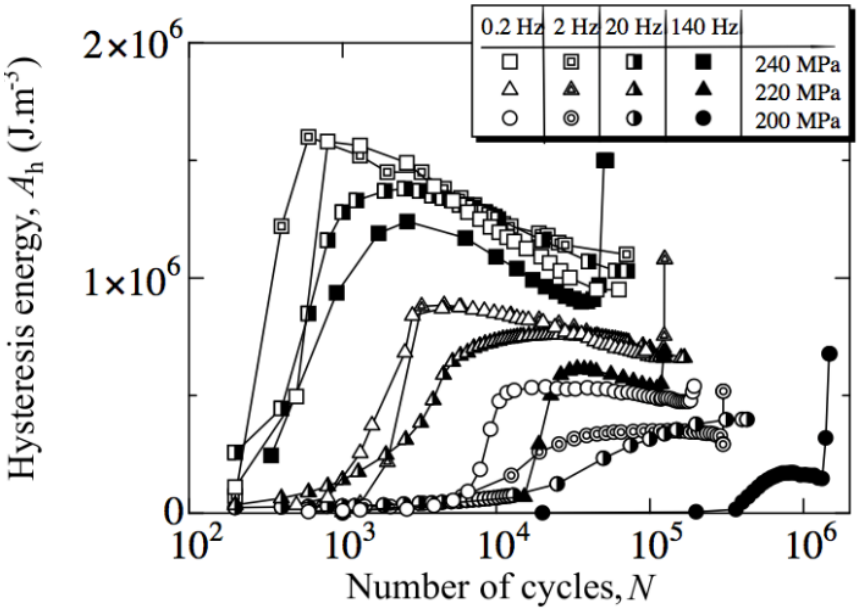

Figure 26 General behavior of stress-strain hysteresis energy

Let us now make a focus of the effect of the frequency on the hysteresis energy A_h. As a general trend, the higher the frequency is, the less severe the initial energy increase is. Some similar results have been reported by Hattori[28]. One can note that variation of the hysteresis energy along the cyclic loading is within a narrow range in the case of σ_a = 240 MPa (square dots). On the other hand, hysteresis energy curves are more and more distant at lower stress levels of 220 MPa and 200 MPa. Indeed, at low stress levels, the initial increase of the curve is retarded with an increase of the loading frequency. This result is also related with the general fatigue properties at the respective loading frequencies, already depicted in Fig. 24. Indeed, fatigue lives at high stress levels for respective loading frequencies are very close each other, but some differences appear as stress level decreases.

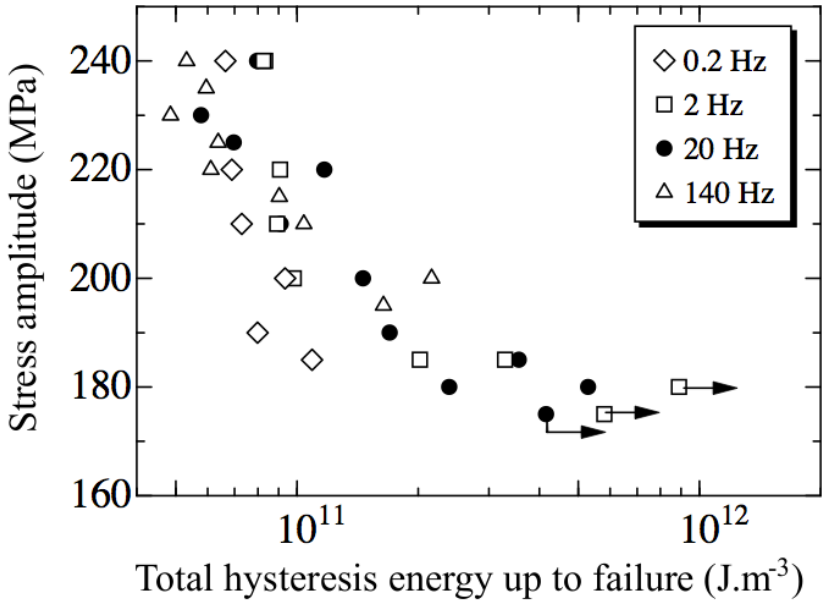

Figure 27 Effect of the frequency on the total hysteresis energy up to failure

Integrating the curves of hysteresis energy depicted in Fig. 26 allows us to compute the whole energy accumulated in the specimen up to failure. Results thus calculated are presented in Fig. 27. As one can see, total hysteresis energy up to failure tends to increase as stress level decreases. Such a general aspect had been already mentioned a long time ago by Inglis[29] in the case of low carbon steel. In addition, Fig. 27 implies that total hysteresis energy is not sensitive to the loading frequency, even though results for 0.2 Hz fatigue tests show a relative lower energy values.

Let us now have a look on the cyclic behavior of S15C steel. Figure 28 shows main results on the frequency dependence of cyclic stress-strain characteristics at the loading stage of $N = N_f / 2$. Figure 28(a) makes a comparison of the monotonic (tensile test) and cyclic (fatigue tests) stress-strain curves at respective frequencies. Obviously, regardless the loading frequency of fatigue tests, peaks of cyclic hysteresis loop are below the monotonic stress-strain curve. This is another proof of the cyclic strain softening behavior of S15C steel[30]. Figure 28(b) makes a focus on the cyclic curves. Paying an attention to the differences among the respective regression lines in this diagram, the peak value of the hysteresis loop becomes higher when the loading frequency is increasing. As a consequence, the cyclic softening behavior is less severe under high frequency fatigue tests.

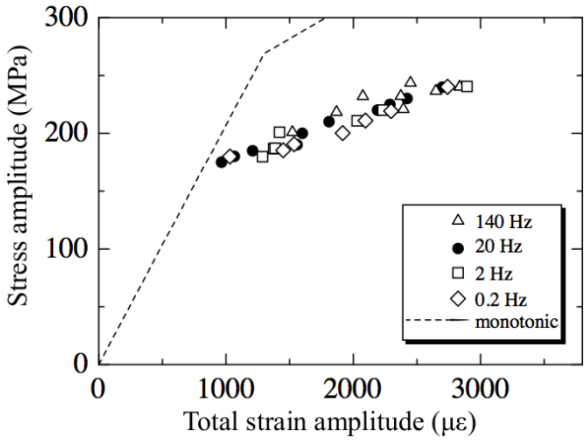

(a) Monotonic and cyclic stress-strain curve

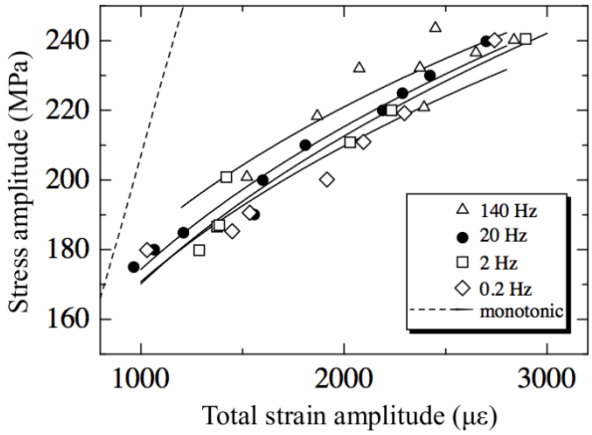

(b) Details on cyclic stress-strain curve

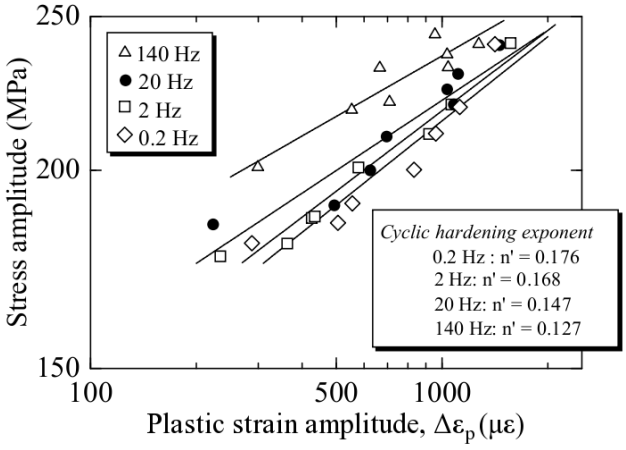

(c) Plastic behavior of hysteresis phenomenon

Figure 28 Frequency dependence of cyclic stress-strain characteristics at $N = N_f / 2$

By considering only the plastic deformation amplitude, *i.e.* half width of stress-strain hysteresis loop $\Delta\varepsilon_p$, one can obtain the results presented in Fig. 28(c), in a *log-log* diagram. Based on this diagram, one can find that, at a definite stress level, the cyclic plastic deformation tends to decrease when the frequency is increasing. Such a diagram also allows us to calculate the cyclic hardening exponent n', which corresponds to the slope of respective regression lines. Values obtained, listed in the diagram, are close to the usual estimation of 0.15 for most of metallic materials[31]. Nevertheless, one can find that cyclic hardening exponent tends to decrease as loading frequency is increasing. As already discussed about Fig. 26, hysteresis energy curves are close each other at high stress levels. Thus, the plastic strain amplitudes at respective loading frequency are also close to one other in this high stress region. On the other hand, in the low stress region, high frequency tests provide very low plastic strain amplitude. Therefore, cyclic hardening exponent tends to decrease at high frequency tests.

3.3.3. Local misorientation observation

One other possibility to get some information on the micro-plasticity behavior of fatigued steel is to undertake measurement of the orientation of crystal lattice of this metal by using EBSD device. Even though EBSD mapping has some drawbacks[32], some literatures have reported a good correlation between the local misorientation and the density of geometrically necessary dislocations (GND)[33-36]. Statistically stored dislocations (SSD) cannot be detected by this technique, but this kind of misorientation analysis is a first step before conducting direct dislocation observations to assess cyclic plasticity behavior and dislocation arrangement of S15C steel fatigued at respective loading frequencies. In this study, we will analyze the local misorientation in the ferrite phase. It should be noted that the angular precision of the measure of the lattice orientation is usually reported to be the order of 1 %[32].

Due to the fact that the fatigue strength is depending on the loading frequency, two particular stress levels based on respective fatigue limits have been chosen. Indeed, for each loading frequency studied, S_w+10 and S_w+30 are respective fatigue limit plus 10 MPa and plus 30 MPa, respectively. For both stress levels, different specimens have been fatigued up to 5%, 10% and 25% of the respective fatigue lives. Then, the tested portions of specimens have been sliced along the cross section. Loading frequencies involved in this study are 140 Hz and 20 Hz.

Some examples of local misorientation maps of ferrite phase obtained by EBSD are depicted in Fig. 29. One can see that surface condition is good enough to obtain meaningful results of the lattice misorientation. This figure is composed of three maps. Figure 29(a) represents an example at the initial stage without cyclic loading, where dominant color is roughly yellow; and Fig. 29(b) indicates an example for a sample fatigued at f = 20 Hz, where dominant color is rather green. According to the respective color scale indicated at the bottom edge of each map, one can find the fact that misorientation within each grain / subgrain tends to decrease by applying the cyclic loading.

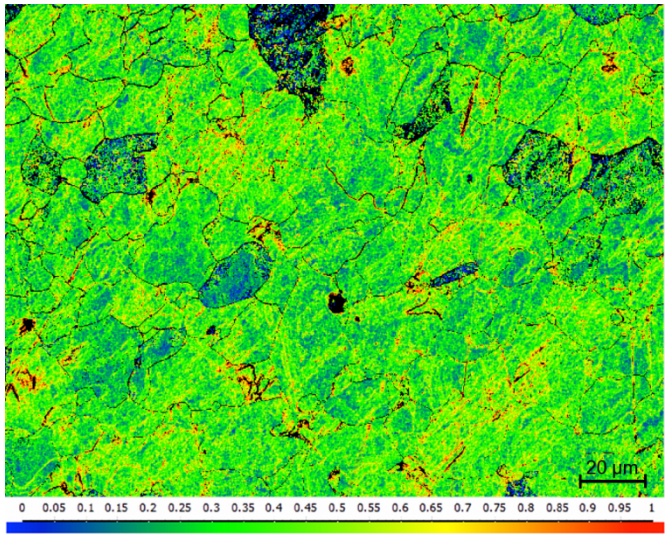

(a) At initial stage

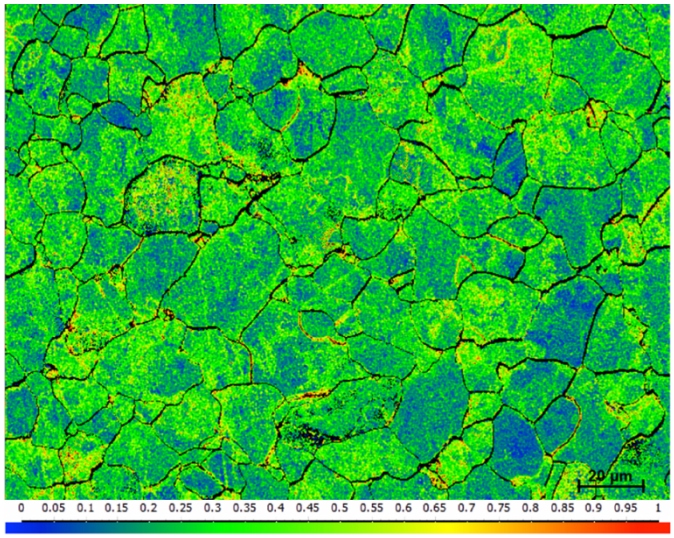

(b) f = 20 Hz, $\sigma_a = S_w+30$, N = 5% N_f

Figure 29 Examples of local misorientation maps

To obtain a more precise point of view of the effect of the fatigue conditions on the variation of the local misorientations values, local misorientation distributions have been studied. The patterns of local misorientation distribution, presented in Fig. 30, have been obtained as follows; on each specimen, two distinct map scans for two different sites representing a surface of 200 μm × 150 μm have been carried out, obtaining the distribution pattern of each map scan. Distribution of the local misorientation was analyzed by setting a sufficiently fine step. Width of the step has been chosen as 0.025 deg., *i.e.* misorientation distribution is defined by 40 points in the misorientation range from 0 to 1 deg. Then, we have calculated the average of misorientation at a couple of sites and the distribution patterns thus obtained are shown in Fig. 30. One can see that the local misorientation distributions are close to a lognormal distribution pattern. Such an observation has already been reported by Kamaya[34].

First, make a focus of the fatigue stage on the variation of the distribution pattern, presented in Fig. 30(a), in the case of 20 Hz. Thick solid line in each diagram represents the distribution curve for non-fatigued specimen. Peak of the distribution pattern for fatigued specimens tends to appear at

lower misorientation values comparing with non-fatigued one. However, differences between these three loading stages are very tiny.

Figure 30(b) depicts the distribution patterns of the local misorientation observation at N = 25% N_f for respective loading frequencies. Clearly, fatigued specimens have a lower local misorientation than non-fatigued one. The main point here is that distributions after fatigue loadings at 140 Hz show higher misorientation values than at 20 Hz.

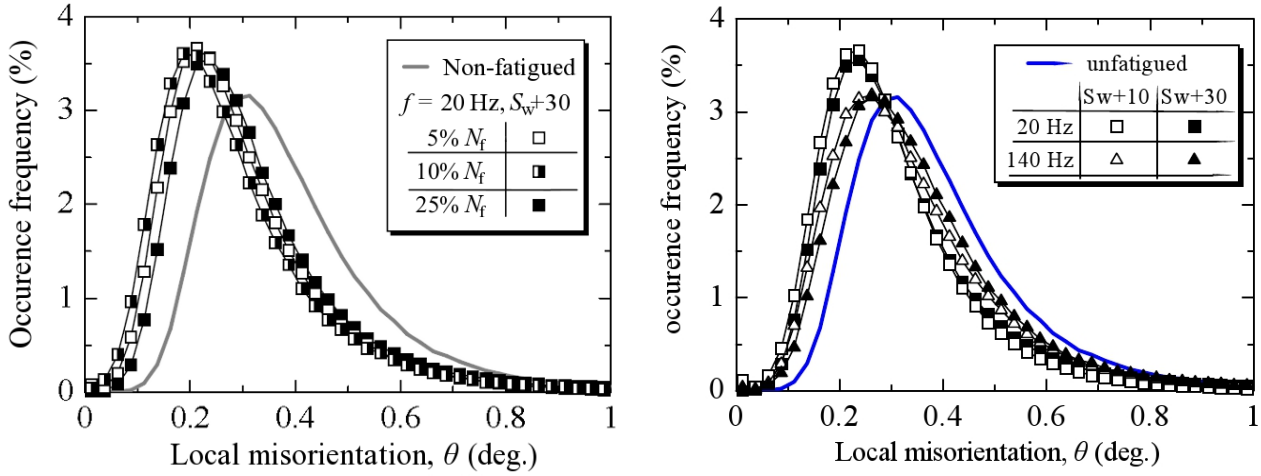

(a) 20 Hz tests **(b) Misorientation distribution, at N = 25% N_f**

Figure 30 Local misorientation distributions

3.4. Discussion on frequency effect of S15C steel

3.4.1. Strain rate influence on the yield stress

It has been widely reported a clear strain rate effect on the yield stress of metallic materials, including low carbon steels[37-39]. From this viewpoint, some tensile tests on S15C steel have been conducted at different loading speeds. These tests have been performed in accordance with JIS Z2201 standard, using tensile specimen already presented in Fig. 21. Results obtained are depicted by open marks in Fig. 31, as a function of the strain rate. One can clearly see that the lower yield stress tends to increase with an increase of the strain rate. Such a phenomenon is due to the fact that higher strain rate provide a higher density of dislocations inside cell walls[38]. Thus, there is a smaller mobility of dislocations at higher strain rate, and then plastic deformation will be more difficult to happen.

According to Tsuchida *et al.*[37] in the case of JIS SM-490 (0.15 %C steel), a linear regression line can be found between the lower yield stress and the strain rate on a semi-logarithmic diagram, represented in solid marks in Fig. 31. Value of the correlation coefficient of this regression for S15C steel is very large as 0.998.

In order to estimate the effect of this change of the yield stress on the fatigue properties of S15C steel, *S-N* diagram in Fig. 24 was replotted by taking the applied stress level normalized by the lower yield stress as the ordinate in Fig. 32. One can clearly see that results within usual frequency range of 0.2 to 140 Hz, is similar to a common *S-N* curve. As a consequence, fatigue limit values obtained at respective frequencies are also close each other: 0.628, 0.625 and 0.635 for

140 Hz, 20 Hz and 2 Hz, respectively. Thus, it seems sensible to consider that, in this frequency range, the slight frequency effect observed in Fig. 24 can be attributed to the fact that yield stress tends to increase with an increase of the loading frequency. In addition, such a result also allows us to make an estimation of the fatigue limit value in the case of 0.2 Hz as follows; the normalized fatigue limit of 0.630 and the lower yield stress of 282 MPa give the fatigue limit of 178 MPa.

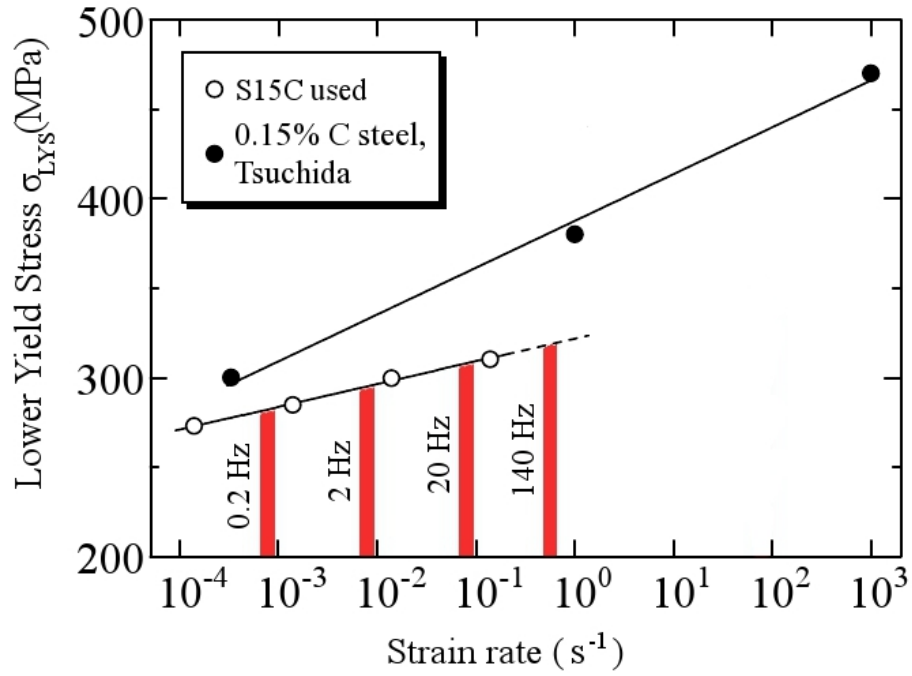

Figure 31 Strain rate effect on yield stress

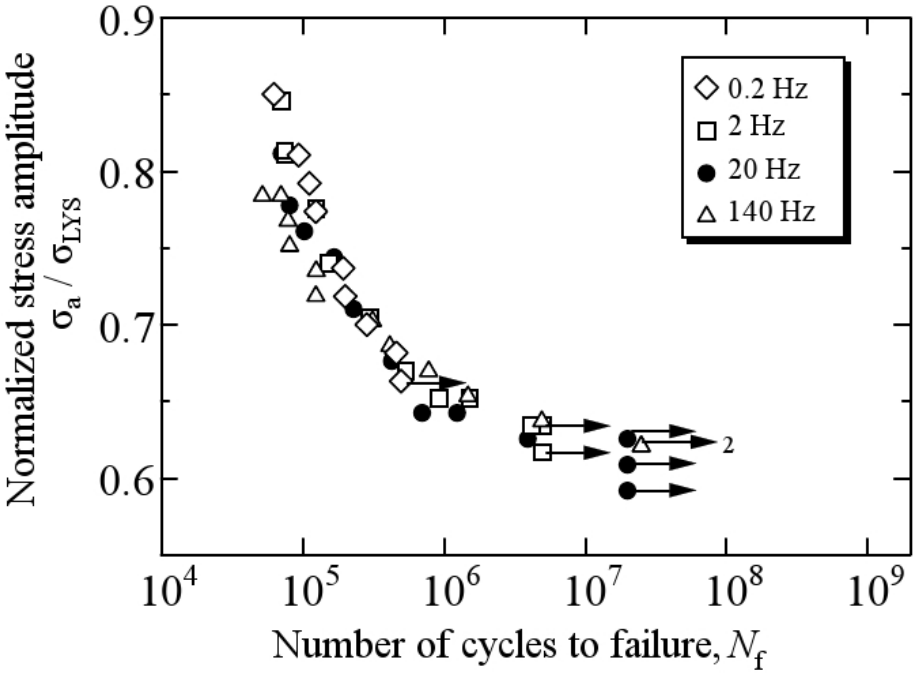

Figure 32 Evaluation of yield stress variation influence on *S-N* properties

3.4.2. Analysis of the micro-plasticity phenomenon

Let us now make a discussion related to the results obtained from lattice local misorientation study. One can find that fatigued specimens reveal lower misorientation values comparing with specimens before fatigue tests. This result is in a good accordance with the general softening behavior already discussed. In such a discussion, it is assumed that the dislocation density, and also GND density, would decrease in the case of cyclic softening.

In order to interpret the physical meaning of the local misorientation results, additional discussions are developed here, based on data in Fig. 30(b). Misorientation distributions obtained at f = 20 Hz let appear lower values than at f = 140 Hz fatigue tests. When the local misorientation has a high value, the GND density becomes higher, as mentioned earlier [33-36]. On the other hand, the cyclic softening is weakened as the loading frequency is increasing. Therefore, specimen fatigued at 140 Hz is supposed to show a higher GND density than fatigued specimen at 20 Hz. On can note that both results from stress-strain behavior and the local misorientation observation are in accordance with each other.

Thus, the micro-plasticity phenomenon of the S15C steel, in the frequency range of 0.2 Hz to 140 Hz, can be well described. Indeed, all the different results obtained from the stress-strain study (Section 3.3.2) and from the misorientation analysis (Section 3.3.3) are in agreement each other. According to Fig. 28(b), a higher loading frequency implies a less severe cyclic softening due to a higher dislocation density, detected by less distinct decrease of misorientation values.

3.5. Conclusion

Fatigue properties of JIS S15C low carbon steel have been studied by carrying out fatigue tests in the loading frequency range from 0.2 Hz to 140 Hz in this Chapter 3. Discussions have been focused on the effect of loading frequency on the fatigue properties and on the micro-plasticity behavior of S15C steel. Following points present the main findings of this work;

(1) An effect of the loading frequency on the *S-N* property was confirmed on S15C low carbon steel, where both of the fatigue strength and the fatigue life increased with an increase of the loading frequency. However, such an effect tends to be low at high stress levels in the frequency range of 0.2 Hz to 140 Hz.

(2) In the usual frequency range of 0.2 Hz to 140 Hz, effect of the loading frequency is well connected to the effect of strain rate on yield stress. Indeed, a common *S-N* curve has been obtained by normalizing the stress amplitude by the lower yield stress at the respective loading frequency.

(3) In the same frequency range, the frequency effect can be connected to the micro-plasticity through a change of the stress-strain behavior at the respective loading frequencies. A higher frequency will implies lower hysteresis energy, *i.e.* the cyclic softening behavior is less severe.

3.6. Future plans

Future plans consist mainly to undertake fatigue tests at the ultrasonic frequency of 20 kHz. First objective is to make the reconfirmation of the frequency effect at such high loading frequency. Then, we will pay a particular attention to determine if such a frequency effect is the direct consequence of the change of the micro-plasticity behavior in a similar way to the case of fatigue

tests performed in the usual frequency range, or if the high loading frequency of ultrasonic tests could initiate other phenomena influencing the fatigue properties of S15C low carbon steel.

Chapter 4. Comparison of the fatigue properties of S15C low carbon steel at usual and ultrasonic frequencies[iv,v]

4.1. Objectives of the studies presented in this section

As already mentioned in the previous Chapter 3, effect of the loading frequency on the fatigue property of JIS S15C low carbon steel is pretty well understood in the loading frequency range of 0.2 to 140 Hz. As second step of this study, we will now involve the case of the ultrasonic loading tests, performed at 20 kHz.

After introducing the experimental procedure related to ultrasonic fatigue tests and discussing on the validity to compare results from usual and ultrasonic tests, we will examine several fatigue properties at ultrasonic frequency and compare it with corresponding tests at usual frequencies. In addition to essential results of *S-N* curves or lattice local misorientation, the slip band formation and crack initiation mechanism will be studied.

4.2. Experimental procedures

4.2.1. Ultrasonic fatigue tests

In order to be able to compare the fatigue tests results at usual and ultrasonic frequencies, some common conditions are readmitted. Particularly, ultrasonic fatigue tests are performed in air, at room temperature, with a stress ratio R = -1. Configuration of the specimen used for ultrasonic fatigue tests is presented in Fig. 33. One can note that the same tested diameter of 5 mm has been admitted for fatigue tests at usual frequencies, according to Fig. 20. In addition, specimen surface was also finished by electrolytic polishing. Thus, these previous conditions are strictly equivalent to the corresponding ones for fatigue tests conducted in the frequency range of 0.2 Hz to 140 Hz.

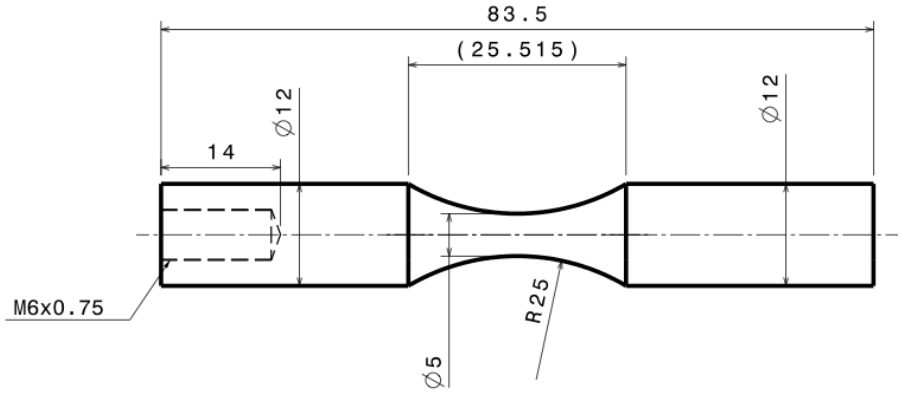

Figure 33 Configuration of specimen for ultrasonic type machine

[iv] [International Journal of Fatigue][In press]© Elsevier Ltd.

[v] [International Journal of Fatigue][Work in progress]© Elsevier Ltd.

However, since the ultrasonic fatigue test technique is different, it is impossible to control directly the stress pattern. Instead, ultrasonic test is using the displacement of the free edge of the specimen as the reference. In other words, ultrasonic test is a strain-controlled test, which is naturally different to the stress-controlled tests performed in the usual frequency range. Nevertheless, Zettl *et al.*[40] have reported that S15C steel is not subjected to high plastic strain amplitudes. Indeed, a quick calculation reveals that, even at high stress levels, peak of plastic strain at failure of the specimen is approximately 1 % of the total strain amplitude. Thus, the plastic behavior of S15C steel does not affect significantly the stress level applied to the specimen during ultrasonic fatigue tests.

Ultrasonic tests are known to cause a significant self-heating phenomenon. In order to keep the specimen surface temperature below 40°C, an air-cooling system in addition to an intermittent loading condition (110 ms of loading time followed by 2500 ms of rest time) were admitted. An ageing effect during the short time lapse of 2.5 seconds is considered to be negligible, as hot-rolled S15C steel does not have high solute carbon content and consequently should have a low ageing rate[41]. At last, intermittent loading condition will introduce short transition periods at initial and end stages of every testing "pulse". However, as already discussed above, significant plasticity does not occur at ultrasonic frequency. Thus, these cycles at a low stress regime do not have a significant effect on the plastic behavior of S15C steel.

4.2.2. Microstructure analysis

This part of the study consists of making some verification on the microstructure of S15C steel after fatigue loading, and particularly after ultrasonic loading tests. Grain size distribution in addition with local misorientation axis will be analyzed by EBSD observation in both transversal and longitudinal sections of the fatigue specimens. EBSD observations have been conducted by using a *Hitachi SU6600* SEM equipped with a *NordlysF* camera for orientation acquisition. In order to prepare these samples to the EBSD analysis, OP-AA (Acidic Aluminum Oxide Polishing, *Struers*) followed by a 4 min. argon ion milling at 6 kV acceleration voltage finishing have been used.

4.2.3. Fatigue slip band study

Observation of the slip bands has been conducted by using plastic film replica, in order to reproduce the specimen surface condition. This technique allows us to observe the surface condition of specimen surface at different fatigue stages. As one can note, specimen surface is not flat. It thus induces that surface effectively replicated by replica films is rather limited. Nevertheless, a particular attention has been taken to reproduce almost the same area of the fatigue specimen.

We have duplicated the surface of specimen fatigued at 0.2 Hz, 20 Hz, 140 Hz and 20 kHz. In order to estimate the density of these slip bands during the fatigue process at both stress amplitude S_w+10 and S_w+30, surface condition has been replicated before fatigue test, and after 5%, 10%, 15% and 25% of fatigue lives at respective frequencies.

Optical microscope has been used to undertake the observation of the replicas. However, such a procedure limits the magnification up to 1000×. In order to proceed to more precise

observation, some observations by SEM have been conducted directly on the specimen surface, after 25% N_f.

4.3. Experimental results

4.3.1. *S-N* data at ultrasonic loading frequency

Figure 34 is presenting the most fundamental fatigue results as *S-N* curves for the wide range of loading frequency from 0.2 Hz to 20 kHz. Naturally, results indicated here in the usual frequency range are exactly the same than shown in Fig. 24. One can see obviously a significant difference of fatigue strengths between ultrasonic and usual loading frequencies less than 140 Hz. Indeed, fatigue limit found in the case of ultrasonic tests is 248 MPa, whereas other frequencies let appear fatigue limits lower than 200 MPa.

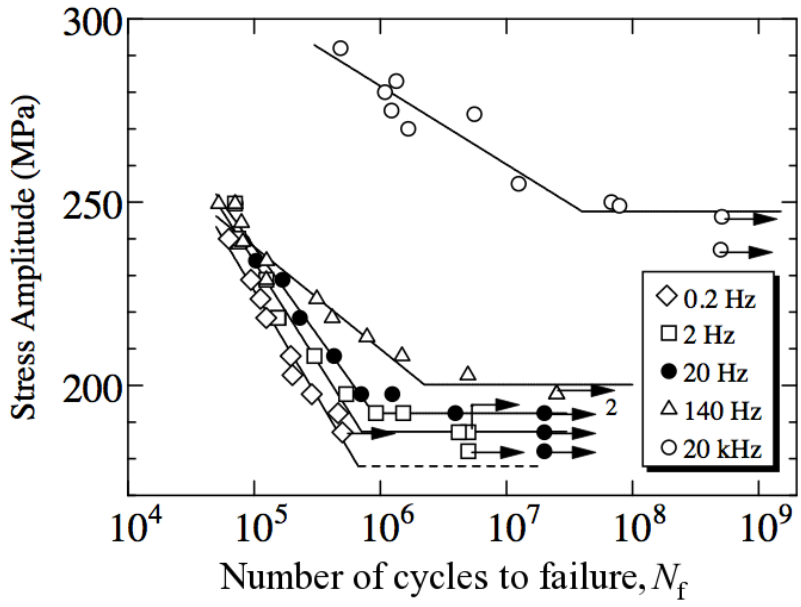

Figure 34 *S-N* diagram of S15C steel in the whole loading frequency range

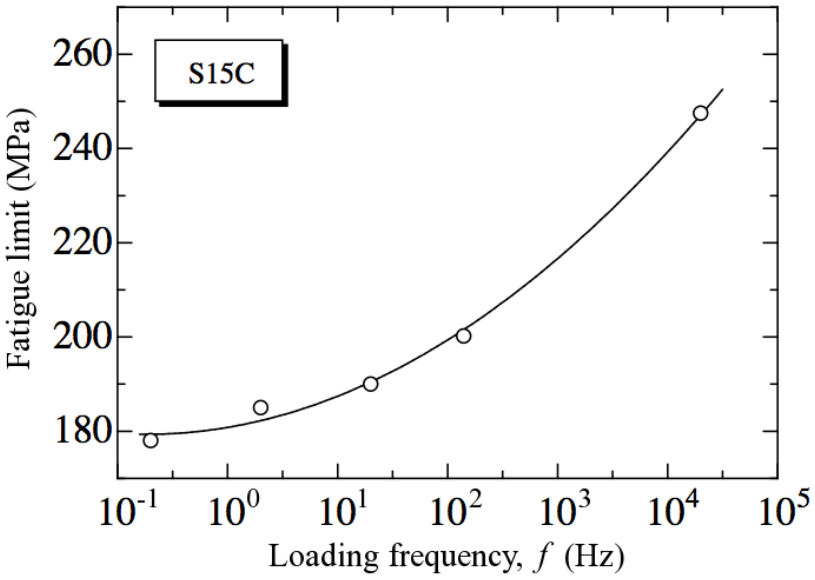

Figure 35 Frequency dependence of the fatigue limit obtained in this work

Fatigue limit thus obtained are replotted as a function of the loading frequency in Fig. 35, in a similar way as Kikukawa *et al.* in Fig 8. One can note that aspects of the curves obtained in both diagrams are equivalent.

According to these results, one can calculate the numerical values of both stress levels so-called S_w*+10* and S_w*+30*. Corresponding data are listed in Table 4. These stress levels will be used in the rest of this report to compare in an effective way the fatigue properties at respective loading frequencies.

Table 4 Numerical values of S_w*+10* and S_w*+30* stress levels

Loading frequency *f* (Hz)	S_w (MPa)	S_w*+10* (MPa)	S_w*+30* (MPa)
0.2	178	188	208
20	192	202	222
140	200	210	230
20,000	248	258	278

4.3.2. Grain size distribution

In this section, by means of EBSD technique, we will verify particularly that the high strain rate induced by ultrasonic fatigue loading will not affect the grain size of S15C steel. Indeed, very high strain rates (approximately 10^3 s^{-1} or higher) may lead to grain refinement[42]. Even though possibility of such a refinement under ultrasonic fatigue tests performed here is low, due to an average strain rate of approximately 10^2 s^{-1}, we will check the grain size distribution using EBSD technique. All data accepted here come from EBSD scans, which represent a 300 μm × 225 μm area with a spatial step size of 0.5 μm between two adjacent points.

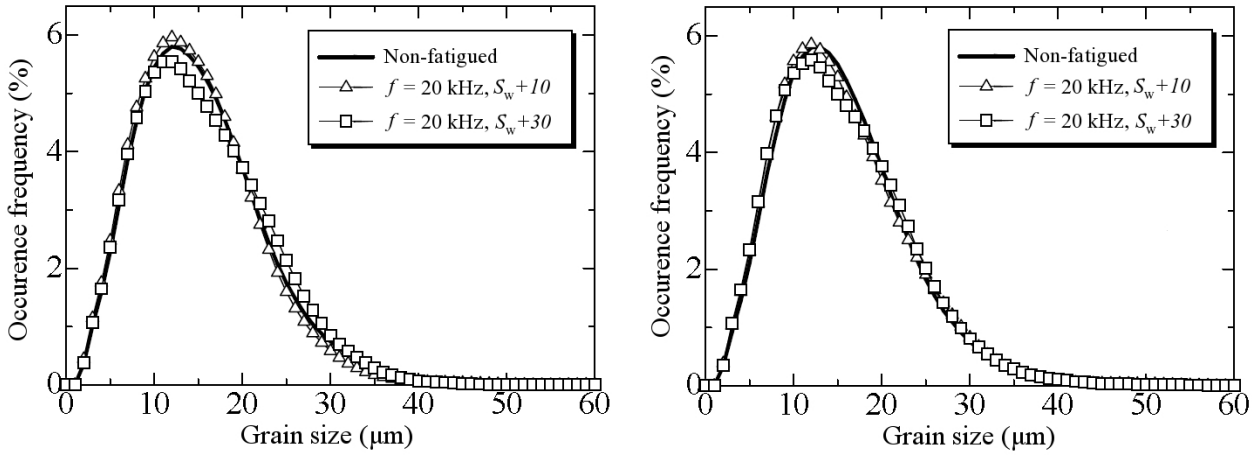

(a) Transversal section **(b) Longitudinal section**

Figure 36 Grain size distribution of ferrite grains, S15C steel

Distributions of the grain size in transversal and longitudinal sections are depicted in Fig. 36(a) and (b), respectively. Calculation of each distribution here is based on four different sites of the same sample, where initial grain size class width was 1 μm. Then, we have calculated the average occurrence in each class over the four sites to get the distributions presented in Fig. 36.

As one can see in Fig. 36, in both transversal and longitudinal sections, grain sizes distributions seem to be not influenced by fatigue loadings at ultrasonic frequency. Indeed, differences between the curves here are very tiny. In addition, the average grain sizes found from these distributions are presented in Table 5.

Table 5 Average grain size obtained from grain size distribution

	Average grain size (μm)			
Section	Transversal		Longitudinal	
Non-fatigued	15.3		15.7	
Stress amplitude	S_w+10	S_w+30	S_w+10	S_w+30
f = 20 kHz	14.7	15.4	15.3	15.5

We can thus presume that the slight change observed in Fig. 36 comes from a dispersion phenomenon of the grain size depending on the specimens, rather than any grain refinement process. In order to make anyway an assessment of the influence of thus slight changes, let us consider as an approximation the Hall-Petch equation in Eq. (9), focusing to the lower yield stress as reported by Yokobori *et al.*[43] for a S15C steel.

, (9)

where σ_y = 90 MPa and k_y = 21.6 MPa.mm$^{1/2}$

A slight change from diameter D to diameter $D + \Delta D$ will induce:

$$\sigma_y(D+\Delta D) = \sigma_0 + k_y(D+\Delta D)^{-1/2}$$

$$\sigma_y(D+\Delta D) = \sigma_0 + k_y(D)^{-1/2} \times \frac{1}{\sqrt{1+\frac{\Delta D}{D}}}$$

Assuming that term $\Delta D/D$ is close to 0, Taylor development up to 1st order gives:

(10)

According to Table 5, average grain size changes are within a range of 0.6 μm. Numerical application of the last term in Eq. (10) gives the value of 7.3 MPa change, where D is taken equal to 15 μm. Comparing this value with the lower yield strength in quasi-static condition in Table 3, one can find that this change of 0.6 μm in grain size implies a variation of approximately 1.3 % in lower yield strength. We can thus consider that such a change has a negligible influence on the fatigue properties of S15C steel.

4.3.3. Fatigue Slip band analysis

Before failure of the specimen, fatigue slip bands have been observed mainly by using plastic replica, as mentioned in Section 4.2.3. Before introducing results, let us have a look on the initial condition of the specimen surface, in Fig. 37. Since the specimens are polished by electrolytic method, some corrosion pits are formed on the surface. In order to remove as much as possible the corrosion pits, alumina polishing up to 0.3 μm diameter has been used. Nevertheless, a few pits are still present even after alumina polishing, as one can see on Fig. 37. For all the pictures from replicas, axial loading direction is vertical.

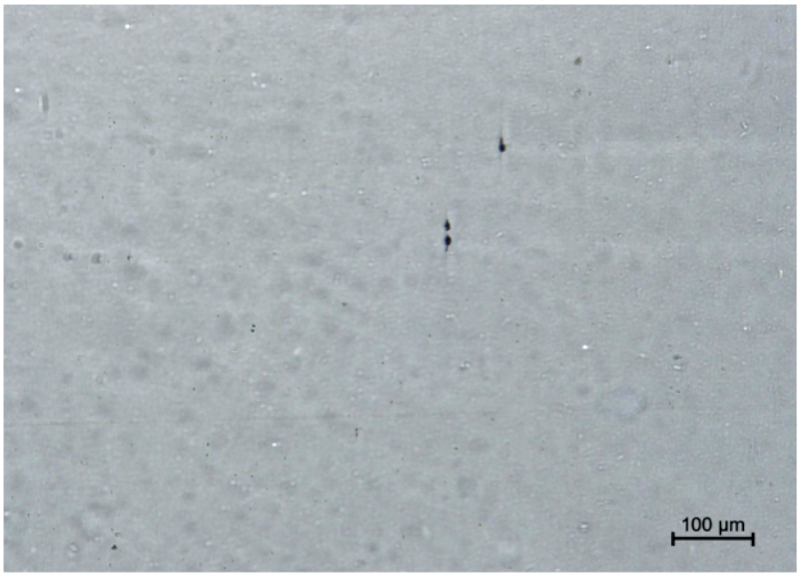

Figure 37 Replica observation of initial condition of specimen surface, S15C

Main results concerning the formation of the fatigue slip bands in the case of fatigue tests performed at usual frequencies are shown in Figs. 38 and 39. In the case of f = 20 Hz, Fig. 38 shows the change of the slip band concentration at different stages of the fatigue process. One can note in Fig. 38(a) that even after only 5 % N_f, some slight fatigue slip bands are formed. This behavior of low carbon steel has also been reported by Sasaki *et al.*[44]. At 10 % and 15 % of N_f, Figs. 38(b) and (c) highlight a continuous increase of the concentration of fatigue slip bands. Finally, at 25 % N_f, slip bands are formed in numerous grains, as shown in Fig. 38(d).

Another interesting point is to make a comparison of fatigue slip bands in the loading frequency range of 0.2 to 140 Hz. Such a comparison is presented in Fig. 39, for f = 0.2 Hz and 140 Hz, in (a) and (b), respectively. For these pictures, stress amplitude is S_w+*30* and N = 25 % N_f. Thus, the corresponding picture at f = 20 Hz is already depicted in Fig. 38(d). According to the results presented in Fig. 28(c) (Section 3.3.3), considering that plastic strain amplitude does not vary significantly between 25 % and 50 % of fatigue life, one can estimate the plastic strain amplitude at each frequency: 833×10^{-6}, 1020×10^{-6} and 813×10^{-6} at f = 0.2 Hz, 20 Hz and 140 Hz, respectively. Thus, at this stress amplitude of S_w+*30*, plastic strain amplitude applied at f = 20 Hz is higher than at other frequencies. Such a point is in correlation with the higher volume fraction affected by slip bands in Fig. 38(d) than in Figs. 39(a) and (b). Nevertheless, one can note that overall fatigue slip band formation and their progress are quite similar for every loading frequency in the range of 0.2 to 140 Hz.

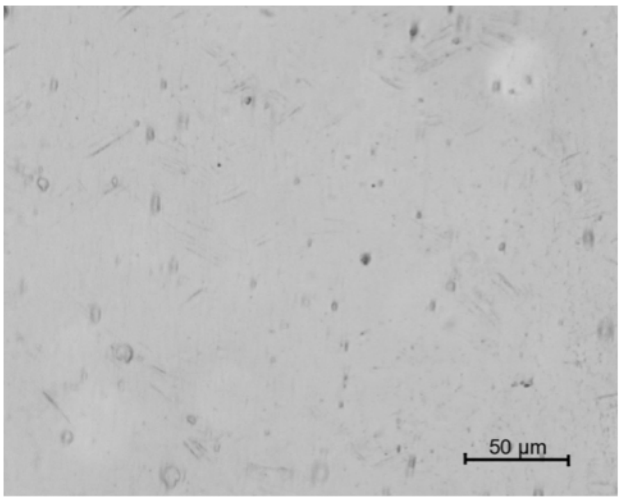

(a) At N = 5 % N_f

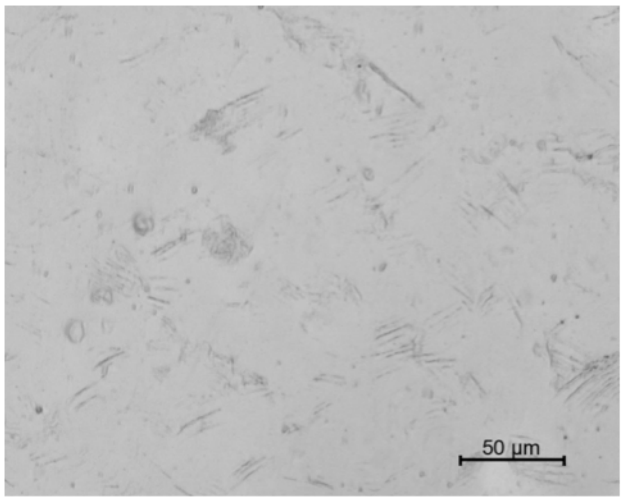

(b) At N = 10 % N_f

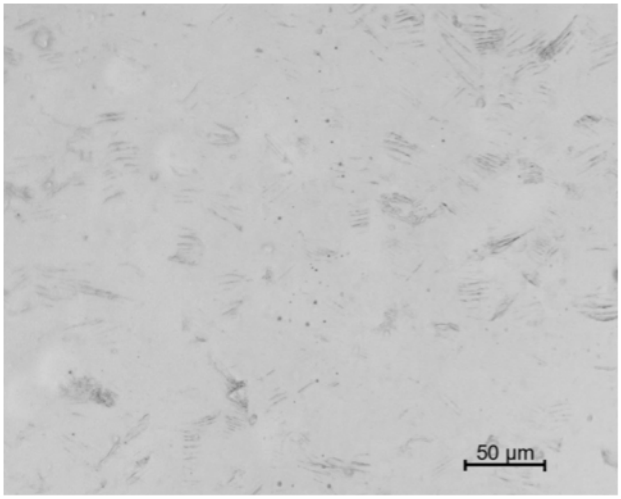

(c) At N = 15 % N_f

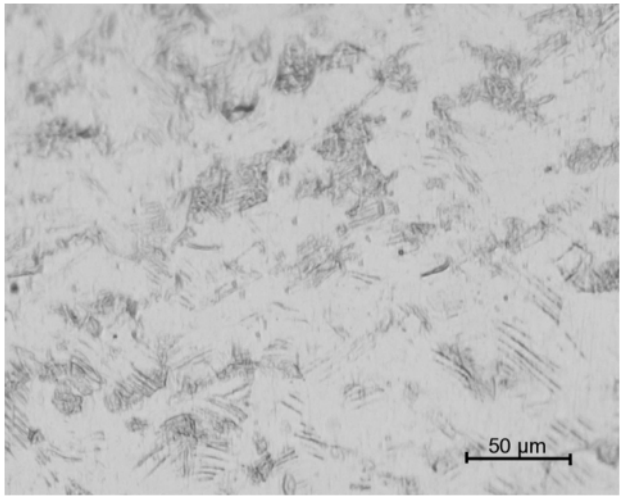

(d) At N = 25 % N_f

Figure 38 Formation of fatigue slip bands, f = 20 Hz, S_w+*30*, S15C

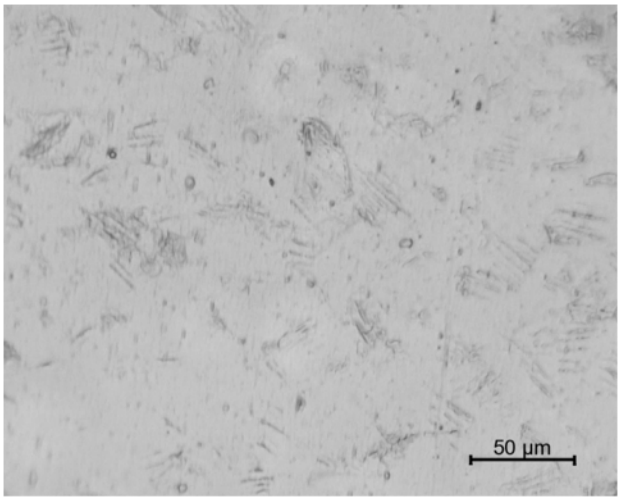

(a) f = 0.2 Hz

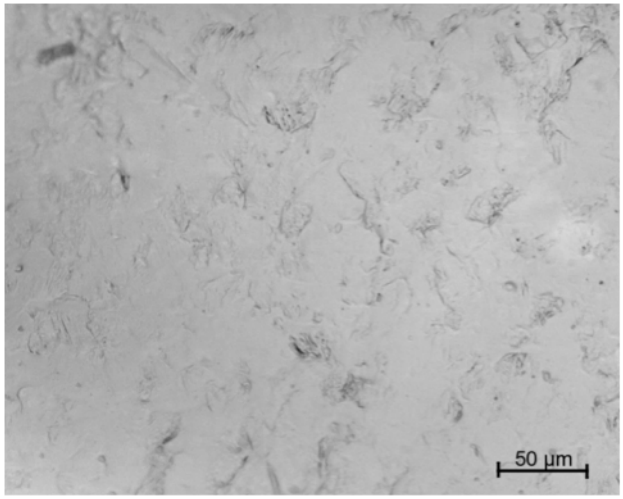

(b) f = 140 Hz

Figure 39 Comparison in usual loading frequency range, S_w+*30*, N = 25% N_f, S15C

The results obtained by means of replica films for specimen fatigued at ultrasonic frequency are presented in Figs. 40 and 41. All replicas here are from specimen surface fatigued up to 25 % of

fatigue life. Nevertheless, it should be noted that in the case of S_w+*30* stress level, some slight fatigue slip bands can be detected after 10 % of fatigue life. However, since it was particularly difficult to take meaningful photographs of these slight slip bands by optical microscope, only results at 25 % N_f are shown here. Results at S_w+*10* and S_w+*30* stress levels are depicted in Figs. 40 and 41, respectively.

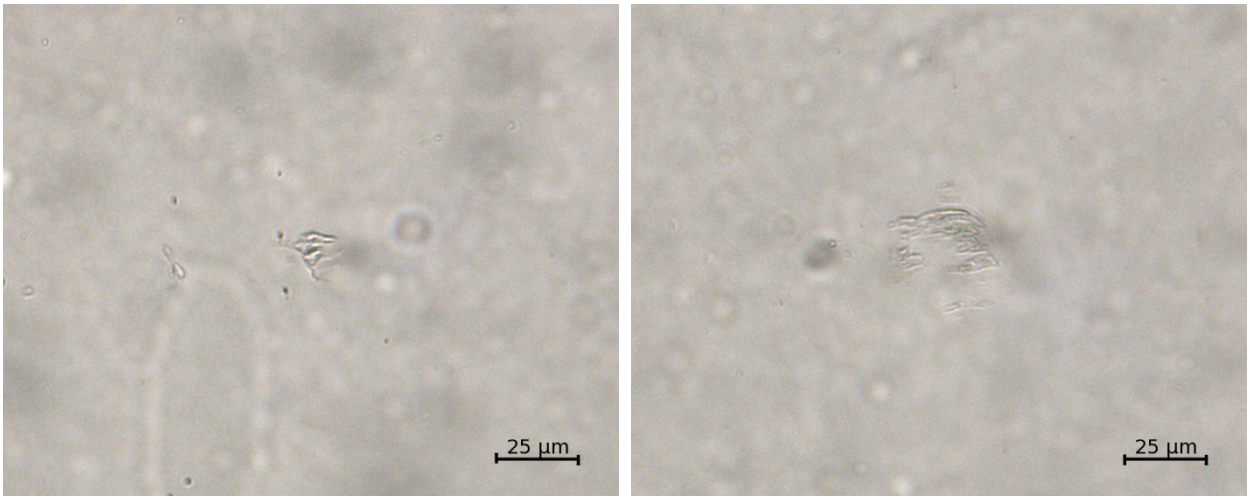

Figure 40 Replica observation of specimen fatigued at S_w+*10*, N = 25% N_f, f = 20 kHz

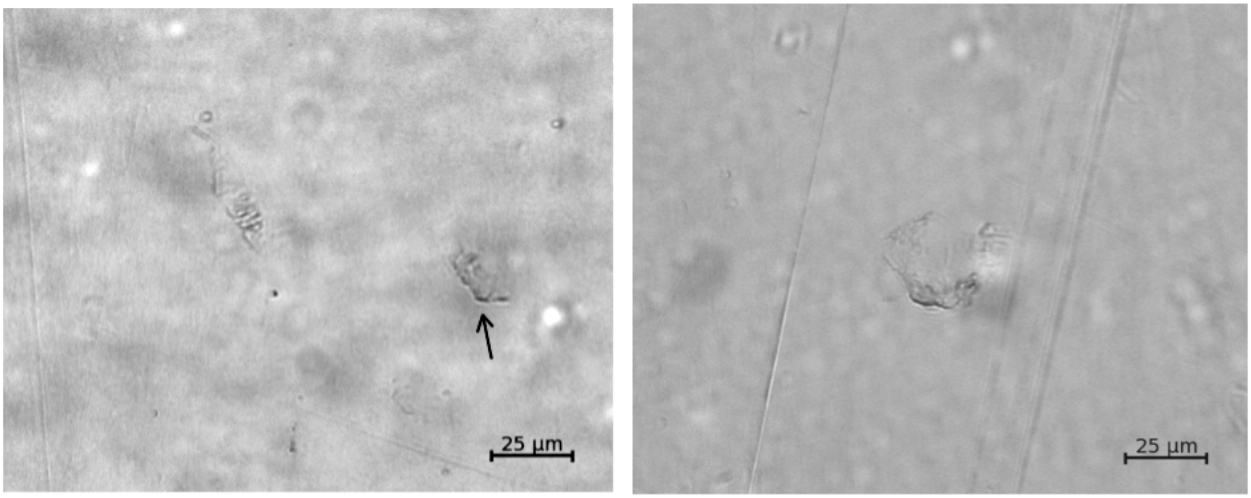

Figure 41 Replica observation of specimen fatigued at S_w+*30*, N = 25% N_f, f = 20 kHz

At both stress levels, fatigue slip bands observation is quite equivalent. In the case of specimen fatigued at f = 20 kHz, only a few grains have fatigue slip bands. Thus, only a small fraction of the material seems to be plastically deformed. In other words, slip bands are created only in a few localized areas. Such a result is in agreement with the low macroscopic plastic strain during ultrasonic test for S15C steel, as reported by Zettl *et al.*[40]. Consequently, the few grains deformed plastically provide an extensive strain inhomogeneity at grain boundaries surrounded by non-plastically deformed grains. Due to such a characteristic behavior, local plastic deformation can be observed, as one indicated by an arrow in Fig. 41.

In order to investigate the slip band behavior in more details, some direct observations of the specimen surface were conducted by SEM. These observations are presented in Fig. 42, for a specimen fatigued at stress level of S_w+*30*, up to 25 % of fatigue life. Unlike the photographs taken

from replica films, loading direction is here horizontally oriented. Two particular types of strain inhomogeneities have been detected. In the case of Type I, a distinct step is formed at only one edge of the grain, as shown in Fig. 18(a). In the other hand, in the case of Type II, an extruded step and an intruded step are formed at a pair of edges of a grain, as indicated in Fig. 18(b). Accordingly, the corresponding grain with the fatigue slip band in Type I is bent, whereas a slight tilted deformation is found in the corresponding grain in Type II.

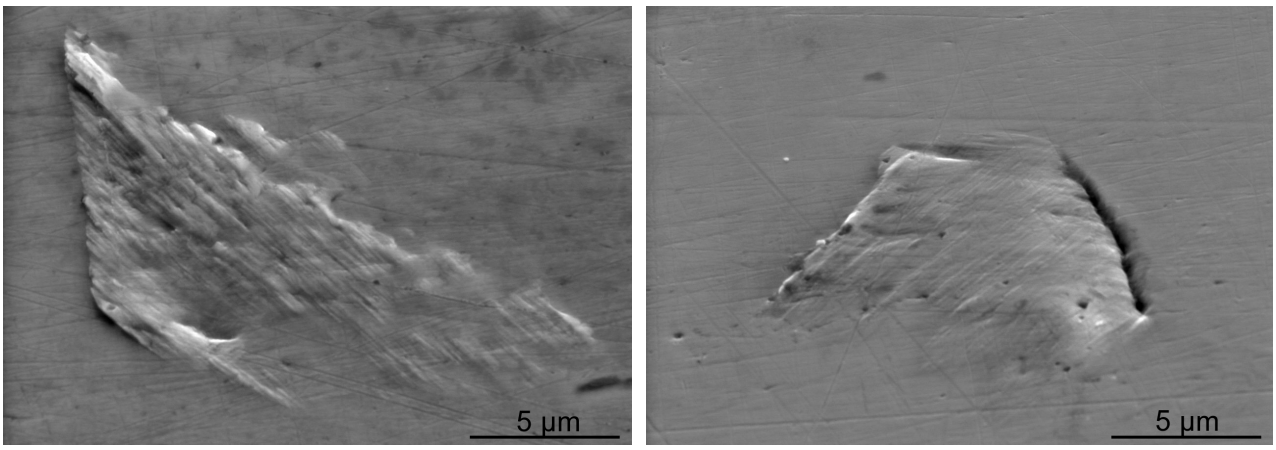

(a) Type I **(b) Type II**

Figure 42 Direct observation of slip bands by SEM, f = 20 kHz, S_w+*30*, N = 25% N_f

We can also point out that this kind of the very dense fatigue slip band structures is less likely to form persistent slip bands (PSB) than the structure of fatigue slip bands found after usual fatigue tests. This point is in agreement with several literatures in this field [45-47], where it is reported that PSB under fatigue loading tends to occur in a specific macroscopic plastic strain range of approximately 10^{-5} to 10^{-3}. According to Zettl *et al.*[40], S15C steel is outside this range for ultrasonic fatigue tests.

4.3.4. Fracture mechanism

4.3.4.1. Classification of number of fatigue cracks

Macroscopic observations of fracture surfaces have been undertaken in this study. Some examples of these fracture surfaces are presented in Fig. 43. Based on these photographs, one can find that failures take place in the mode of surface-induced fractures. No any specimen has failed in the mode of interior inclusion-induced fracture, even under ultrasonic loading tests. A similar behavior has been reported by Zettl *et al.*[40] for a material equivalent to a S15C steel. This aspect can be related to the fact that stress concentration around an inclusion is easily released by the local plasticity in the vicinity of the inclusion due to relative low yielding stress of this kind of steels. Assuming such a distinct drop of stress concentration around interior inclusion, feasibility of the crack initiation there becomes drastically low. As a consequence, fatigue crack tends to initiate at specimen surface.

Figures 43(a), (b) and (c) makes the distinction between a final fracture consecutive to the crack propagation of only one crack, or multiple cracks. Figs. 43(a) and (b) presents the case where multiple cracks were induced on the specimen surface as indicated by several arrows. On the other hand, in Fig. 43(c), only one crack has induced the specimen fracture. Occurrences of single crack

and multiple cracks are distinguished by hollow and solid marks in the *S*-*N* diagram in Fig. 44, respectively. It is not surprising to see that multiple cracks are more likely to happen in the high stress region, whereas a single crack occurs generally at low stress levels. One can note that multiple cracks tends to occur in the life range of $N < 10^6$ cycles, although the single crack mode is observed in some specimens in the case of 0.2 Hz fatigue tests.

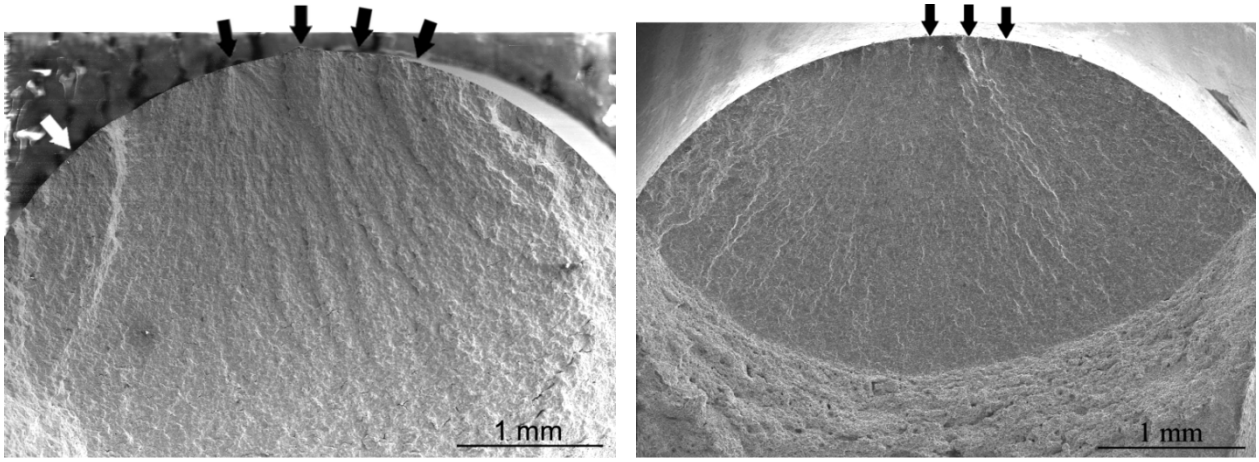

(a) f **= 0.2 Hz,** σ_a **= 240 MPa,** $N_f = 6.29\times10^4$ **(b)** f **= 20 Hz,** σ_a **= 239.2 MPa,** $N_f = 8.14\times10^4$

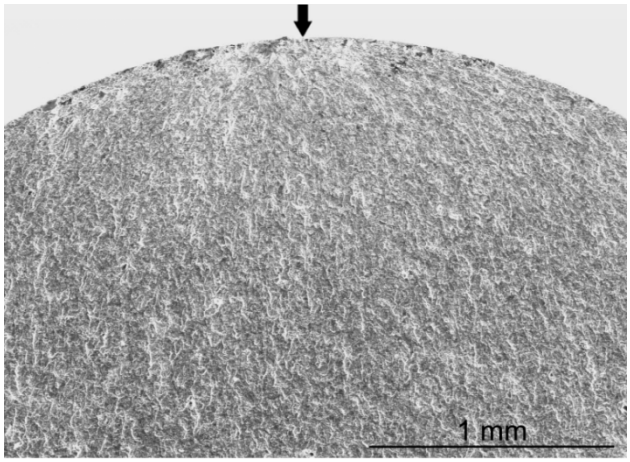

(c) f **= 20 kHz,** σ_a **= 249 MPa,** $N_f = 7.88\times10^7$

Figure 43 Several examples of fatigue fractures

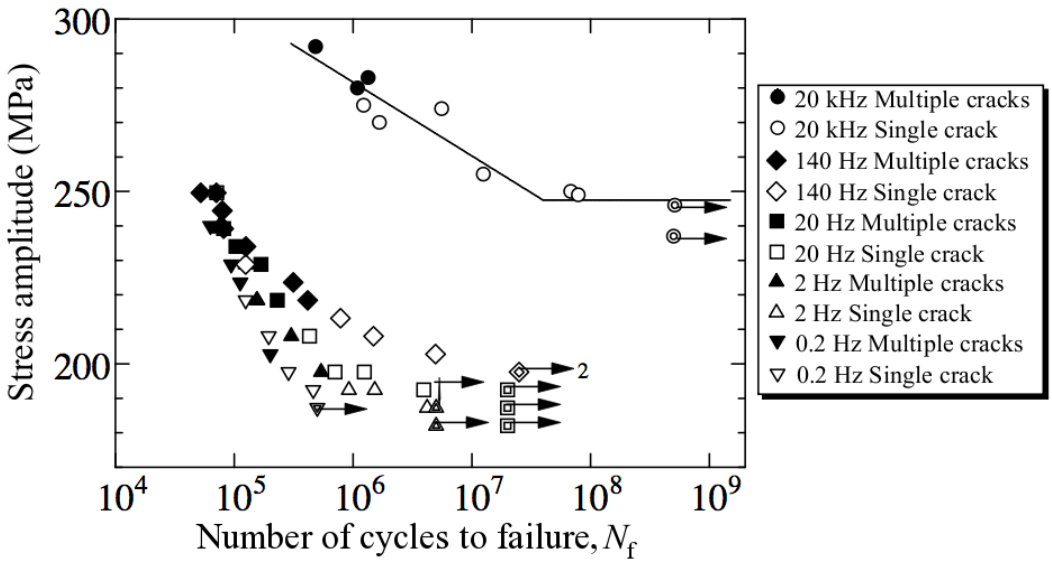

Figure 44 Summary of fracture behavior of S15C steel

4.3.4.2. Crack initiation mechanism

The crack initiation behavior has also been observed by SEM microcopy. Figure 45 presents some pictures taken from a specimen fatigued at f = 0.2 Hz. Main crack initiation site is depicted in Fig. 45(a), where the crack is clearly initiated along slip bands. This intragranular crack initiation mechanism has been observed in a high majority of specimens failed in the usual frequency range of 0.2 to 140 Hz. Nevertheless, some secondary crack initiation sites on the specimen surface reveal also intergranular crack, as in Fig. 45(b). Such type of crack initiation can be attributed to debonding of the weakened grain boundaries introduced during the process of material fabrication. More discussions will be further made in Section 5.4.2.

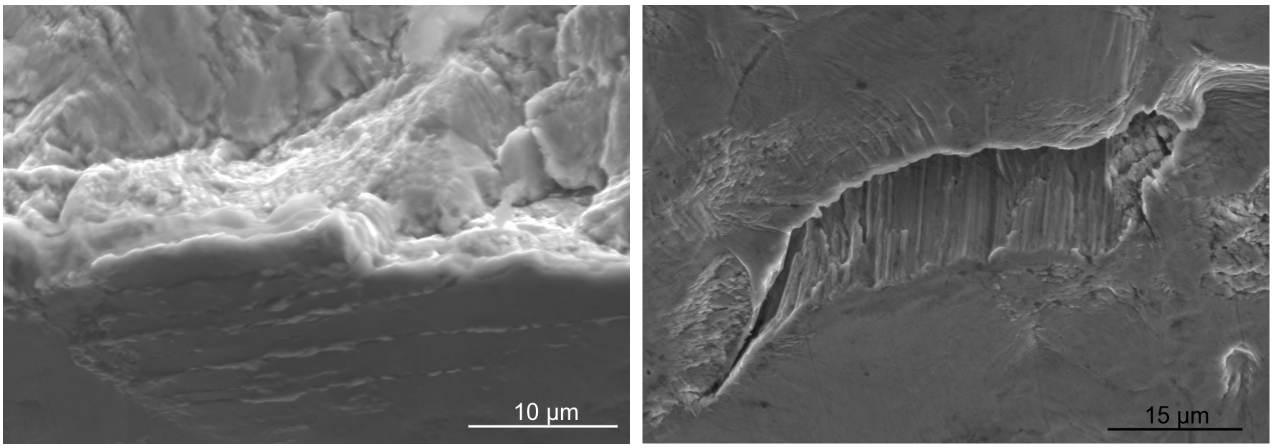

(a) Main crack initiation site **(b) Secondary crack initiation site**

Figure 45 Crack initiation mechanism (f = 0.2 Hz, σ_a = 223.6 MPa, N_f = 1.12×10^5)

In the case of specimens fatigued at 20 kHz, crack initiation mechanism was exclusively intergranular, as depicted in Fig. 46. The crack origin is represented by an arrow "O" and the crack grows along a grain boundary. The early stage crack tends to bifurcate along a pair of grain

boundaries at the triple point “T”, contacting three grains. It is a characteristic aspect that any slip band is not visible on the specimen surface in this micrograph.

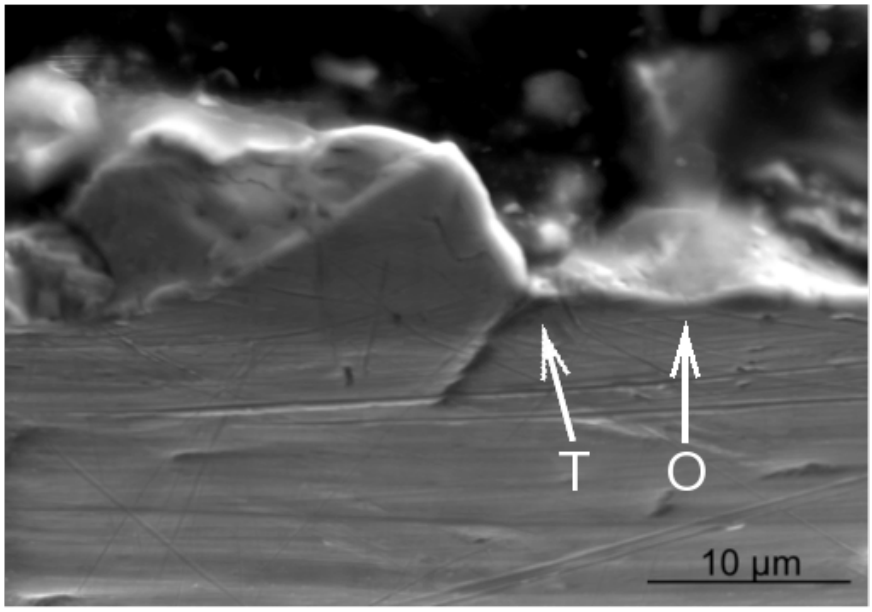

Figure 46 Crack initiation mechanism at ultrasonic frequency (σ_a = 270 MPa, $N_f = 1.67\times10^7$)

Such an intergranular crack initiation behavior has already been reported in several literatures. Zhang *et al.*[48] have found that low carbon steel has an intergranular crack initiation for tests at an average strain rate of 300 s^{-1}. Wang *et al.*[49] have reported that iron at room temperature under ultrasonic loading has an intergranular crack initiation mechanism. Puskar[50] has also reported intergranular crack initiation for an iron fatigued at ultrasonic frequency. Besides, at room temperature, crack initiation can also occur without any slip band on the specimen surface.

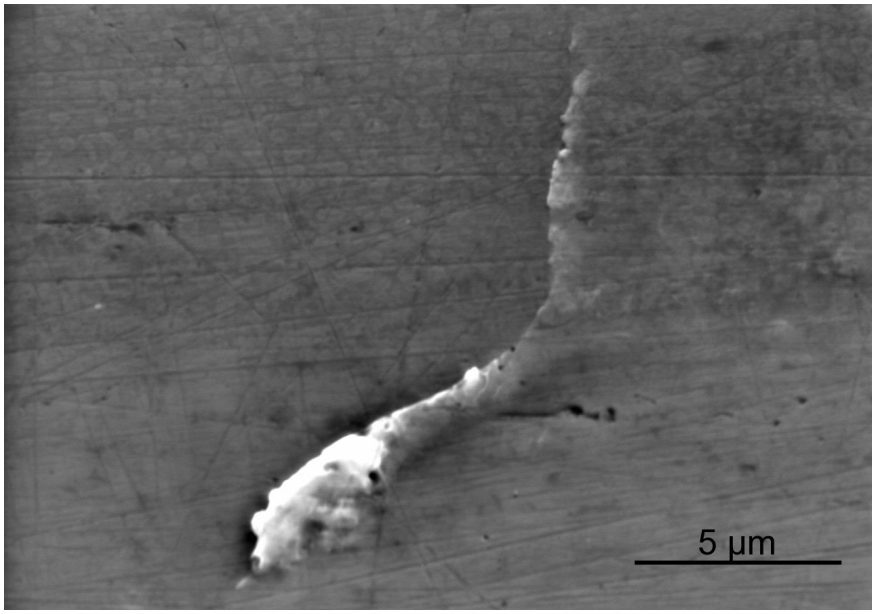

Figure 47 Strain inhomogeneity at GB without slip bands (f = 20 kHz, S_w+*30*, N = 25% N_f)

It should be noted that a few severe strain inhomogeneities, without any slip band, have been found on direct observation on the specimen surface after 25% N_f at a stress level of S_w+*30*.

One typical example indicating such an inhomogeneity is depicted in Fig. 47. This type of inhomogeneity can be induced along some grains boundaries in the long sequence of cyclic loadings, and the most severe site can be the crack initiation site leading the specimen to the fatigue failure.

4.3.5. Local misorientation study

The lattice local misorientation of the ferrite phase has been studied also in the case of fatigue tests performed at 20 kHz. We will check here the misorientation change due to the cyclic loading at 20 Hz, 140 Hz and 20 kHz, for both transversal and longitudinal sections. Results from such a study are expected to give fruitful data in order to better understand the micro-plasticity behavior.

4.3.5.1. Local misorientation in cross section

In the case of the transversal section, experimental procedure to obtain the misorientation distribution was exactly the same as presented in Section 3.2.5 and Section 3.3.3. For such a reason, one can compare the results found in Fig. 30 and corresponding new curves at 20 kHz. Such a comparison is made in Fig. 48.

Obviously, the distributions for specimen fatigued at 20 kHz reveal the lowest values. However, as already discussed in Section 3.4.2, distributions at 140 Hz show higher misorientation values than the values at 20 Hz. In other words, there is no linear relation between the misorientation values and the loading frequency. One can note, as experimental evidence, the distinct decrease of misorientation value, which takes place in the case of ultrasonic loading condition.

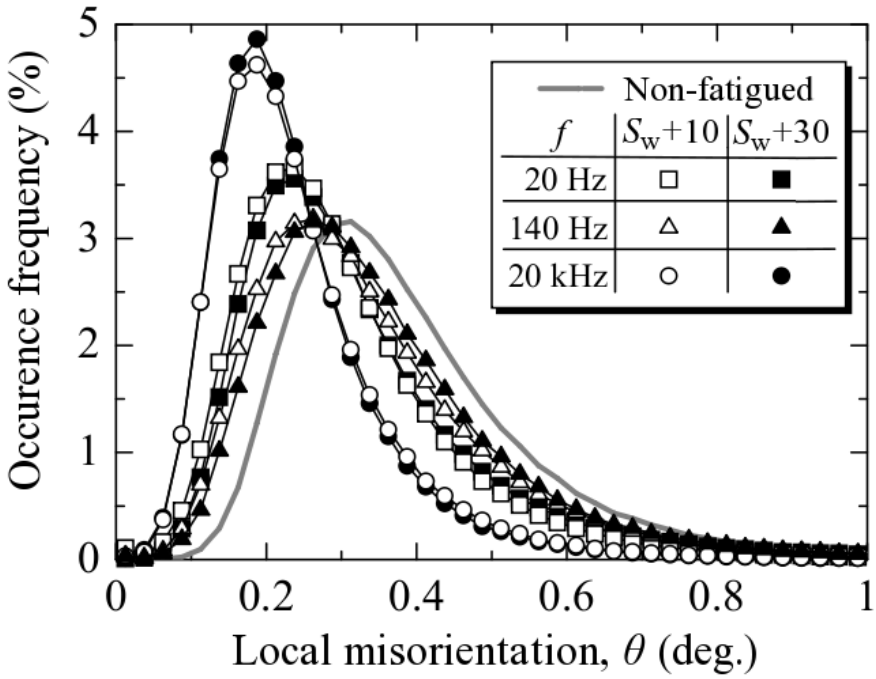

Figure 48 Local misorientation distributions at $N = 25\%\ N_f$, cross section

4.3.5.2. Local misorientation in longitudinal section

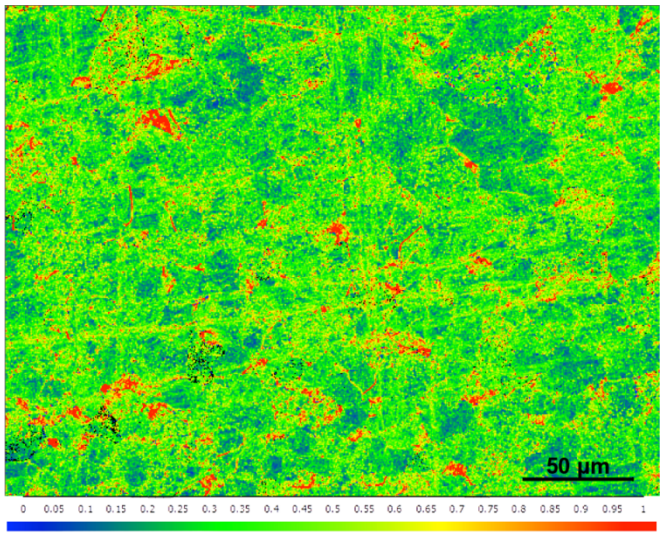

(a) At initial stage

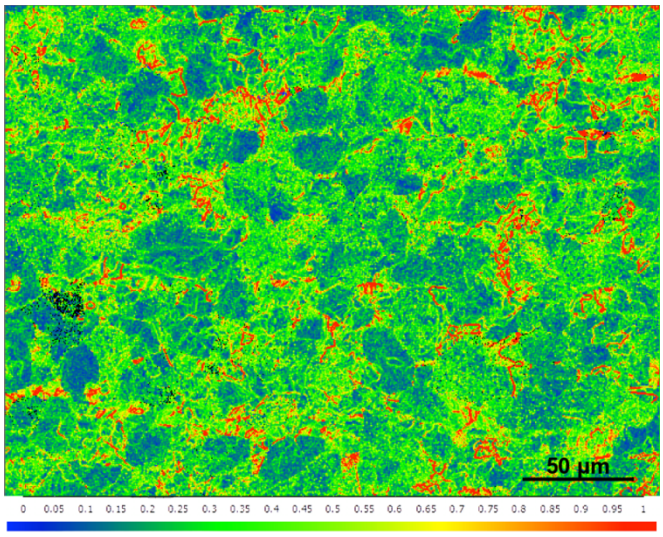

(b) f = 20 Hz, S_w+30, N = 25% N_f

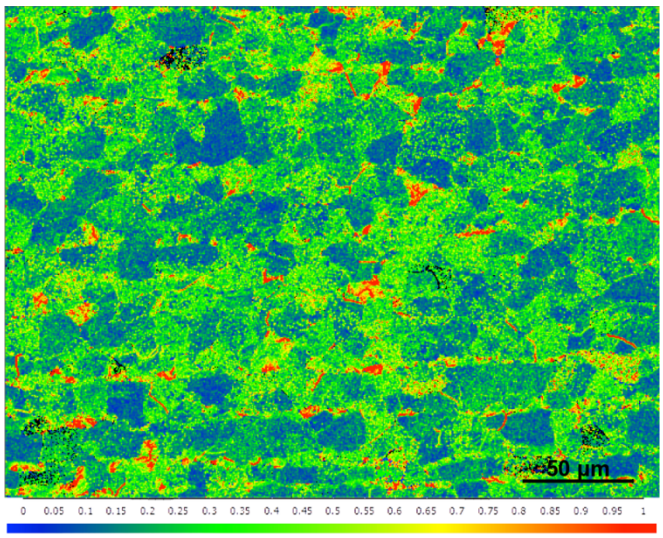

(c) f = 20 kHz, S_w+30, N = 25% N_f

Figure 49 Examples of local misorientation maps, longitudinal section, S15C

A similar study has been made in the case of longitudinal section, in order to verify if such an irregularity of the local misorientation distribution at 20 kHz can be reconfirmed. Calculation of the local misorientation is based on exactly the same procedure as explained in Section 3.2.5. Nevertheless, the spatial step size is slightly different. In transversal axis, step size was equal to 0.3 µm, whereas it is equal to 0.5 µm here. Such a change can affect the local misorientation values[33]. However, change is supposed limited as both step sizes are sufficiently small.

Some examples of local misorientation maps are depicted in Fig. 49 for non-fatigued specimen, after f = 20 Hz loadings and after f = 20 kHz loadings, in (a), (b) and (c) respectively. Loading direction is horizontal for all maps. As indicated at the bottom edge of each map, color scale is representing a misorientation range from 0 to 1 deg. Since very few locations reveal misorientation values larger than 1 deg. in each map, the color scale is adjusted to be sensitive in the range of 0 to 1 deg. for the sake of convenience. One can see that general surface condition is good enough to provide meaningful results.

The local misorientation distributions presented in Fig. 50 are based on the average of 4 different sites. In this work, a class width of 0.025 deg. has been used. In accordance with the results presented in Section 3.3.4, one can see a clear decrease of the local misorientation values after fatigue loadings. In addition, ultrasonic fatigue tests at f = 20 kHz cause the largest decrease. However, it is noteworthy that large occurrence frequency values at f = 20 kHz in Fig. 48 has not been reached in Fig. 50. This aspect can be attributed to the change of the sectional direction in these two studies.

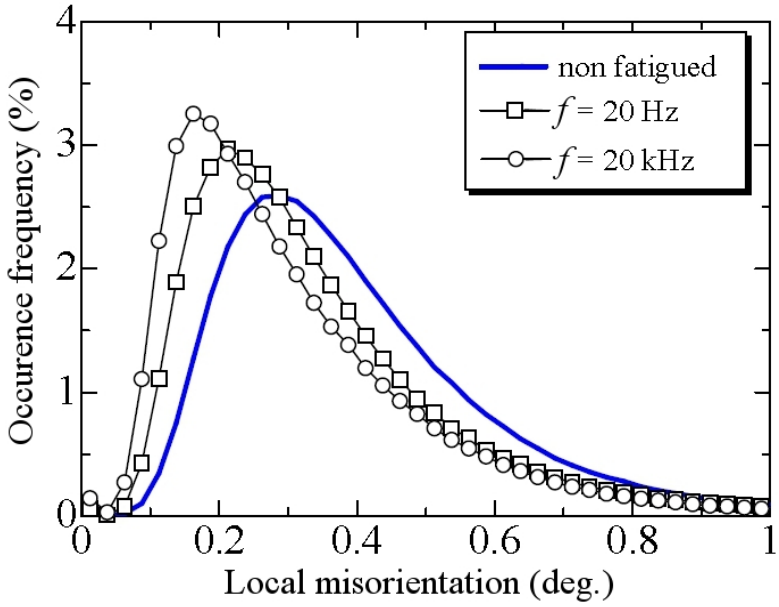

Figure 50 Local misorientation distributions along longitudinal axis, S_w+*30*, S15C steel

4.4. Discussion

4.4.1. Effect of the variation of the yield stress

In a similar way to the section 3.4.1, we will again assess the effect of the strain rate at ultrasonic frequency on the yield stress by normalizing the stress amplitude of the fatigue test by the

lower yield stress at respective strain rate. Due to restriction of the available speed to conduct tensile tests, we are unable to perform a similar test up to a strain rate level equivalent to ultrasonic loading conditions, *i.e.* approximately 10^2 s^{-1} strain rate. Therefore, regression line has been extrapolated up to this value in order to assess the yield stress under 20 kHz fatigue loading condition, as indicated by a dashed line, in Fig. 51. The *S-N* diagram thus obtained is presented in Fig. 52.

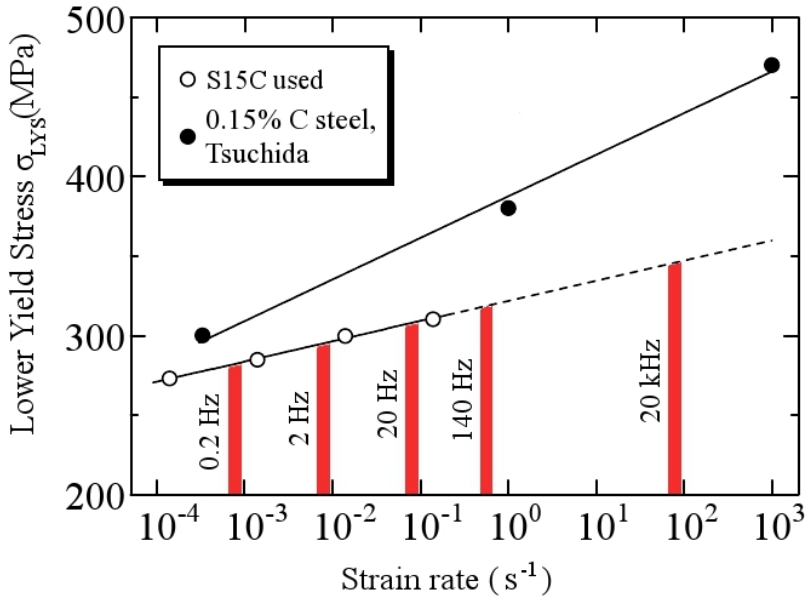

Figure 51 Extrapolation of the yield stress assessment

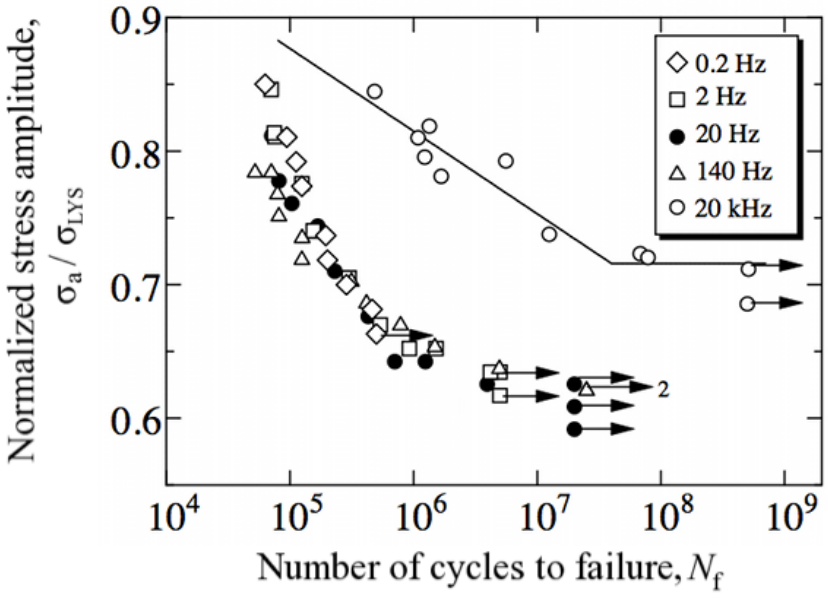

Figure 52 Evaluation of yield stress variation influence on *S-N* properties from 0.2 Hz to 20 kHz

Clearly, Fig. 52 lets appear a gap between *S-N* curves at usual frequencies and ultrasonic frequencies. Even though such a gap is smaller than that observed in usual *S-N* curve diagram in Fig. 34, it still remains a clear difference. Fatigue limit found here at ultrasonic frequency is 0.717, which is a significantly higher value than corresponding ones in usual frequency range around

0.630. In other words, the effect of the strain rate on the yield stress seems to not be able to give an entire explanation of the frequency effect on fatigue properties of low carbon steels up to ultrasonic frequencies.

4.4.2. Analysis of the local misorientation results

As already discussed in Section 3.4.2, local misorientation distribution gives a good indication of the GND density inside the material. According to the results obtained at 20 Hz and 140 Hz, we were able to detect a cyclic softening behavior of the S15C steel. In addition, fatigue tests performed at 20 Hz induce a more severe cyclic softening than at 140 Hz. In such a discussion, it is assumed that the dislocation density, and also GND density, would decrease in the case of cyclic softening

If we are now considering the misorientation distributions from ultrasonic tests, local misorientation has the lowest values in both transversal and longitudinal sections, according to Figs. 48 and 50. Since the lowest misorientation is corresponding to the lowest GND density, S15C steel can be a typical material showing a severe cyclic softening, or a rearrangement of dislocations at 20 kHz.

However, as already mentioned in Section 3.2.2, S15C steel does not show high plastic strain amplitudes at 20 kHz. Thus, the hypothesis of a severe cyclic softening is not so sensible. The drastic loss of local misorientation after 20 kHz fatigue loadings is more certainly related to a significant change of dislocation structures. This fact is correlated to the evidence that *S-N* property at only 20 kHz cannot be normalized by the lower yield stress as a common *S-N* property, in a similar way to the results in the usual frequency range of 0.2 Hz to 140 Hz. In addition, the fatigue slip band formation and crack initiation mechanism is clearly affected by the ultrasonic loading frequency. In other words, the *S-N* property at 20 kHz cannot be fully explained by only the strain rate effect on the yield stress. This aspect suggests us that we have some other potential factors affecting the frequency effect on the ultrasonic *S-N* property of S15C steel.

4.5. Conclusion

The aim this Chapter 4 was to analyze several essential fatigue properties of S15C low carbon steel at ultrasonic frequency of 20 kHz. All these fatigue properties have been compared with the corresponding ones induced by fatigue tests performed at usual loading frequencies. The following points introduce the main findings of this work;

(1) Even though the strain rate induced by ultrasonic fatigue test is as high as 10^2 s^{-1}, it is not sufficient to cause a significant refinement of S15C steel grain structure. This result is in accordance with several literatures, where such a refinement is detected from 10^3 s^{-1} strain rate.

(2) There is a clear effect of the ultrasonic loading frequency on the *S-N* property of S15C steel. Increase of the fatigue strength at 20 kHz is in accordance with some previous outstanding researches.

(3) Instead an intragranular fatigue crack initiation due to fatigue slip band formation for almost all the specimens fatigued in the usual frequency range, specimens failed at ultrasonic frequency show exclusively an intergranular crack initiation. Such a behavior is the direct

consequence of the formation of the slip bands at ultrasonic frequency, which reveals very strong strain inhomogeneities at some grain boundaries.

(4) The local lattice misorientation distributions at 20 kHz present a clear irregularity in both transversal and longitudinal sections. Such an observation urges us to expect a possible dislocation rearrangement inside the ferrite phase of S15C steel.

All the previous points, in addition to the fact that *S*-*N* curve at 20 kHz normalized by the lower yield stress do not match the common *S*-*N* curve in the frequency range of 0.2 to 140 Hz, implies that, in addition to the strain rate effect on the yield stress, some other potential factors should be taken into consideration under ultrasonic loading condition. Thus, the fatigue properties of S15C steel at 20 kHz are not fully understood.

4.6. Future plans

The future plan consists to undertake the observation of the dislocations inside the ferrite grains of S15C low carbon steel. It is expected to found some typical dislocation arrangements, which explain the distinct loss of local misorientation values.

If such a dislocation rearrangement is found, it would give very precious indications in order to give the reason(s) of the change of several fatigue properties reported in this Chapter 4, as the fatigue slip band formation or the crack initiation mechanism. Finally, it could be the final step to understand the longer fatigue lives obtained at ultrasonic loading frequency.

Chapter 5. The low temperature regime and its consequences on the fatigue properties of S15C low carbon steel[vi]

5.1. Objectives of the further studies

The main objective of the works presented in this Chapter 5 is to explain in details the reason of the high discrepancy between *S-N* properties of S15C low carbon steel from fatigue tests at usual frequencies (from 0.2 to 140 Hz) and ultrasonic frequency at 20 kHz.

Indeed, only a slight frequency effect in the usual frequency range can be detected from the *S-N* properties. As presented in Chapter 3, the reason of this effect is a slight change of the micro-plasticity behavior, causing a variation of the cyclic softening effect. Nevertheless, in the usual frequency range, other essential fatigue properties are similar, as the fatigue slip band formation and the crack initiation mode, already discussed in Chapter 4.

However, specimens fatigued at 20 kHz have revealed some clear irregularities on the fatigue properties studied in the Chapter 4. Thus, all these particular phenomena have to be explained in order to fully understand the *S-N* properties in the wide frequency range from 0.2 Hz to ultrasonic frequency of 20 kHz. According to the lattice local misorientation study, dislocation observations are expected to give fruitful results to indentify such phenomena.

Finally, a second objective is, if possible, to give a potential reason of the absence of such a significant effect of the ultrasonic frequency for other types of structural steels with higher carbon content.

5.2. Experimental details on the dislocation observation

In order to obtain direct observation of dislocations, several techniques are available. Recently, the Electron Channeling Contrast Imaging (ECCI) technique is more and more used, as it requires only an EBSD device with some specific configurations. This technique is supposed to allow a larger observation surface than usual TEM (Transmission Electronic Microscope) technique. Nevertheless, in the present study, we were unable to find dislocations by ECCI method. As a consequence, usual TEM method has been chosen instead.

More precisely, dislocation observations have been performed simultaneously by two different devices: *JEOL JEM 2010* TEM and *Hitachi HD-2700* STEM, both with an acceleration voltage of 200 kV. Preparation of specimens was slightly different to perform the dislocation observations. After specimen has been fatigued at the chosen configuration, center portion has been sliced in the cross-section direction. Then the samples were polished to obtain a thickness of 0.15~0.20 mm.

In the case of *JEM 2010* TEM, final preparation of the specimens requires perforation by etching method (electrolytic polishing) with 90% acetic acid / 10% hydrochloric acid solution at 20

[vi] [International Journal of Fatigue][Work in progress]© Elsevier Ltd.

V. On the other hand, samples for observation with *HD-2700* TEM have been prepared using FIB cut and finishing by argon ion milling at 500 V.

Observations are performed for samples before and after a definite number of cycles depending on the fatigue strength according to *S-N* data diagram. More precisely, we have undertaken observation after 5 %, 10 % and 25 % of fatigue life at the respective loading frequencies. Specimen fatigued at 0.2 Hz, 20 Hz, 140 Hz and naturally 20 kHz loading frequencies will be observed here, for both stress levels S_w+10 and S_w+30, already presented in Table 4.

5.3. Dislocation observation

Before introducing the dislocation structure obtained after ultrasonic fatigue tests, let us introduce the results obtained before fatigue loading and after fatigue tests performed in the usual frequency range of 0.2 Hz to 140 Hz.

5.3.1. Initial condition of the dislocation structure

As already mentioned, the initial condition of the S15C steel used here is a hot-rolled bar. It is thus expected to get a relatively dense dislocation structure. Overview of the dislocation structure obtained is depicted in Fig. 53. More particularly, it has been found that, a cell structure with unsharpened walls has been found mainly in the vicinity of the grain boundaries as presented in the top right corner of Fig. 53 and in Fig. 54. Nevertheless, low dislocation density areas can be also pointed out, as in the bottom left corner of Fig. 53 and in Fig. 55. Such a structure of hot-rolled low carbon steel is quite equivalent to the structure found by Deva *et al*.[51].

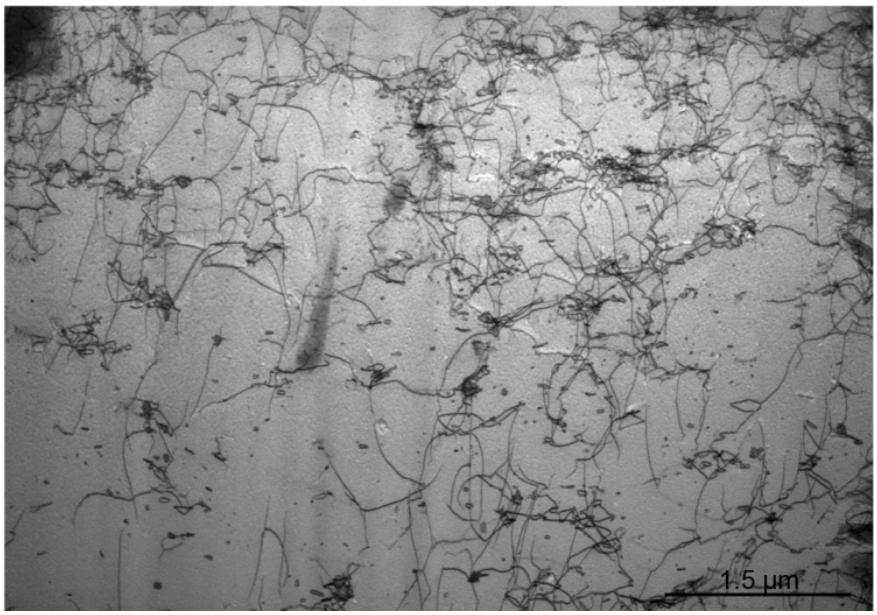

Figure 53 Overview of dislocation structure before fatigue process

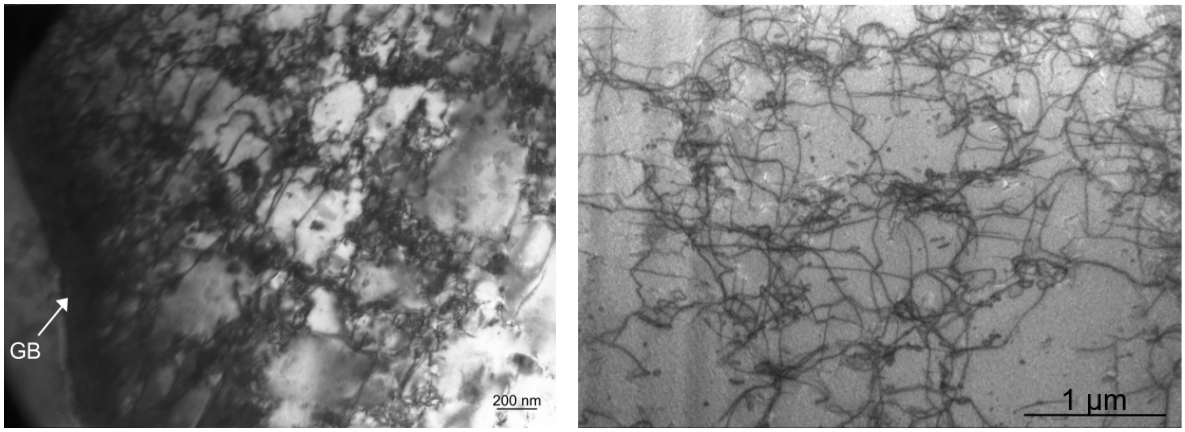

(a) Obtained by TEM **(b) Obtained by STEM**

Figure 54 Cell structure with unsharpened walls

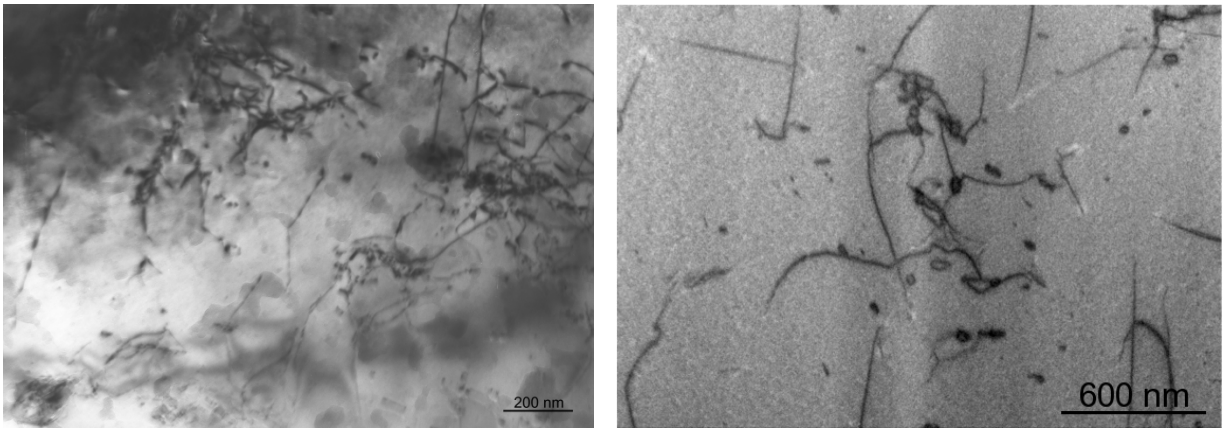

(a) Obtained by TEM **(b) Obtained by STEM**

Figure 55 Low dislocation density locations

5.3.2. Dislocation structure after fatigue test at usual frequencies

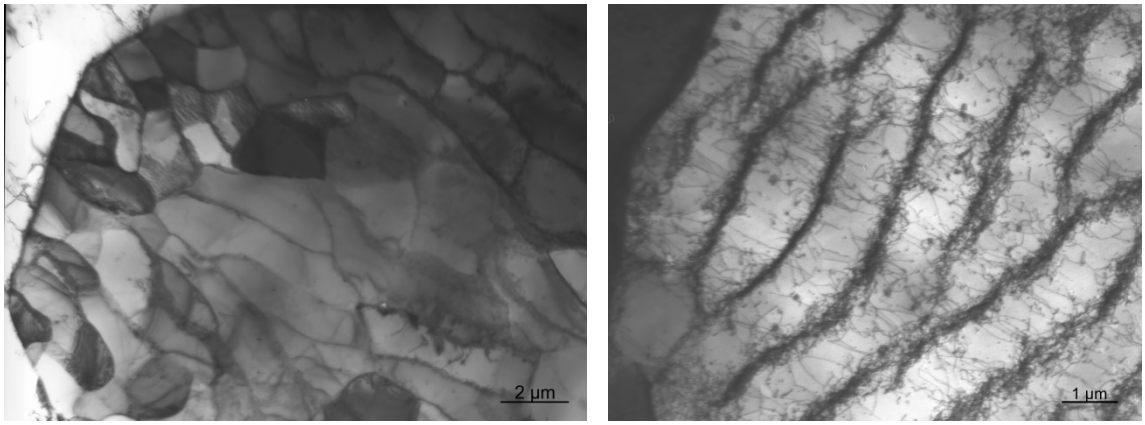

(a) Cell structure **(b) Ladder structure**

Figure 56 General dislocation structures induced by fatigue process (f = 0.2 Hz, S_w+30, 25 % N_f)

An overview of the structures found is shown in Figs. 56 and 57, taken from a specimen fatigued at a stress level of S_w+30, up to 25 % of fatigue life, at a loading frequency of f = 0.2 Hz and f = 140 Hz, respectively. Figure 56(a) let appear a clear grain substructure within the whole grain. One can note that there are very few free dislocations inside distinct dislocation cells. One the

other hand, Figure 56(b) depicts a well-known ladder structure where a significant number of screw dislocations can be seen between walls. Similar observations can be found for f = 140 Hz, as depicted by Fig. 57. Consequently, change of loading frequency from 0.2 to 140 Hz does not induce a significant effect on the dislocation structures of S15C steel. Weisse *et al.*[52] and Min *et al.*[53] have also found similar dislocation structures of low carbon steels after cyclic loading.

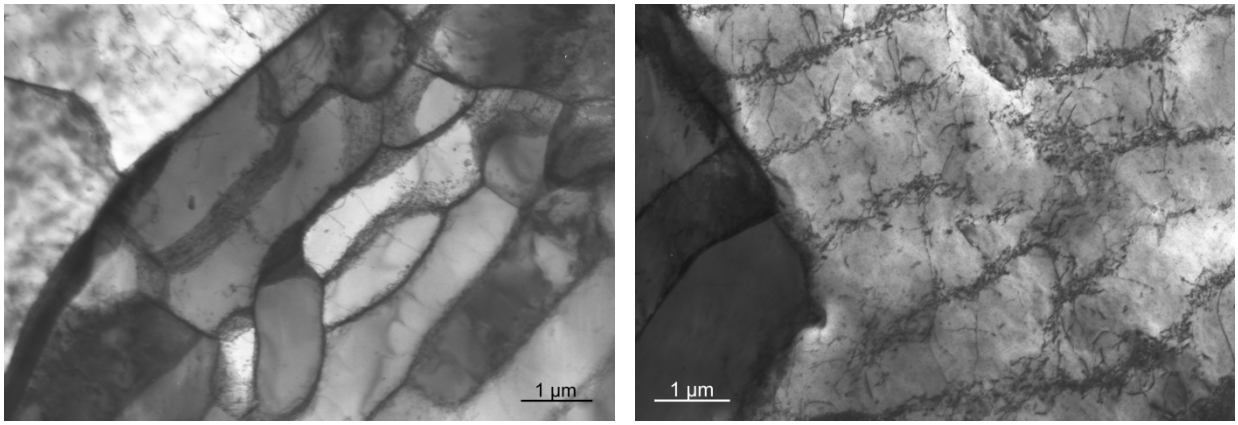

(a) Cell structure **(b) Ladder structure**

Figure 57 General dislocation structures induced by fatigue process (f = 140 Hz, S_w+*30*, 25 % N_f)

Therefore, dislocation structures found after cyclic loading in the usual frequency range from 0.2 Hz to 140 Hz are similar and in agreement with several results found in some literatures.

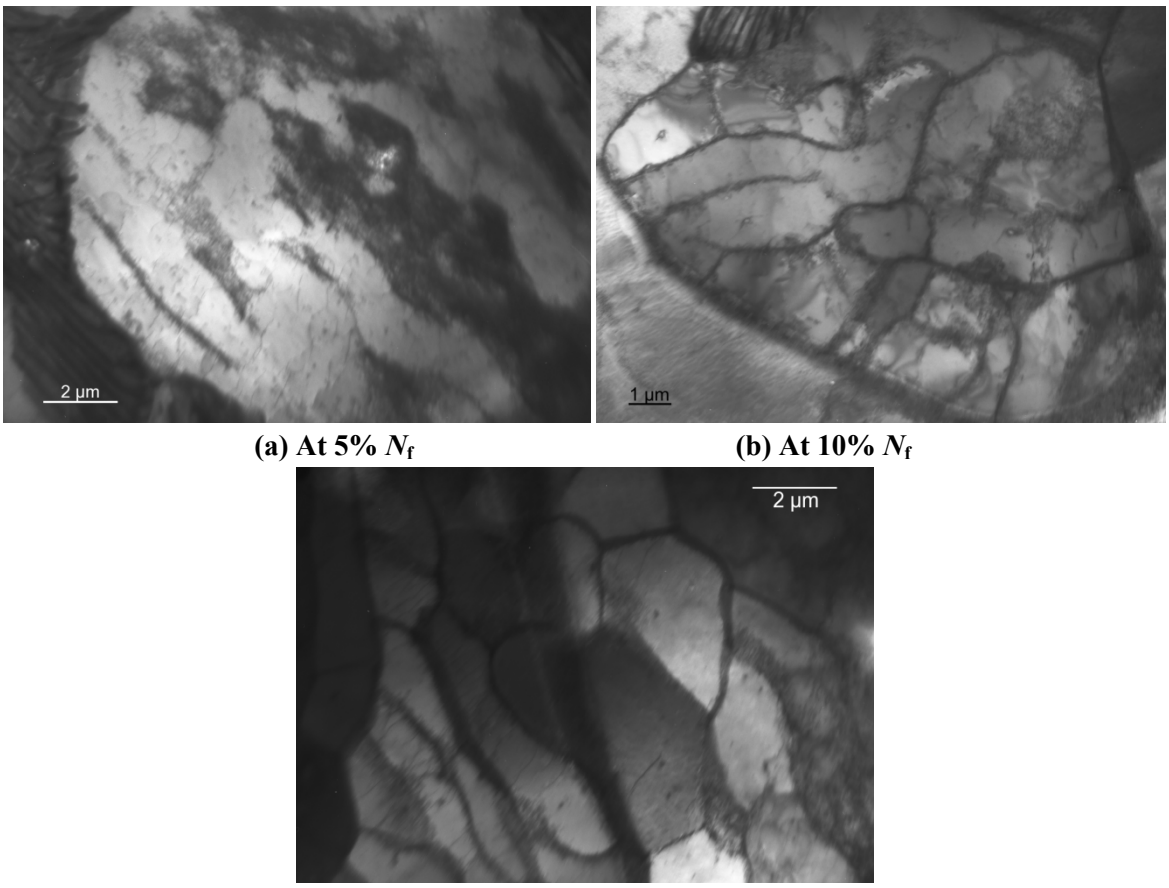

(a) At 5% N_f **(b) At 10% N_f**

(c) At 25% N_f

Figure 58 Effect of cyclic loading on dislocation density inside dislocation walls (f = 20 Hz, S_w+*30*)

Let us make a focus on the changes of dislocation structure, and more particularly about the cell substructure, at the respective fatigue stages of 5 %, 10 % and 25 % of the fatigue life. Discussions here are based on micrographs observed at the respective stages for different specimens tested at f = 20 Hz, with a stress level of S_w+*30*. Figure 58(a) presents a typical cell structure obtained at the stage of 5% N_f, cells are already initiated, but some walls are not so clear. Thus a lot of dislocations are widely distributed over some cells appearing as black areas. At the stage of 10 % N_f, cell walls are more sharply formed, as one can see in Fig. 58(b). Finally, at the stage of 25 % N_f, cell walls are entirely formed, as seen in Fig. 58(c). Such a change of the walls density is an important hint of the dislocation annihilation inside every cell due to the cyclic loading, as pointed out by Chai *et al.*[54]. It is also found that this change of dislocation structure is certainly linked with the S15C steel cyclic softening already verified in our previous work, in the Chapter 3.

5.3.3. Dislocation structure induced by ultrasonic fatigue test

As expected from the results obtained from the misorientation distribution already discussed in our previous work (Chapter 4), ultrasonic loading on the S15C steel induces a totally different dislocation structure. Figure 59 presents the dislocation structure observed for a specimen fatigued at S_w+*30* and 25 % N_f. One can find obviously that the structure obtained in Fig. 59(a) do not reveal clear wall. Details of this structure are given in Fig. 59(b), representing the area marked by the square in Fig. 59(a). One can see long screw segments belonging here to two different slip systems, with some dislocation forests occasionally formed.

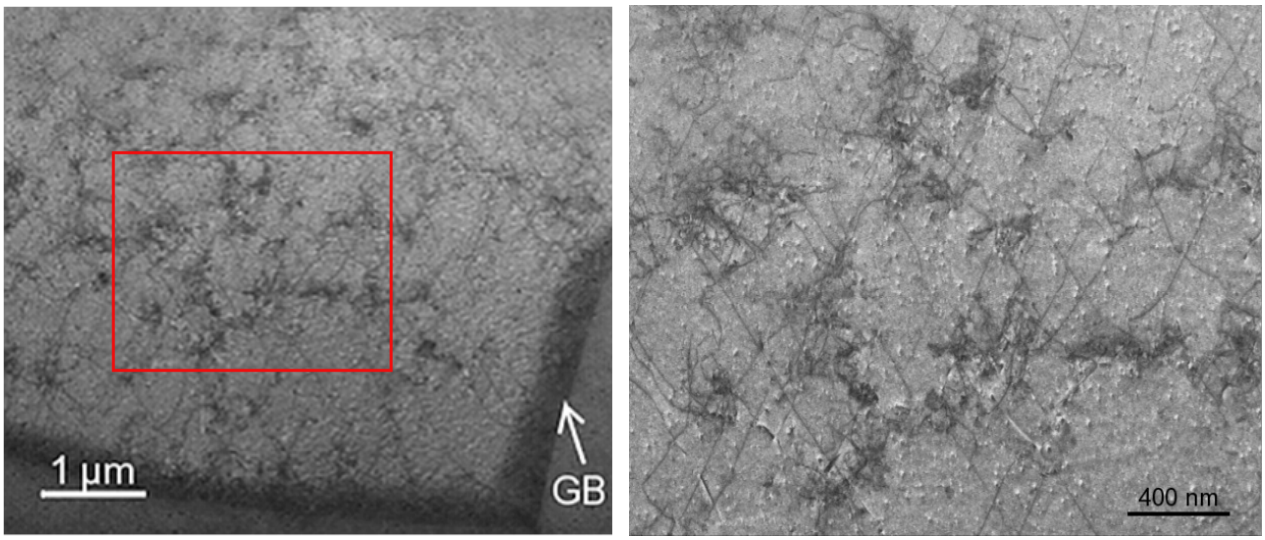

(a) Obtained by STEM **(b) Obtained by TEM**

Figure 59 Dislocation structure induced by ultrasonic loading, S_w+*30* at 25% N_f

Such kinds of dislocation structure are induces by specific dislocation multiplication processes as reported by Saka *et al.*[55]. In this section, we will make a focus on the dislocation multiplication processes observed on iron samples, at an operative temperature of -120°C or -90°C, and compare these multiplication processes with dislocation structures obtained after cyclic loading at ultrasonic frequency here. Even though more recent *in situ* experiments are available, with a better observation resolution, the work done by Saka *et al.* is an outstanding original result on dislocation multiplication mechanisms.

Some dislocation multiplication processes described by Saka *et al.* have been observed in dislocation observation of S15C steel after ultrasonic loadings, as shown in Figs. 60, 61, 62, 63 and 64. These figures are composed of one TEM micrograph of S15C steel fatigued at f = 20 kHz up to 25 % N_f, and a schematic illustration of the multiplication mechanism proposed by Saka *et al.*, in (a) and (b), respectively. Presence of such particular multiplication processes after fatigue tests at ultrasonic frequency at room temperature will be discussed in Section 5.4.

Figure 60 introduces a multiplication process due to the jog J_1 of the screw dislocation itself, which tends to retard the motion and to bow out the segment AJ_1. In the case of the top red square, screw dislocation has not already bowing out, even though a jog can be detected as a slight angle appears. The bottom red square indicates a dislocation bowed by the jog.

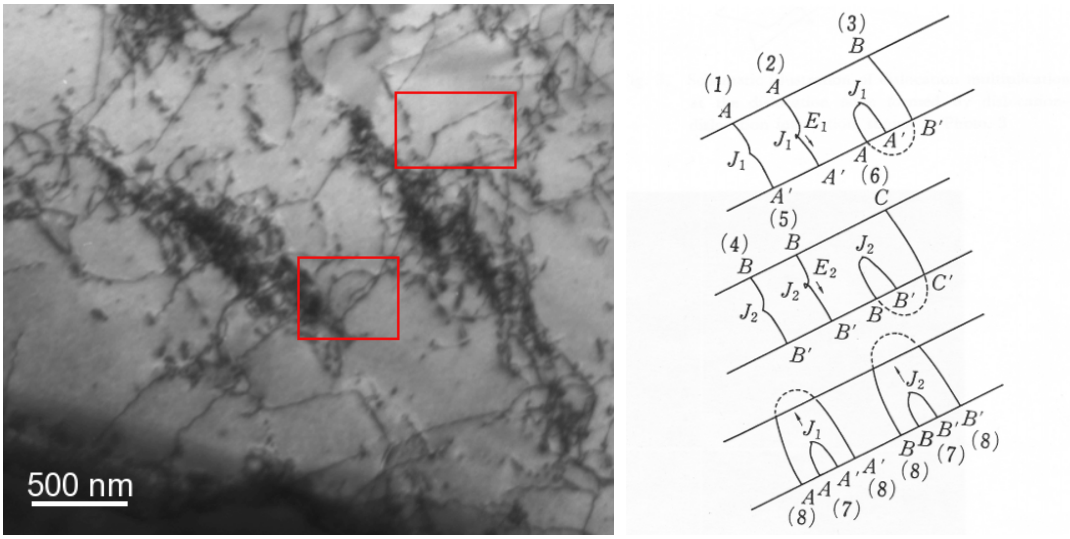

(a) Observation by TEM **(b) Schematic illustration**

Figure 60 Multiplication mechanism at super jogs on screw dislocations, S15C steel

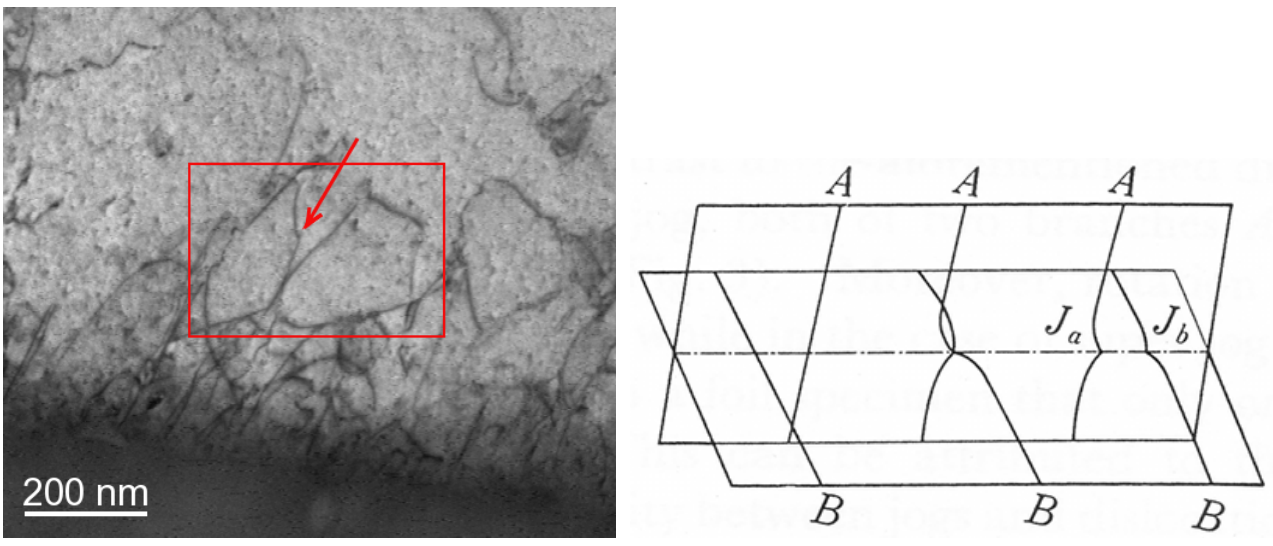

(a) Observation by STEM **(b) Schematic illustration**

Figure 61 Formation of jogs by dislocation-dislocation interaction, S15C steel

One possible mechanism to create these jogs on the screw dislocation is presented in Fig. 61. It consists to formation of jogs due to the interaction of two screw dislocations belong to different slip systems, as depicted in the schematic illustration Fig. 61(b). In the STEM micrograph

in Fig. 61(a), one can see obviously the location of the interaction between two dislocations, indicated by the red square. Slightly higher to this location, a jog has been formed due to this interaction, as pointed out by the arrow.

Another possible multiplication process of the dislocations is due to the interaction of two dislocations, in a way rather similar to the Frank-Read source. Due to this interaction, the segment *AB* will bow out, as illustrated in Fig. 62(b). In order to better understand the overall situation, letters with similar meanings have been reproduced in the STEM micrograph, in Fig. 62(a).

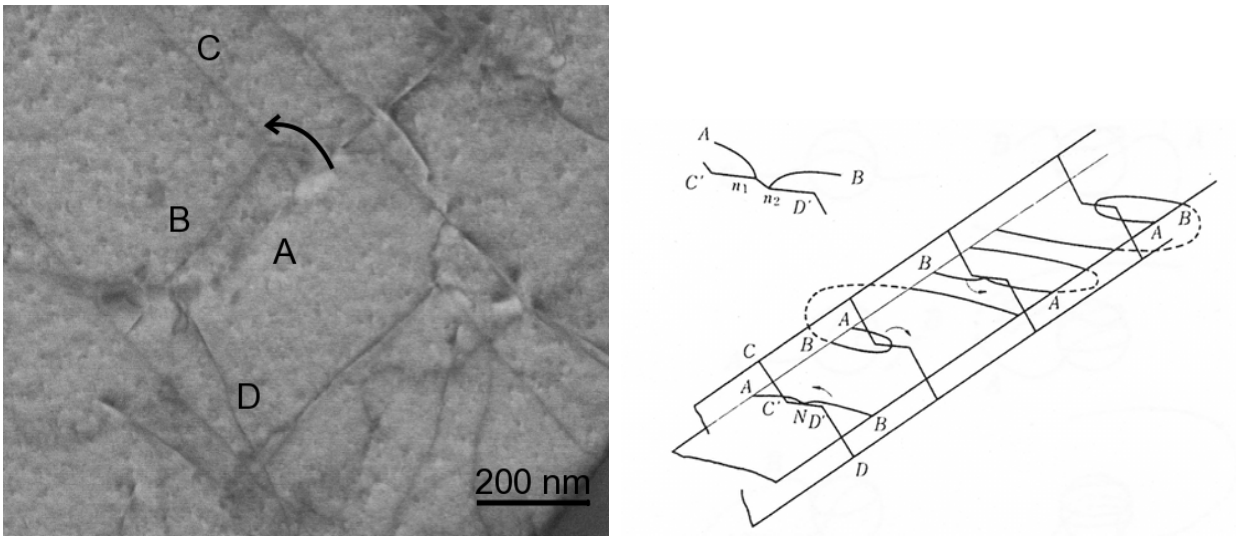

(a) Observation by STEM **(b) Schematic illustration**

Figure 62 Multiplication mechanism due to dislocation-dislocation interaction, S15C steel

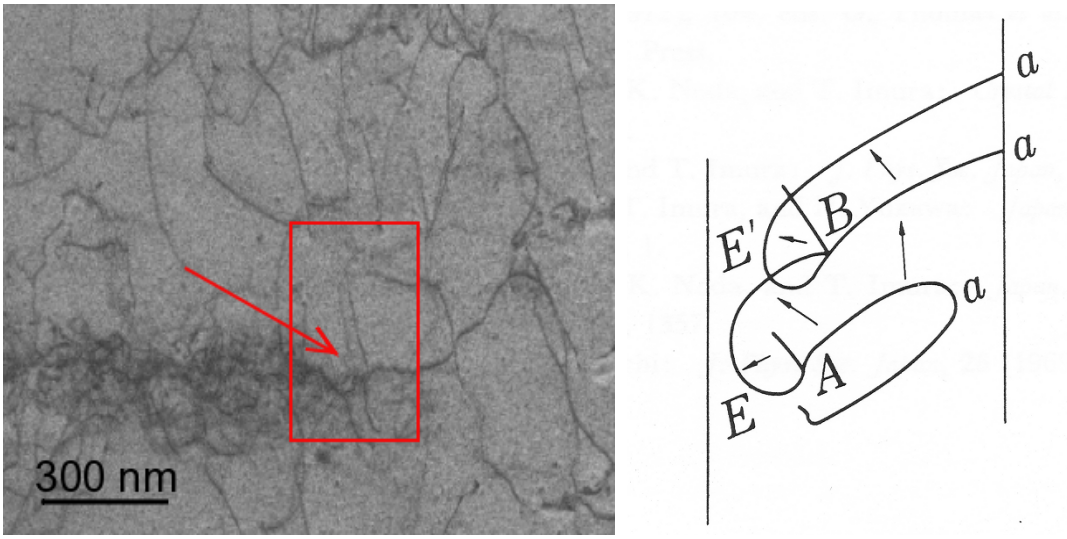

(a) Observation by TEM **(b) Schematic illustration**

Figure 63 Multiplication mechanism at the grown in sub-boundary, S15C steel

The dislocation multiplication mechanism presented in Fig. 63 is usually observed as a result of the interaction of a moving dislocation with one of the forest dislocation, which constitute a sub-boundary. In the illustration Fig. 63(b), the screw segment *Ea* met a forest dislocation *B*, and thus stopped. Resulted screw segment *Ba* bows out around *B*. Then the dislocation segment *E'Ba* rotates around B, multiplying dislocations. This mechanism is really difficult to detect as it occurs near a forest of dislocations, and thus where dislocation concentration is already relatively high.

Nevertheless, Fig. 63(a) highlights a dislocation multiplication process due to the presence of a dislocation loop pointed out by the arrow.

Influence of a particle inside ferrite lattice will increase the cross-glide of screw dislocation, as shown in Fig. 64(b). The two branches of the screw dislocation *A* and *B* rotated independently around this particle *P*, creating a new dislocation for each rotation. This aspect is presented in the red rectangles, in Fig. 64(a).

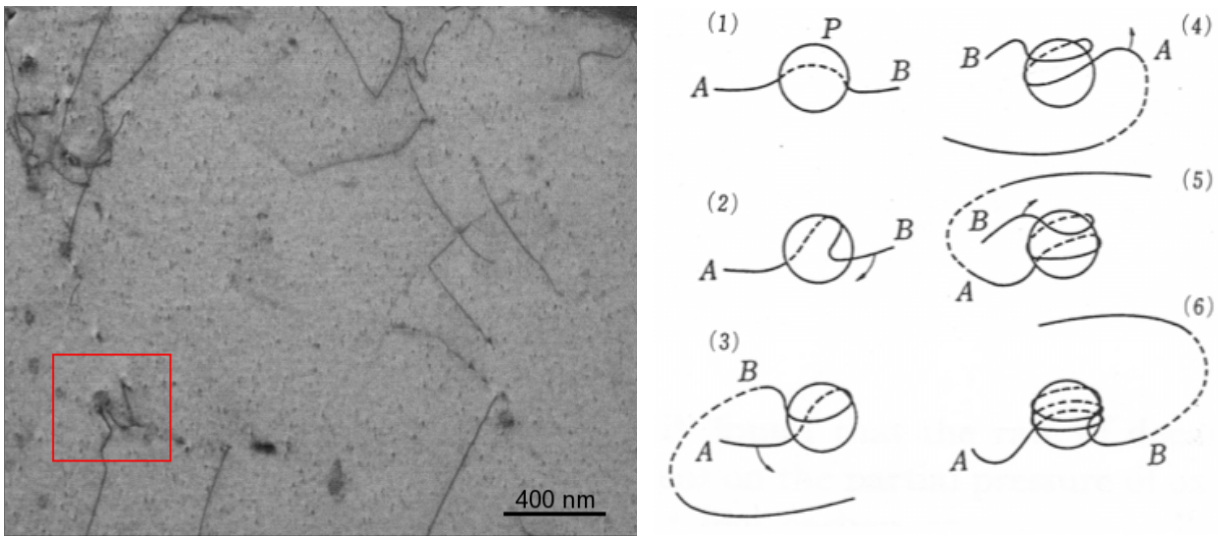

(a) Observation by STEM **(b) Schematic illustration**

Figure 64 Multiplication mechanism due to inclusion particle, S15C steel

Thus, one can note that the overall dislocation structure of S15C steel is extremely sensitive to the loading frequency. Conventional fatigue tests performed at 0.2 to 140 Hz let appear similar dislocation structures, particularly ladder or cell structures. On the other hand, ultrasonic loading induces long screw dislocations, with possibly some dislocation forests rather than clear walls. A detailed analysis of the dislocation multiplication processes at ultrasonic frequency has pointed out significant agreement with processes observed for iron uniformly deformed at low temperature[55].

5.4. Discussion

5.4.1. The Seeger theory and related works

This theory deals with a special plastic property of B.C.C. materials, first proposed by Seeger[56], in 1954. According to this theory, the flow stress σ consists of a sum of an athermal component σ_G , and a thermal component σ^*, as presented in Eq. (11). σ_G is indeed the stress requires for a gliding dislocation to bow out and to overcome the elastic interaction with other dislocations. As a consequence, this athermal component is related to the density of dislocation ρ and their arrangement. The thermal component σ^*, frequently so-called the "effective stress", is a supplement stress needed to allow screw dislocations to glide at a given temperature and strain rate. This thermal component is practically negligible above a transition temperature T_0 (or below a transition strain rate $\dot{\varepsilon}_t$), given in Eq. (12).

$$\sigma = \sigma_G + \sigma^*(\dot{\varepsilon}, t) \quad (11$$

The transition temperature T_0 and the transition strain rate $\dot{\varepsilon}_t$ are linked each other, in accordance with Eq. (12)

$$U_0 = kT_0 \ln\left(\frac{\rho A b \nu_0}{\dot{\varepsilon}_t}\right), \tag{12}$$

where

U_0: activation energy for jog formation at zero stress,
k: Boltzmann's constant,
ρ: density of mobile dislocations,
A: displacement surface done by a dislocation after intersecting a screw dislocation,
b: Burger vector norm,
υ_0: Debye's frequency.

In the literatures, this particular phenomenon of B.C.C. materials have been most of the time studied under tensile tests, by decreasing the temperature as low as 77 K (liquid nitrogen), for example. Thus, this particular region where σ^* is not negligible has been so cold the "low temperature regime". Such a region can be reached at higher temperature, if a sufficient high strain rate is applied to the material, in accordance with Eq. (12). In the present work, for the sake of coherency with such literatures, authors will use the same expression, even though all experiments, and particularly fatigue tests, are actually performed at room temperature.

Literatures have already discussed some particular properties of B.C.C. materials placed into this low temperature regime. One of these properties is related to the multiplication processes of dislocations, as clearly shown by Saka *et al.*[55] in the Section 5.3.3. Since B.C.C. structure introduces deep valleys into Peierls energy function aligned with Burgers vector ***b*** directions[57], dislocation multiplication processes can be affected. In the low temperature regime, dislocations tend to adopt low-energy configurations, and thus cannot overtake the amount of energy needed to glide in another valley as described in Fig. 65. It leads to an essential property of dislocation motion in the low temperature regime: mobility of edge dislocations is higher than mobility of screw dislocations. For a Fe-Si alloy, J.R. Low *et al.*[58] have found that edge dislocation mobility can reach a 25 times higher value than screw dislocation mobility in this domain.

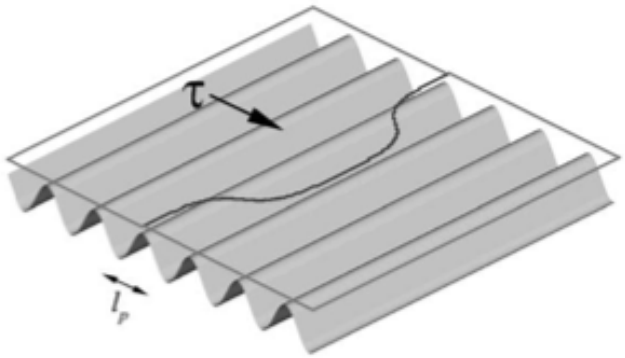

Figure 65 Illustration of Peierls valley and kink mechanism in B.C.C. structure[57]

As a consequence, dislocation observation of a B.C.C. material placed into this low temperature regime let appear long screw segments[58-60]. It is thus not possible to get a dislocation structure composed with clear screw and edge dipoles, as cell or ladder dislocation structures, if the gap between screw and edge dislocation mobilities is large enough. Recently, by the means of *in situ* TEM observation, Caillard[61] has reported another screw dislocation displacement in pure iron at very low temperature based on "jerky motions", where the screw segment jumps over several Peierls valley. Such a motion mechanism will not be further discussed as only detected in pure iron samples[62].

In the case of applicability of this theory into fatigue test experiments, Mughrabi *et al.*[59] have performed fatigue tests, at room temperature on pure iron specimens, to determine the effect of the (average) strain rate on dislocation structure. It has been found that dislocation structure is extremely sensitive to the strain rate, according to the Seeger theory. On the one hand, below the transition strain rate $\dot{\varepsilon}_t$ (approximately 10^{-4} s^{-1} under these conditions), dislocation cell dipole structures can be clearly seen, which is a proof of equivalent screw/edge dislocation mobility. On the other hand, the same material fatigued at a strain rate larger than $\dot{\varepsilon}_t$ will leads to long screw dislocation observations, characteristic of the low temperature regime, as depicted in Fig. 66.

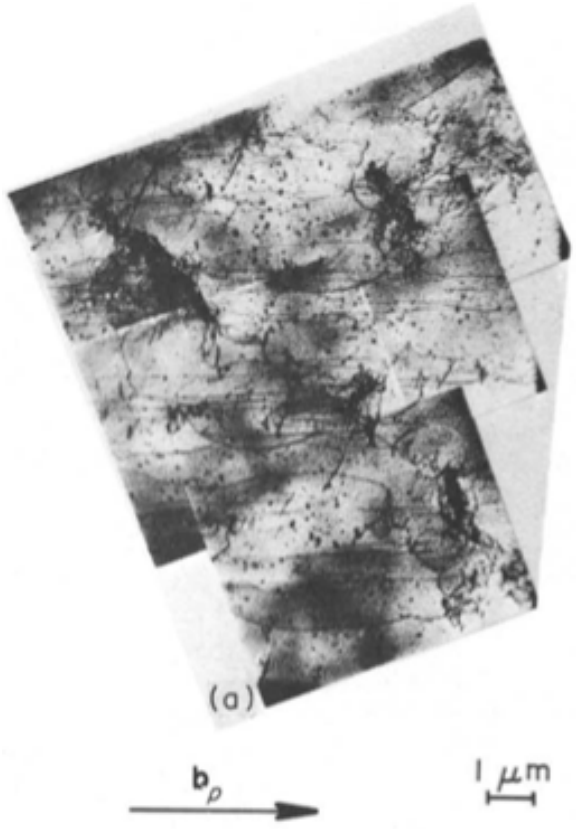

Figure 66 Long screw dislocations after cyclic loading, $\dot{\varepsilon} > \dot{\varepsilon}_t$, iron[59]

A second property affected by this low temperature regime is the fatigue crack initiation mechanism. Indeed, Magnin *et al.*[63], Guiu *et al.*[64], Sommer *et al.*[65] and Mughrabi[66] have identified a transition of the fracture initiation, in the case of pure iron. Outside the low temperature regime, transgranular fracture initiation phenomenon has been reported, as illustrated in Fig. 67(a).

Such a mechanism is due to the local stress concentration at slip bands. However, if the pure iron specimen is placed into the low temperature regime, intergranular fracture initiation mechanism is predominant, as shown in Fig. 67(b). Such a transition is explained by a significant stress asymmetry and a large shape change. Shape change will be particularly effective at free surface of the specimen, implying deformation. Since these deformations differ according to the grain orientations, it results incompatible deformations at the grain boundaries, and thus favors intergranular fracture initiation mechanism. Sommer *et al.*[67] have proposed also that this mechanism could be related to highly inhomogeneous strain level between different grains, even though only a very small fraction of grains is plastically deformed.

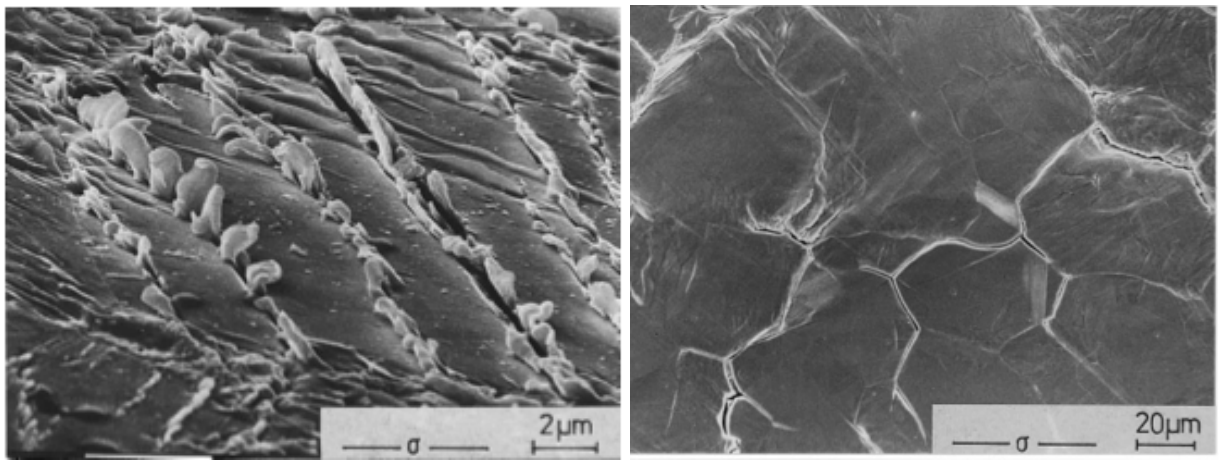

(a) Transgranular fracture initiation **(b) Intergranular fracture initiation**

Figure 67 Fracture initiation mode, outside (a) and inside (b) the low temperature regime, iron[65]

5.4.2. Effect of other chemical elements inside ferrite lattice

The Seeger theory presented in the previous section has been widely studied for B.C.C. pure iron, due to the absence of other elements inside ferrite grains. Nevertheless, some publications are discussing about the influence of some additional elements inside ferrite grain on the applicability of the Seeger theory. Addition of interstitial (or substitution) elements into a pure lattice is supposed to harden the material. This is the reason why steel, iron plus solute carbon atoms, is significantly harder than pure iron due to the pinning of the dislocations.

However, in a certain temperature range inside the low temperature regime, addition of carbon will soften the material, as shown in Fig. 68 from Quesnel *et al.*[68]. One can see that at a moderate low temperature range, yield stress from pure iron is higher than carburized iron. It seems also that the higher carbon concentration is, the more obvious the softening effect is. Sommer *et al.*[67] has observed this softening behavior for a 74 ppm Carbon iron at a temperature of 220K and a strain rate of 10^{-3} s^{-1}, under axial fatigue tests. Such a softening can be easily detected by *in-situ* experiments, since mobility of screw segments will be drastically increased by addition of carbon atoms at a similar temperature[62,69]. Thus the gap between screw and edge segment mobility will be significantly decreased.

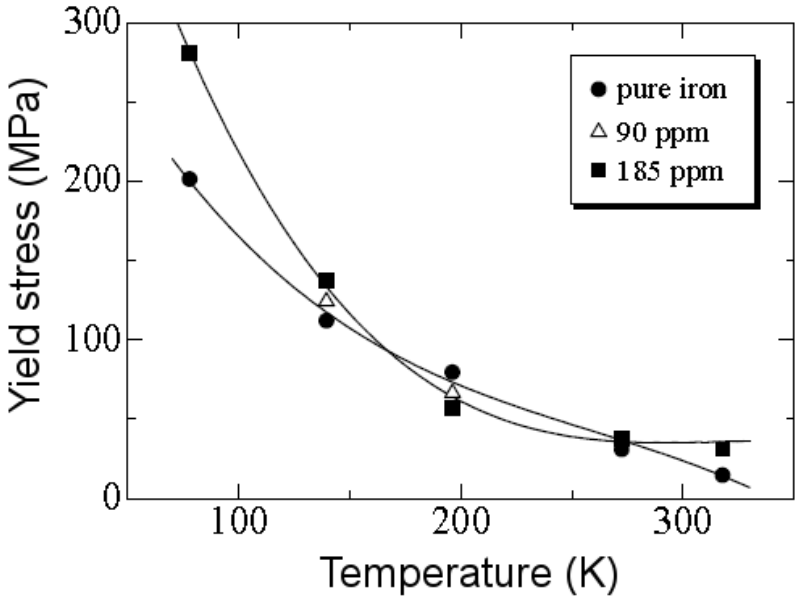

Figure 68 Resolved shear yield stress at 0.05% plastic strain of pure and carburized iron[68]

The reason of the effect of interstitial elements inside iron lattice has been the subject of some controversies. Sato *et al*.[70] have pointed out a decrease of the activation energy of kink mechanism due to addition of interstitial elements. Solomon *et al.*[71] have considered these impurities as barriers to the motion of non-screw dislocations in the low temperature regime to explain their experimental results. Kuramoto *et al.*[72] have interpreted the softening effect by analyzing a direct relation with disappearance of peak of activation area of dislocation by addition of carbon. Recently, Caillard[61] has found that the main mechanism related to this softening effect of carbon solute atoms, in a 110 ppmC iron, is due to the disappearing of activation area peak, as proposed by Kuramoto *et al.*[72]. A similar conclusion has also been reported for Si, Ni or Cr additions at relatively low concentrations[73].

Such a softening effect has a direct consequence on the transition temperature T_0 giving the temperature bound of the low temperature regime. In order to assess this transition temperature, one can undertake experiments on the strain rate sensitivity of the flow stress. To perform this experiment, the flow stress difference from tensile tests carried out at two distinct strain rates is calculated. Such strain rate sensitivity in a function of temperature presents a peak[74]. This peak means that the effective stress σ^* is negligible for the lowest strain rate, but becomes significant for the highest strain rate. In other words, the transition temperature T_0 is located at the peak temperature for a strain rate between the two strain rates applied during tensile tests. According to Quesnel *et al.*[68] in Fig. 69, the higher the carbon solute atom element composition up to 400 ppm is, the more distinct the shift to low temperature domain of the strain sensitivity is. Therefore, the higher the carbon solute atom element composition up to 400 ppm is, the lower the transition temperature T_0 is. Based on the transition equation of the Seeger theory, the transition strain rate $\dot{\varepsilon}_t$ of ferrite grains in S15C steel will be higher than that for pure iron, at the same temperature. Such an important effect of the chemical composition for α-iron based metallic materials on the transition conditions was found by Magin *et al.*[63].

According to Table 2, ferrite grain lattice of S15C steel includes, in addition to carbon atoms, also Mn, Si and Cr solute atoms. All these elements will induce a shift of the transition

condition to higher strain rates. Besides, Vaynman *et al.*[75] have discussed that the addition of nanosize precipitates inside B.C.C. lattice tends to decrease locally the Peierls stress over the length of a double kink pair along the dislocation. Due to the chemical composition of S15C steel, it seems reasonable to have a relatively high number of precipitates inside ferrite phase. Such a point is confirmed by the Fig. 64(a), where one can see those precipitates. Since the Peierls stress is locally decreased, leading to a reduction of the activation energy U_0, the transition strain rate tends to increase according to Eq. (12). Unfortunately, an estimation of this transition strain rate in the case of S15C steel is not given here, as it requires very specific experiments.

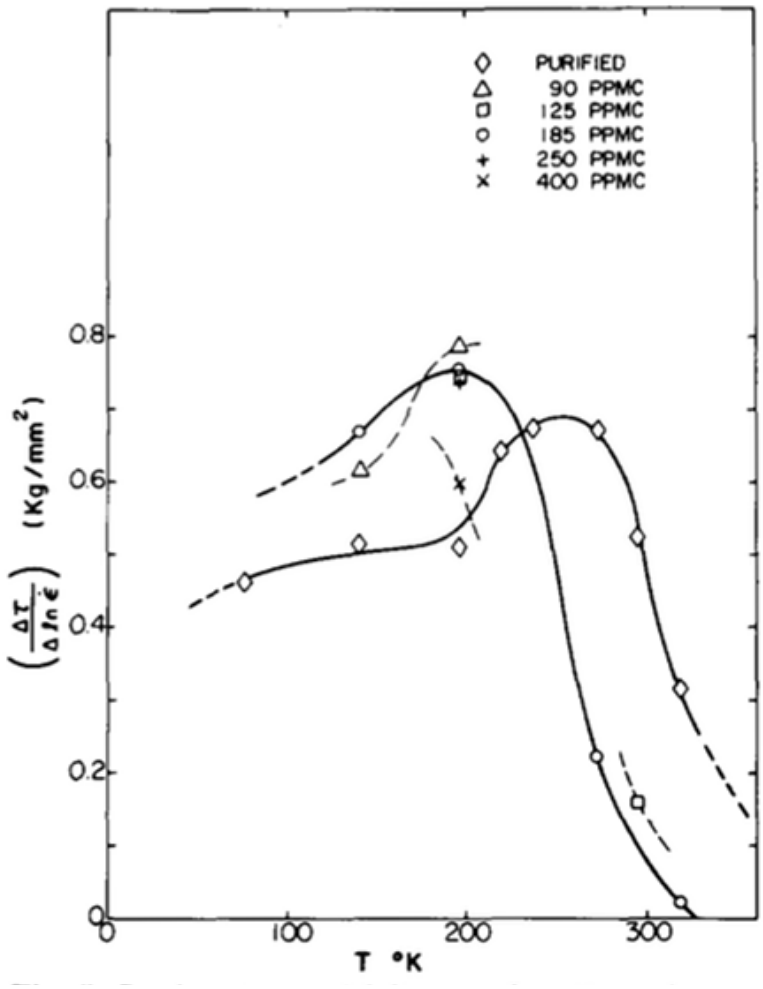

Figure 69 Strain rate sensitivity of yield stress, Fe-C sytem[68]

In addition, it should be noted that addition of other elements has also a typical effect on the fatigue crack initiation, due to possible grain boundary embrittlement. Indeed, it is usually reported that segregations of Mn[76], S[77] or P[78] impurities tend to weak the grain boundaries. On the other hand, addition of carbon tends to strength the grain boundaries by replacing the other segregation elements in the vicinity of grain boundary[79]. We have thus a competition of the segregation elements between carbon and other atoms at grain boundaries. According to chemical composition listed in Table 3, it is thought that intergranular crack initiation mechanism is facilitated in the S15C steel studied in the present work compared to pure iron.

5.4.3. Strain rate effect on the fatigue properties of S15C steel

In the work done in Chapter 3 of this report, slight change of fatigue strength of S15C steel in the usual frequency range of 0.2 Hz to 140 Hz has been detailed. The strain rate affects slightly the cyclic strain softening of S15C steel, due to the change of the lower yield stress. However, since such an explanation cannot explain the drastic loss of local misorientation for fatigue tests at ultrasonic frequency, a similar explanation is not reasonable.

The significant change of the dislocation structure observed in Section 5.3 causes a decrease of geometrically necessary dislocations (GND) density, and thus gives the reason of the drastic loss of local misorientation seen in both transversal and longitudinal directions (Section 4.3.5). Instead of cell or ladder structures caused by fatigue loadings performed in usual frequency range of 0.2 to 140 Hz, samples fatigued at 20 kHz reveal long screw segments. Such a structure is characteristics of B.C.C. materials deformed at sufficiently low temperature and / or sufficiently high strain rate.

The effect of the strain rate on the fatigue properties of pure α-iron, due to this change of dislocation structure, is schematically depicted in Fig. 70. As already mentioned in Section 5.4.1, at room temperature, the transition strain rate $\dot{\varepsilon}_t$ is approximately 10^{-4} s^{-1}. At a strain rate lower than this transition value, mobility of screw and edge parts of dislocations are similar. Thus, dislocations dipoles, as clear dislocation walls, can be formed. In addition the crack initiation mechanism is intragranular. If the average strain rate has overcame the transition strain rate, due to Peierls stress profile in B.C.C. lattice, mobility of the screw part of dislocations becomes very low compared to non-screw part. So, long screw segments are formed, and an intergranular crack initiation mechanism is reported. Such a change of the crack initiation mechanism implies a drastic increase of the fatigue life of α-iron [63,66].

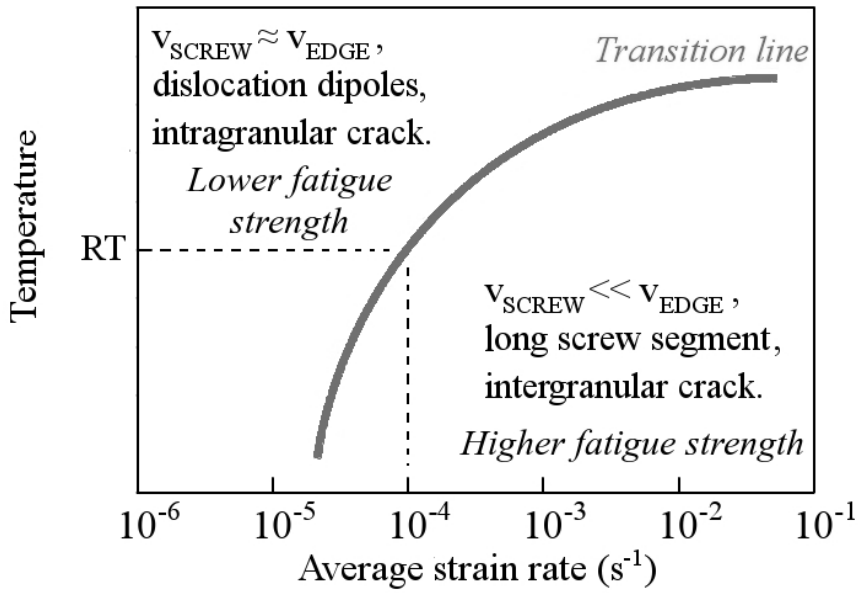

Figure 70 Strain rate effect on fatigue properties of pure α-iron

In the case of the S15C low carbon steels, even though the base matrix is also B.C.C. α-iron, we have to consider some complexities of the microstructure as follows; (1) the interstitial and substitution elements and precipitates inside the ferrite lattice; (2) the existence of cementite and thus a volume fraction of pearlite grains.

As already discussed in Section 5.4.2, addition of such solute elements inside the ferrite lattice will macroscopically induce a softening effect in the low temperature regime compared with the case of pure iron. Indeed addition of solute elements and formation of precipitates inside ferrite lattice decrease the gap between screw and edge dislocation mobilities. This aspect is directly related with the decrease of the transition temperature T_0 with an increase of carbon content as shown in Fig. 69, at a constant strain rate. Similarly, at the same temperature, the transition strain rate $\dot{\varepsilon}_t$ is increased by the effect of other elements inside the ferrite lattice, as already mentioned in Section 4.2.

In the case of low carbon steels with carbon content higher than its solubility inside the ferrite lattice, volume fraction of pearlite grains is expected to have a significant effect on the athermal stress term σ_G of the flow stress, but the effective stress σ^* is expected to keep negligible small. Indeed, the fine lamellar structure of pearlite grains is supposed to prevent the formation of long segments of screw dislocations. Besides, one can note that most of the high misorientation values left after ultrasonic loadings are induced inside the pearlite grains in Fig. 49(c). Such an experimental evidence implies that dislocation structure in α-phase of pearlite grains is slightly affected by ultrasonic loadings. In other words, the effective stress σ^* of S15C steel is caused by B.C.C. α-phase in ferrite grains only. In addition, pearlite grains do not affect neighboring ferrite grains behavior in the low temperature regime, since long screw segments were observed in all ferrite grains in this work. For S15C steel, a quick calculation based on the Fe-C phase diagram gives a volume fraction of pearlite grain of 16.9 %. This result seems to be in a good agreement with the microstructure shown in Fig. 19. It is thus sensible to consider that the small pearlite volume fraction inside S15C steel has a limited influence on the macroscopic effective stress σ^*.

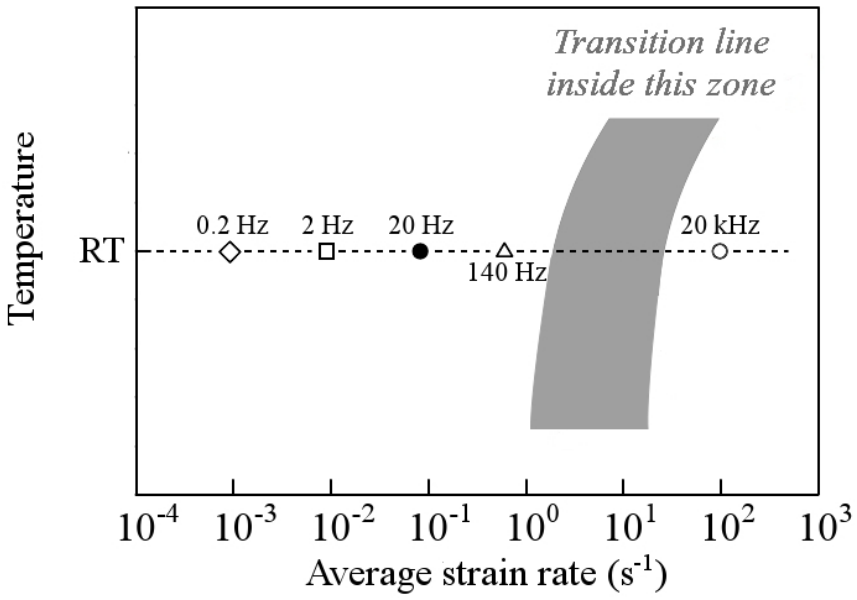

Figure 71 Strain rate effect on fatigue properties of S15C steel

According to the above discussion, a scheme representing the strain rate effect on the fatigue properties of S15C steel is shown in Fig. 71. This schematic overview is roughly similar to the situation for pure iron. However, due to the dissolved elements in the ferrite lattice, the transition strain rate $\dot{\varepsilon}_t$ has drastically increased. In accordance with results from dislocation micrographs, the

transition is set between corresponding average strain rate of fatigue tests performed at f = 140 Hz and f = 20 kHz, at room temperature.

At strain rate lower than the transition, dipole dislocation structures can be observed in ferrite grains, and the crack initiation mostly occurs due to slip bands, inducing an intragranular fatigue crack. The rare case of intergranular crack initiation mode in this domain is certainly caused by diffusion of impurities increasing the segregation concentration along grain boundaries. On the other hand, at strain rate higher than the transition, mobility of screw and edge dislocations differ from each other. Thus, long screw segments are formed, according to the Peierls stress profile. In this domain, crack initiation becomes exclusively intergranular. Such a change of crack initiation mode is the main reason why the *S-N* property in ultrasonic fatigue test differs significantly from that at usual frequencies, in a way similar to pure α-iron.

Finally, it should be noted that this discussion is valid as long as the macroscopic behavior of the carbon steel studied in the low temperature is governed by the effective stress σ^*. As already mentioned, the effective stress is caused by B.C.C. α-phase in ferrite grains only, excluding the α-phase in pearlite grains due to its lamellar structure. In the case of S15C steel with a very slight pearlitic volume fraction, it seems reasonable to consider that its macroscopic behavior is governed by the effective stress σ^* of ferrite grains. However, an increase of pearlitic volume fraction reduces the effective stress of the whole structural steel, due to decrease of ferritic volume fraction. Thus, fatigue properties of carbon steels with a higher content of carbon, *i.e.* higher volume fraction of pearlite, should be less sensitive to the peculiar behavior of ferrite grains, inducing a lower sensitivity to the loading frequency

As an example, Zettl *et al.*[40] have studied the fatigue properties, at ultrasonic frequency, of a 0.15 %C and 0.61 %C, with 20 % and 80 % pearlitic volume fractions, respectively. *S-N* curve found for 0.15 %C at f = 20 kHz is close to the results found in Fig. 34. In the case of 0.61 %C, the *S-N* curve obtained has been compared with S58C conventional rotating bending tests results, at a loading frequency of 51.7 Hz, in air, at room temperature, in Fig. 72[80]. One can see clearly that *S-N* curves, and particularly the fatigue strengths, are close to the agreement. Such a phenomenon can be explained by the discussion above. Nevertheless, this general approach of the frequency effect for a wide range of carbon steels requires strong experimentations for various kinds of middle and high carbon steels to be validated.

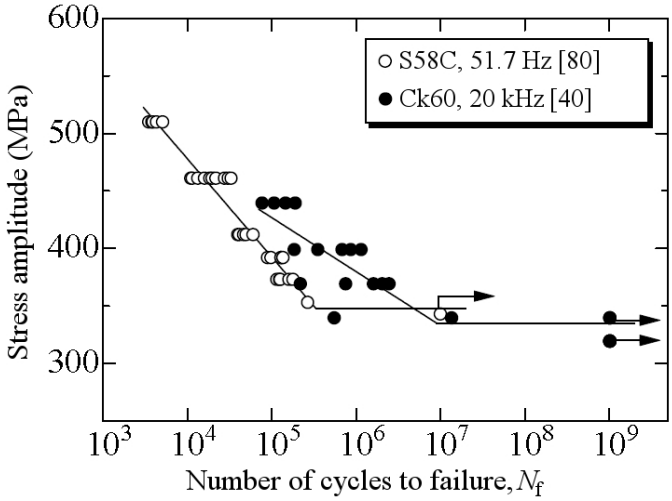

Figure 72 Brief comparison of *S-N* curves for high carbon steel

5.5. Conclusion

Experiments presented in this Chapter 5 deals exclusively with the dislocation observations obtained in ferrite grains of S15C low carbon steel. Such observations have been carried out in the wide range of loading frequency of 0.2 Hz to 20 kHz. Main findings are summarized in several points as follows;

(1) A clear effect of the loading frequency on the dislocation structures in ferrite grains of S15C steel has been found. Fatigue tests conducted in the usual frequency range of 0.2 to 140 Hz have caused clear dislocation dipole structures (cell or ladder), whereas ultrasonic loading has induced formation of long screw dislocation structures without clear dislocation walls.

(2) Such long screw dislocation structures are characteristic of B.C.C. materials deformed in a certain domain, depending on the temperature and the strain rate, so-called the "low temperature regime", in accordance with the Seeger theory.

(3) Inside this low temperature regime, pure α-iron is reported to show some particular fatigue properties based on shape change of the specimen, inducing a concentration of stress at grain boundaries and thus an intergranular crack initiation. Such results have been already detected for S15C steel in the Chapter 4.

(4) Due to the dissolved elements and precipitates inside ferrite lattice, the transition conditions (temperature and strain rate) for S15C low carbon steel is different from those in pure α-iron. In accordance with the dislocation micrographs, the transition strain rate for S15C steel is supposed to be within a range between fatigue tests performed at f = 140 Hz and f = 20 kHz, at room temperature. Consequently, the significantly higher fatigue strength of S15C steel at f = 20 kHz than usual frequencies is due to the transition of crack initiation mechanism, in a way similar to the case of pure α-iron.

(5) The effective stress σ^* is expected to be caused only by ferrite grains, excluding α-phase in pearlite grains due to its lamellar structure. Since the pearlitic volume fraction of S15C steel is very slight, its macroscopic behavior in the low temperature regime is governed by the effective stress σ^* of ferrite grains. However, an increase of the pearlitic volume fraction reduces the effective stress of the structural steel due to the decrease of the ferritic volume fraction. Thus, fatigue properties of carbon steels with a higher content of carbon should be less sensitive to the peculiar behavior of ferrite grains, inducing a lower sensitivity to the loading frequency.

Chapter 6. Conclusions and Perspectives

The aim of the experiments presented in this report is to deliver a better understanding of the frequency effect on fatigue properties of metallic materials. This work has been divided into the Chapters 2, 3, 4 and 5 of this report.

First study, presented in the Chapter 2, is dealing with a meta-synthesis of the frequency effect for a wide range of metallic materials. In addition, specific discussions were added in the case of structural steels and aluminum alloys. According to the results, effect of the ultrasonic loading frequency is rather limited for numerous kinds of metallic materials, even though some extents of discrepancy were found for steels in the high cycle regime. Nevertheless, this meta-synthesis highlighted also the special case of the low carbon steels, which are known to be particularly sensitive to the loading frequency, compared to other structural steels.

Thus the second study has been focused on the particular case of S15C low carbon steel and due to its length, was presented in Chapters 3, 4 and 5 of this report. The Chapter 3 presents the fundamental fatigue results at usual frequency range from 0.2 to 140 Hz, and found a slight frequency effect. Such a frequency effect found is due to the change the yield stress depending on the strain rate applied on the material. Besides, by normalizing the stress amplitude by the lower yield stress at respective strain rates, a common *S*-*N* curve has been found.

Then, ultrasonic fatigue test results were introduced in the Chapter 4. In addition, this section deals with a comparison of some essential fatigue properties at usual and ultrasonic frequencies. According to the experimental results, some discrepancies were detected. Indeed, the slip band formation and the crack initiation mode differ from at usual and ultrasonic frequencies. In addition, a strong irregularity of the local misorientation distributions urges us to consider a drastic dislocation rearrangement inside ferrite grains.

In order to better grasp the ultrasonic fatigue properties of S15C steel, observation of the dislocation structures is presented in the Chapter 5. Indeed, the dislocation arrangements differ totally after usual and ultrasonic fatigue loadings. Samples fatigued at ultrasonic frequency reveal long screw dislocation structure in ferrite grains. This structure is characteristic to B.C.C. materials placed into the “low temperature regime”, as observed for pure iron. This regime can be also reached if a sufficient strain rate is applied on the material, which is experimentally the case for S15C steel fatigued at 20 kHz, exclusively. Inside this “low temperature regime”, the crack initiation is reported to be intergranular, whereas intragranular crack initiation mode is reported outside this regime. S15C steel presents a similar behavior.

Thus, the significant increases of both fatigue strength and life at ultrasonic frequency are explained by this change of crack initiation mechanism, also reported in the case of pure iron. It is noteworthy that a change of crack propagation rate was also found for low carbon steels between usual and ultrasonic fatigue tests[81]. However, the rather slight change reported is unlike to explain the large discrepancy of the fatigue life found in the *S*-*N* data.

Nevertheless, carbon steels do not have exactly the same microstructure compared with pure iron. Presence of solute elements and particles inside ferrite has a critical influence on the transition condition of the Seeger theory. Consequently, these elements shift the low temperature regime to higher strain rate domain. In addition, long screw dislocation structures are unlike to be formed in

the lamellar ferrite structure of pearlite grains. Such a point is confirmed by the high values of local misorientations in α-phase of pearlite grains even after ultrasonic loadings. Thus, pearlitic structure is considered to have a negligible impact on the effective stress σ^*. Thus, S15C macroscopic behavior in the low temperature regime is governed by the effective stress σ^* of ferrite grains. This assumption is valid as long as the pearlitic volume fraction is slight. An increase of the pearlitic volume fraction will decrease the ferritic volume fraction, reducing the effective stress σ^*. This is certainly the reason why the carbon steels close to eutectoid point of Fe-C phase diagram do not show a frequency effect as significant as low carbon steels.

Further studies dealing with the effect of the loading frequency on the fatigue properties of carbon steels should be undertaken in order to better grasp all the phenomena related to this low temperature regime. One major improvement of this work would be to determine the transition strain rate of ferrite grains of carbon steel, at room temperature. However, such a study seems almost impossible due to the very high strain rates as high as 10^0 or 10^1 s^{-1} involved, which will cause undoubtedly a self-heating phenomenon.

One could also carry out series of comparisons between usual and ultrasonic frequencies on carbon steels with various carbon contents as S10C, S20C, S45C, etc… Such an experiment would consist to calculate the amplitude of the frequency effect for each kind of carbon steels studied and thus could compare the frequency effect as a function of the carbon content. Simultaneously, it would be also fruitful to confirm that the dislocation structure in the ferrite grains at 20 kHz is the same for all carbon steels, regardless the carbon content, *i.e.* regardless the pearlite volume fraction.

In order to better grasp the mechanisms of severe strain inhomogeneities revealed by SEM microscopy on the specimen surface after 20 kHz cyclic loadings, it would also interesting to carry out some dislocation observations inside grains plastically deformed, and precise the characterizations and differences between grains plastically deformed revealing very dense slip band structure and other grains without any slip band.

Finally, it is also a huge interest to analyze the case of quenched steels behavior depending on the loading frequency and particularly the B.C.C. martensite microstructure. Since the martensite crystallographic structure is similar to the ferrite one with a higher concentration of carbon atoms, the transition condition should be even more shifted to higher strain rates. Nevertheless, particular influence of needle-shaped microstructure can induce some other phenomena. It is thus difficult to expect the behavior of martensite under ultrasonic loadings from this work.

REFERENCES

[1] B. Hopkinson, *Proceedings of the Royal Society of London, Series A*, Vol.86 (1911), p.101.

[2] C. F. Jenkin, *Proceedings of the Royal Society of London, Series A*, Vol.109 (1925), p.119.

[3] W. P. Manson, *Piezoelectric Crystal and their Application in Ultrasonics*. (1950) New York: Van Nostrand.

[4] F. Girard and G. Vidal, Rev. Metall., Vol.56 (1959), p.25.

[5] M. Kikukawa, K. Ohji and K. Ogura, Push-Pull Fatigue Strength of Mild Steel at Very High Frequencies of Stress Up to 100 kc/s, *Journal of Basic Engineering Transaction of the ASME D*, Vol.87 (1965), pp.857-864.

[6] Y. Murakami, "The Mechanism of Fatigue Failure of Steels in the Ultra long Life Region of N>107 cycles, Metal Fatigue Effetct of Small Defects and Non metallic Inclusions, (2002) pp.273-303.

[7] T. Wu, J. Ni, C. Bathias, An automatic ultrasonic fatigue testing system for studying low crack growth at room and high temperatures, *Automation in Fatigue and Fracture: Testing and Analysis* (1994), pp.598-607, C. Amzallag, ASTM STP, ASTM Philadelphia.

[8] J. Ni, C. Bathias, Development of an ultrasonic fatigue device and its application in fatigue behaviour studies, *Recent Advances in Experimental Mechanics* (1994), pp.1121-1126, Silva Gomes et al, Rotterdam, Balkerma.

[9] M. Yamane, High Speed Plane Bending Fatigue Test (4th Report, Theoretical Consideration on the Speed Dependency, Part 2), *Transactions of the Japan Society of Mechanical Engineers*, Vol.30, No.215 (1964), pp.772-779. (In Japanese).

[10] S. Taira and K. Emura, Investigation on the High Frequency Fatigue (the 1st Report), *Journal of the Society of Materials Science, Japan*, Vol.12, No.118 (1963), pp. 536-541. (In Japanese).

[11] Y. Furuya, Specimen size effect on gigacycle fatigue properties of high strength steel under ultrasonic fatigue testing, *Scripta materiala*, Vol.58 (2008), pp.1014-1017.

[12] E. Takeuchi, Y. Furuya, N. Nagashima, K. Miyahara and S. Matsuoka, Effect of Frequency on Giga-cycle Fatigue Properties for Ti-6Al-4V Alloy, *Transactions of the Japan Society of Mechanical Engineers Series A*, Vol.70, No.696 (2004), pp.1124-1130. (In Japanese).

[13] S. Setowaki, Y. Ichikawa and I. Nonaka, Effect of Frequency on High Cycle Fatigue Strength of Railway Axle Steel, *Proceedings of the Fifth International Conference on Very High Cycle Fatigue VHCF-5* (2011), pp.153-158.

[14] E. Bayraktar, I. Marines and C. Bathias, Failure mechanisms of automotive metallic alloys in very high cycle fatigue range, *International Journal of Fatigue*, Vol.28 (2006), pp.1590-1602.

[15] I. Marines, G. Dominguez, G. Baudry, J.-F. Vittori, S. Rathery and C. Bathias, J.-P. Doucet and C. Bathias, Ultrasonic Fatigue Tests on Bearing Steel AISI-SAE 52100 at Frequency of 20 and 30 kHz, *International Journal of Fatigue*, Vol.25 (2003), pp.1037-1046.

[16] H. Mayer, M. Papakyriacou, B. Zettl and S.E. Stanzl-Tschegg, Influence of Prosity on the Fatigue Limit of Die Cast Magnesium and Aluminum Alloys, *International Journal of Fatigue*, Vol.25 (2003), pp.245-256.

[17] Y. Furuya, Ultrasonic Fatigue Properties of High Strength Steel under Testing with Dumbell-type Specimen having a Straight Part, *Transactions of the Japan Society of Mechanical Engineers Series A*, Vol.73, No.732 (2007), pp. 957-964. (In Japanese).

[18] Y. Furuya and S. Matsuoka, Ultrasonic Fatigue Properties of High Strength Steel under Tensile Mean Stress, *Transactions of the Japan Society of Mechanical Engineers Series A*, Vol.71, No.709 (2005), pp.1201-1206. (In Japanese).

[19] Y. Furuya, T. Abe and S. Matsuoka, 10^{10}-cycle fatigue properties of 1800 MPa-class JIS-SUP7 spring steel, *Fatigue & Fracture of Engineering Materials & Structures*, Vol.26 (2003), pp. 641-645.

[20] Q.Y. Wang, J.Y. Bernard, A. Dubarre, G. Baudry, S. Rathery and C. Bathias, Gigacycle Fatigue of Ferrous Alloys, *Fatigue & Fracture of Engineering Materials & Structures*, Vol.22 (1999), pp.667-672.

[21] C. Bathias and J. Ni, Determination of Fatigue Limit between 10^5 and 10^9 cycles using an Ultrasonic Fatigue device (1993), pp. 141-152, Advance in Fatigue Lifetime Predictive Techniques: Second volume, ASTM STP 1211, Philadelphia.

[22] C.C. Engler-Pinto Jr., R.J. Frisch Sr., J.V. Laserckil, H. Mayer and J.E. Allison, Effect of Frequency and Environment on High Fatigue of Cast Aluminum Alloys, *Proceedings of the Fourth International Conference on Very High Cycle Fatigue VHCF-4* (2007), pp.421-427.

[23] C. Bathias, Influence of Metallurgical Instability on the Gigacycle Regime, *International Journal of Fatigue*, Vol.32 (2010), pp.535-540.

[24] K. Shiozawa, T. Sakai *et al*., *Database on Fatigue Strength of Metallic Materials, Elsevier & JSMS*, Vols.1-3 (1996).

[25] NIMS Fatigue Data Sheet No. 106, *Data Sheet on Ultrasonic Fatigue Properties of Alloy Steel SCM 440 (0.4C-1Cr-0.2Mo) for Machine Structural Use* (2009).

[26] *Handbook of Fatigue Design, Chap. 12*, Ed. Society of Material Science Japan, Published by Yokendo Ltd. (1995), p.388 (In Japanese).

[27] T. Sakai *et al*., Standard Evaluation Method of Fatigue Reliability for Metallic Materials, T. Sakai, Soc. Mater. Sci., Japan (2007).

[28] S. Hattori, Study on Stress-Strain Hysteresis Loop Behavior in Fatigue Process of Normalized Carbon Steels, PhD thesis, 1979. (In Japanese).

[29] N.P. Inglis, Hysteresis and Fatigue of Wohler Rotating Cantilever Specimen, *The Metallurgist*, February (1927), pp.23-27.

[30] C.E. Feltner and C. Laird, Cyclic Stress-Strain Response of F.C.C. Metals and Alloys-I, *Acta Metallurgica*, Vol.15 (1967), pp.1621-1632.

[31] L. Landgraft, J. Morrow and T. Endo, Determination of the cyclic Stress-Strain Curve, *Journal of Materials*, Vol.4 (1969), pp.176-188.

[32] B.S. El-Dasher, B.L. Adams and A.D. Rollett, Viewpoint: experimental recovery of geometrically necessary dislocation density in ploycrystals, *Scripta Mater*., Vol.48 (2003), pp.141-145.

[33] M. Kamaya, Measurement of local plastic strain distribution of stainless steel by electron backscatter diffraction, *Materials Characterization*, Vol.60 (2009), pp.125-132.

[34] M. Kamaya, Characterization of microstructural damage due to low-cycle fatigue by EBSD observation, *Materials Characterization*, Vol.60, (2009) pp.1454-1462.

[35] D.P. Field, P.B Trivedi, S.I. Wright and M. Kumar, Analysis of local orientation gradients in deformed single crystals, *Ultramicroscopy*, Vol.103 (2005), pp.33-39.

[36] E. Demir, D. Raabe, N. Zaafarani and S. Zaefferer, Investigation of the indentation size effect though the measurment of geometrically necessary dislocations benath smal indents of different depths using EBSD topography, *Acta Mater*., Vol.57 (2009), pp.559-569.

[37] N. Tsuchida, H. Masuda, Y. Harada, K. Fukaura, Y. Tomota and N. Nagai, Effect of ferrite grain size on tensile deformation of a ferrite-cementite low carbon steel, *Material Science and Engineering A*, Vol.488 (2008), pp.446-452.

[38] W.S. Lee and C.Y. Liu, The effect of temperature and strain rate on the dynamic flow behavior of different steels, *Material Science and Engineering A*, Vol.426 (2006), pp.101-113.

[39] M. Itabashi and K. Kawata, carbon content on high-strain-rate tensile properties for carbon steels, *International Journal of Impact Engineering*, Vol.24, No.2 (2000), pp.117-131.

[40] B. Zettl, H. Mayer, C. Ede and S. Stanzl-Tschegg, Very high cycle fatigue of normalized carbon steels, *International Journal of Fatigue*, Vol.28, No.11 (2006), pp.1583-1589.

[41] B. Mintz and D.V. Wilson, Strain ageing during the fatigue of carbon steels, *Acta Metall*., Vol.13 (1965), pp.947-956.

[42] D. Rittel, G. Ravichandran and A. Venkert, The mechanical response of pure iron at high strain rates under dominant shear, *Materials Science and Engineering A*, Vol.432 (2006), pp.191-201.

[43] T. Yokobori, H. Ishii and S. Koyama, The effect of ferrite grain size on the cyclic stress-strain response of low carbon steel, *Scripta Metallurgica*, Vol.13, No.7 (1979), pp.515-517.

[44] S. Sasaki and Y. Ochi, Some experimental studies of fatigue slip bands and persistent slip bands during fatigue process of low carbon steel, *Engineering Fracture Mechanics*, Vol.12 (1979), pp.531-540.

[45] L.S. Toth, A. Molinari and N. Zouhal, Cyclic plasticity phenomena as predicted by polycrystal plasticity, *Mechanics of Materials*, Vol.32 (2000), pp.99-113.

[46] C. Buque, Persistent slip bands in cyclically deformed nickel polycrystals, *Int. J. Fatigue*, Vol. 23 (2001), pp.459-466.

[47] C.D. Liu, D.X. You and M.N. Bassim, Cyclic strain hardening in polycrystalline copper, *Acta metall. mater.*, Vol.42, No.5 (1994), pp.1631-1638.

[48] M. Zhang, P. Yang and Y. Tan, Micromechanisms of fatigue crack nucleation and short crack growth in a low carbon steel under low cycle impact fatigue loading, *Int. J. Fatigue*, Vol.21 (1999), pp.823-830.

[49] C. Wang, D. Wagner, Q.Y. Wang and C. Bathias, Gigacyle fatigue initiation mechanism in Armco iron, *Int. J. Fatigue*, Vol.45 (2012), pp.91-97.

[50] A. Puskar, Crack and slip band formation in iron during ultrasonic fatigue at various temperatures, *Engineering Fracture Mechanics*, Vol.10 (1978), pp.187-195.

[51] A. Deva, B.K. Jha, N.S. Mishra, Influence of boron on strain hardening behaviour and ductility of low carbon hot rolled steel, *Materials Science and Engineering A*, Vol.528 (2011), pp.7375-7380.

[52] M. Weisse, C.K. Wamukwanba, H.-J. Christ and H. Mughrabi, *Acta metallurgica et materialia*, Vol.41, No.7, (1993), pp.2227-2233.

[53] Z. H. Min, L. Delaey and A. Deruyttere, Fatigue Softening of Severely Cold-Drawn Low Carbon Steel, *Acta mettalurgica*, Vol.33, No.4 (1985), pp.563-570.

[54] H.-F. Chai and C. Laird, Mechanisms of Cyclic Softening and Cyclic Creep in Low Carbon Steel, *Materials Science and Engineering*, Vol.93 (1987), pp.159-174.

[55] H. Saka, K. Noda and T. Imura, Direct observation of dislocation multiplication in iron at low temperature by HVEM, *Transactions ISIJ*, Vol.13, (1973), pp.318-324.

[56] A. Seeger, The temperature dependence of the critical shear stress and of work-hardening of metal crystals, *Philosophical Magazine 7th Series*, Vol.45 (1954), pp.771-773.

[57] L. Stainier, A.M. Cuitino and M. Ortiz, A micromechanical model of hardening, rate sensitivity and thermal softening in bcc single crystals, *Journal of the Mechanics and Physics of Solids*, Vol.50 (2002), pp.1511-1545.

[58] J.R. Low and A.M. Turkalo, Slip band structure and dislocation multiplication in silicon-iron crystals, *Acta Metallurgica*, Vol.10 (1962), pp.215-227.

[59] H. Mughrabi, K. Herz and X. Stark, The effect of strain rate on the cyclic deformation properties of α-iron single crystals, *Acta Metallurgica*, Vol.24 (1976), pp.659-668.

[60] M. Tang, L.P. Kubin and G.R. Canova, Dislocation mobility and the mechanical response of B.C.C. single crystals: a mesoscopic approach, *Acta Materialia*, Vol.46, No.9 (1998), pp.3221-3235.

[61] D. Caillard, Kinetics of dislocations in pure Fe. Part II, *Acta Materialia*, Vol.58 (2010), pp.3504-3515.

[62] D. Caillard, An in situ study of hardening and softening of iron by carbon interstitials, *Acta Materialia*, Vol.59 (2011), pp.4974-4989.

[63] T. Magnin and J.H. Driver, The influence of strain rate on the low cycle fatigue properties of single crystals and polycrystals of two ferritic alloys, *Materials Science and Engineering*, Vol.39 (1979), pp.175-185.

[64] F. Guiu, R. Dulniak and B.C. Edwards, on the nucleation of fatigue crack in pure polycrystalline α-iron, *Fatigue and Engineering Materials and structures*, Vol.5, No.4 (1982), pp.311-321.

[65] C. Sommer, H. Mughrabi and D. Lochner, Influence of temperature and carbon content on the cyclic deformation and fatigue behaviour of –iron, part II, *Acta Materialia*, Vol.46, No.5 (1998), pp.1537-1546.

[66] H. Mughrabi, Wechselverformung und Ermüdungsbruch von α–Eisenvielkristallen, *Zeitschrift für Metallkunde*, Vol.66 (1975), p.719-724. (In German).

[67] C. Sommer, H. Mughrabi and D. Lochner, Influence of temperature and carbon content on the cyclic deformation and fatigue behaviour of iron, part I, *Acta Materialia*, Vol.46, No.5 (1998), pp.1527-1536.

[68] D.J. Quesnel, A. Sato and M. Meshii, Solution softening and hardening in the iron-carbon system, *Materials Science and Engineering*, Vol.18 (1975), pp.199-208.

[69] D. Caillard, Kinetics of dislocations in pure Fe. Part I, *Acta Materialia*, Vol.58 (2010), pp.3493-3503.

[70] A. Sato and M. Meshii, Solid solution softening and solid solution hardening, *Acta Metallurgica*, Vol.21 (1973), pp.753-768.

[71] H.D. Solomon and C.J. McMahon, Solute effects in micro and macroyielding on iron at low temperatures, *Acta Metallurgica*, Vol.19 (1971), pp.291-302.

[72] E. Kuramoto, Y. Aono and K. Kitajima, Thermally activated slip derformation of high purity iron single crystals between 4.2 K and 300 K, *Scripta Metallurgica*, Vol.13 (1979), pp.1039-1042.

[73] D. Caillard, A TEM in situ of alloying effects in iron. I-Solid solution softening caused by low concentrations of Ni, Si and Cr, *Acta Materialia*, Vol.61 (2013), pp.2793-2807.

[74] D. Leemans and M.E. Fine, Solid solution softening and strain rate sensitivity of Fe-Re and Fe-Mo alloys, *Metallurgical Transactions*, Vol.5 (1974), pp.1331-1336.

[75] S. Vaynman, M.E. Fine, S. Lee and H.D. Espinosa, Effect of strain rate and temperature on mechanical properties and fracture mode of high strength precipitation hardened ferritic steels, *Scripta Materialia*, Vol.55 (2006), pp.351-354.

[76] N.H. Heo, J.W. Nam, Y.-U. Heo and S.-J. Kim, Grain boundary embrittlement by Mn and eutectoid reaction in binary Fe-12Mn steel, *Acta Materialia*, Vol.61 (2013), pp.4022-4034.

[77] N.H. Heo, Sulfur segregation and intergranular fracture in α–iron, *Scripta Materialia*, Vol.51 (2004), pp.339-342.

[78] M.C. Inman and H.R. Tipler, Grain-Boundary segregation of phosphorus in an iron-phosphorus alloy and the effect upon mechanical properties, *Acta Metallurgica*, Vol.6 (1958), pp.73-84.

[79] S. Suzuki, M. Obata, K. Abiko and H. Kimura, Effect of carbon on the grain boundary segregation of phosphorus in α–iron, *Scripta Metallurgica*, Vol.17 (1983), pp.1325-1328.

[80] Shiozawa K. *et al*. (1996), *Data base on fatigue strength of Metallic Materials*, Elsevier & JSMS, code 143-550, pp.861-862.

[81] N. Tsutsumi, A. Shiromoto, V. Doquet and Y. Murakami, Effect of test frequency on fatigue strength of low carbon steel, *Transaction of the Japan Society of Mechanical Engineers A*, Vol.72, No.715 (2006), pp.317-325. (In Japanese).

APPENDIX

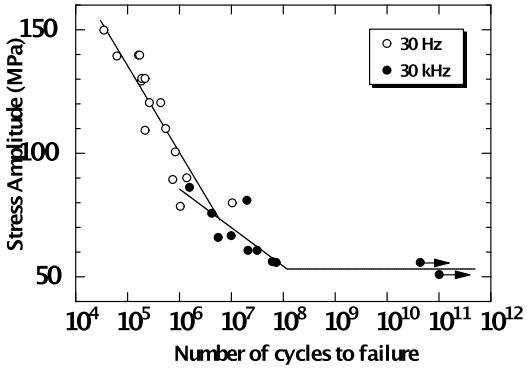

Fig_Apx 1 Aluminum alloy. E. Bayraktar[14]

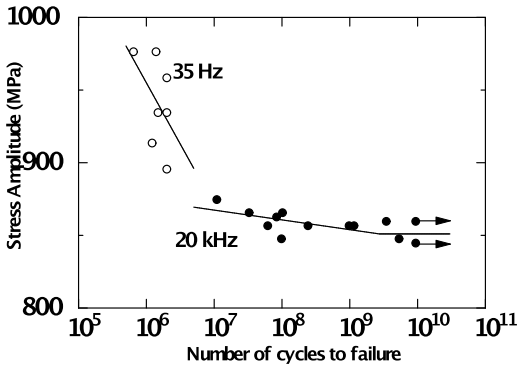

Fig_Apx 2 Bearing steel. I. Marines[15]

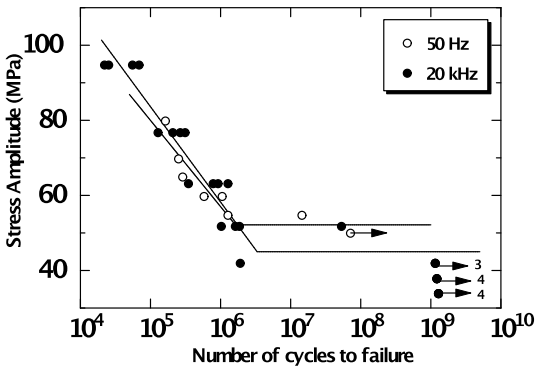

Fig_Apx 3 AZ91 (Mg Alloy). H. Mayer[16]

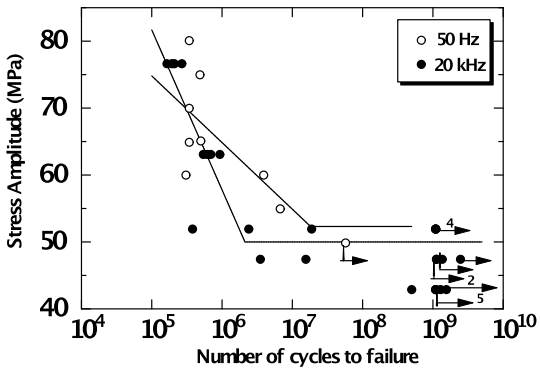

Fig_Apx 4 AM60 (Mg Alloy). H. Mayer[16]

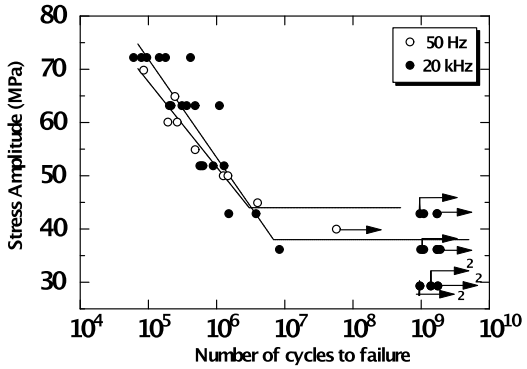

Fig_Apx 5 AE42 (Mg Alloy). H. Mayer[16]

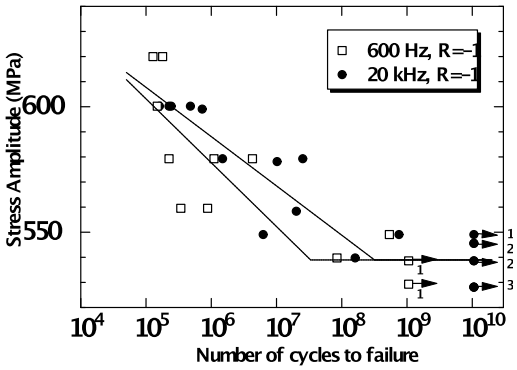

Fig_Apx 6 Ti-6Al-4V. E.Takeuchi[12]

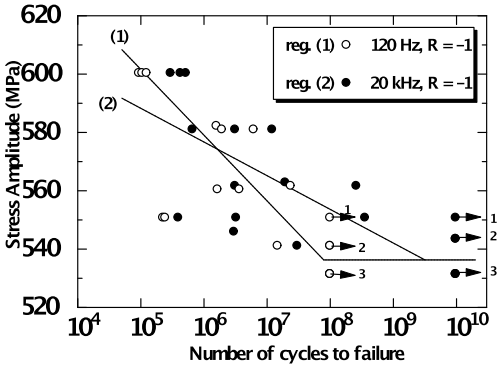

Fig_Apx 7 Ti-6Al-4V. E.Takeuchi[12]

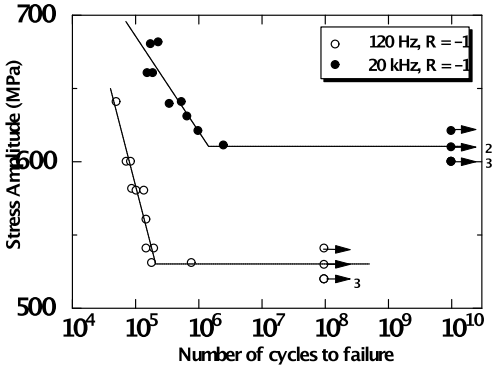

Fig_Apx 8 Ti-6Al-4V. E.Takeuchi[12]

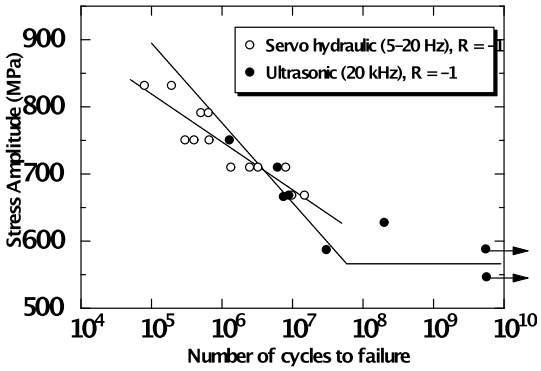

Fig_Apx 9 SCM steel. Y. Furuya[17]

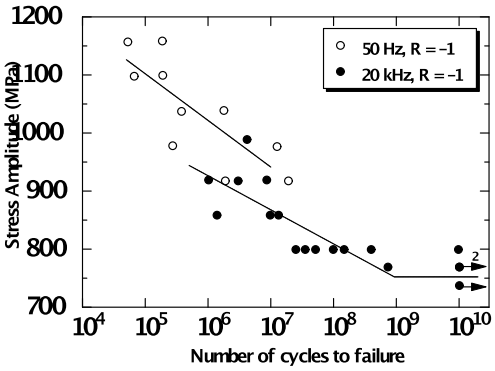

Fig_Apx 10 SCM steel. Y. Furuya[18]

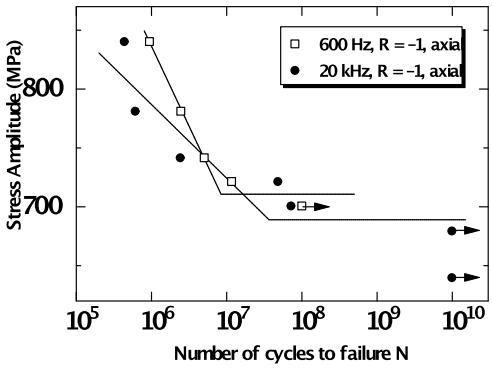

Fig_Apx 11 Spring steel. Y. Furuya[19]

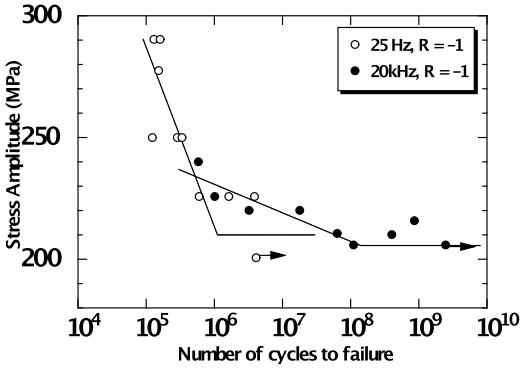

Fig_Apx 12 SG cast iron. Q. Y. Wang[20]

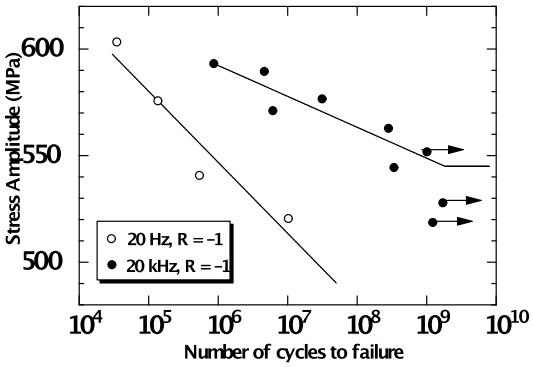

Fig_Apx 13 Ti-6Al-4V. C. Bathias[21]

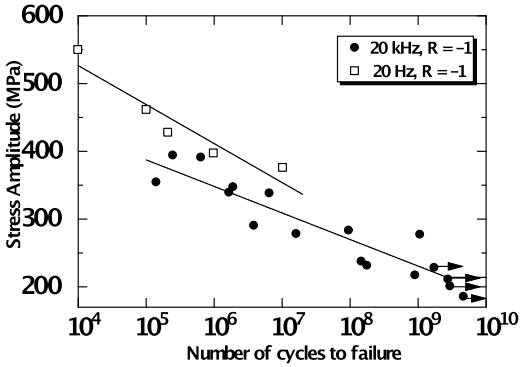

Fig_Apx 14 Ni alloy. C. Bathias[21]

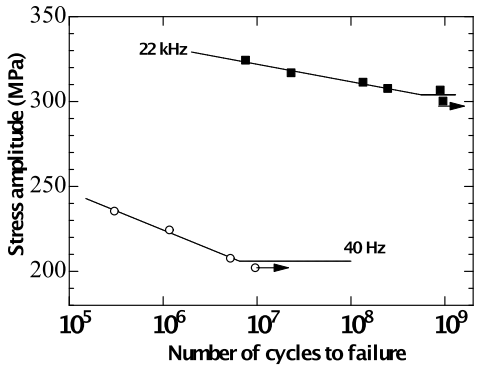

Fig_Apx 15 Mild steel. M. Kikukawa[5]

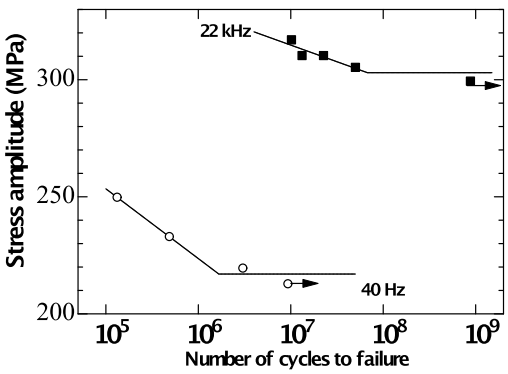

Fig_Apx 16 Mild steel. M. Kikukawa[5]

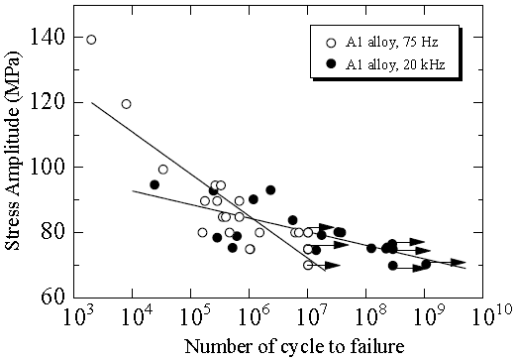

Fig_Apx 17 Al. alloy. Engler-Pinto[22]

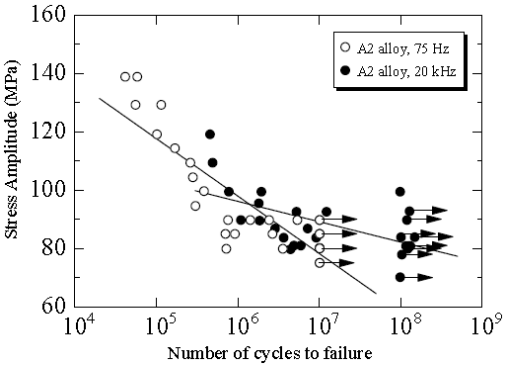

Fig_Apx 18 Al. alloy. Engler-Pinto[22]

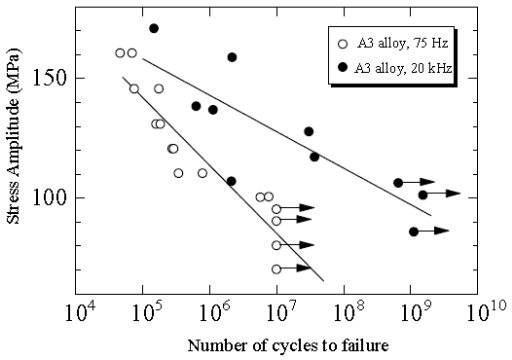

Fig_Apx 19 Al. alloy. Engler-Pinto[22]

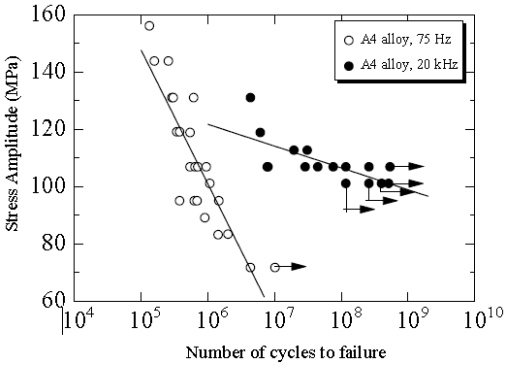

Fig_Apx 20 Al. alloy. Engler-Pinto[22]

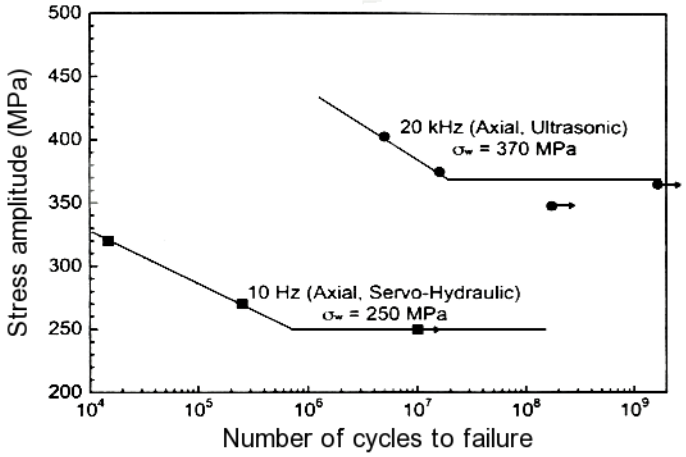

Fig_Apx 21 S38C rail steel. Setowaki[13]

List of Figures

Figures in main body of this report

Figures in the appendix

List of Tables